

# Experimentelle Studie über die fortschreitende Strukturänderung von anisotropen Sandsteinen

**Dissertation  
zur Erlangung des  
Doktorgrades der Naturwissenschaften (Dr. rer. nat.)**

der

Naturwissenschaftlichen Fakultät III  
Agrar- und Ernährungswissenschaften,  
Geowissenschaften und Informatik

der Martin-Luther-Universität Halle-Wittenberg

vorgelegt von  
Frau Feitosa Menezes, Flora  
Geb. am 31.12.1989 in Belém do Pará, Brasilien

Gutachter: Prof. Dr. Christof Lempp

Prof. Dr. Christoph Hilgers

Tag der Verteidigung: 07.10.2019



## Danksagung

Mit dieser Arbeit endet nicht nur meine wissenschaftliche Tätigkeit an der Martin-Luther-Universität, sondern auch eine schöne und unvergessliche Zeit in Halle. Hiermit möchte ich mich bei den vielen Arbeitskollegen und Kommilitonen bedanken, die mich währenddessen mit ihrer Freundschaft begleitet und unterstützt haben.

Ein besonderer Dank geht an Prof. Christof Lempp für das Vertrauen, für die gemeinsame Begeisterung an diesem zerklüfteten Thema und besonders für die konstruktive Betreuung. Auf weiteren Diskussionen über die Umstrukturierung der Geometrie und dementsprechende Fraktalität bleibe ich unendlich gespannt.

In den letzten drei Jahren hatte ich die Gelegenheit an einer vielfältigen und anspruchsvollen Forschungsarbeit teilzunehmen, die mir viele neue Erkenntnisse, fachliche Erfahrungen und Freude gebracht hat. Dafür bedanke ich mich bei den lieben Clusterinos Kristoff Svensson, Andreas Neumann und Prof. Herbert Pöllmann.

Für die enge Zusammenarbeit und hohe Bereitschaft bei allen unvorhersehbaren Labor-Unwägbarkeiten möchte ich mich bei Gerald Tröber und Juri Buchantschenko herzlich bedanken.

Für die Unterweisung und Durchführung der Röntgenmikrotomographie, deren Auswertung und Anregung zu sehr positiven Diskussionen bedanke ich mich bei John Maximilian Köhne, Steffen Schlüter, Maik Lucas und Julius Diel.

Last but not least möchte ich meiner Familie, Thomas Degen, Sabrina Galluccio, Tom Huber und insbesondere meinen Eltern meinen tief empfundenen Dank aussprechen. Vielen Dank für eure Unterstützung, Geduld und Freundschaft während all dieser Zeit!

## Abstract

Natural events such as earthquakes, floodings, volcanic eruptions and even climate change are influenced by innumerable random factors, which interact with each other to different scales and influence themselves perpetually. Deformation of rock mass is a well-known example of a natural event characterized by the interdependency between rock (e.g., lithological parameters, bedding, joints) and boundary conditions (e.g., lithostatic confinement, pore pressure variation, deformation rate). Therefore, the question this study will examine is how far can this relation between material and boundary conditions be understood and assumed as reliable? Is there a path to follow? In order to do so, the lithological variation of two sandstones and their mechanical response to lithostatic stress conditions are characterized, considering behavioural changes in dependency of pressure changes and anisotropy effects. Three kinds of triaxial compression tests were carried out by using saturated specimens (14 cm length and 7 cm diameter) drilled in two directions of anisotropy ( $0^\circ$  and  $90^\circ$ ) with respect to bedding. The sedimentary rocks are the greyish Trendelburg Beds, a silica cemented subarkose Bunter Sandstone of Triassic Age (porosity of ca. 12 %), and the red-brownish Rotliegend Sandstone (Bebertal), a carbonate and silica cemented sandstone of Permian Age, clearly less porous (ca. 6 % of effective porosity) and less permeable ( $3.5 \times 10^{-10}$  m/s) than the Bunter Sandstone. Despite the randomness of the natural boundary conditions, deformation pattern have arisen and could be correlated to lithological parameters. Both materials present a pronounced brittle behaviour and significant anisotropy effects influenced by coring direction. However, Rotliegend and Bunter Sandstone have shown an inversed anisotropic behaviour and distinct deformation paths by pore pressure changes. The contrast between both sandstones may be associated not only with their different values of porosity and permeability, but also with their differently structured pore space distribution – they accommodate strain differently. To conclude, this experimental approach will be illustrated within application-oriented aspects from the Cluster Project, by considering the Trendelburg Beds as an analogue reservoir host rock for geological CO<sub>2</sub> storage. The deformation of rock mass should be understood as a continuous process of matrix and pore space rearrangement, rather than strictly defined in plastic or elastic domains. Consequently, this study provides a comprehensive description of the effects of random factors on the structural change of rocks and thus is of importance for diverse questions concerning pressure change in rock masses.



## Zusammenfassung

Die Deformation von Gebirgen ist ein bekanntes Beispiel für ein Naturereignis, welches durch die Wechselwirkung zwischen Gesteinspaketen (z. B. Schichtung, Klüfte, Adern) und variierenden Randbedingungen (z.B. effektiver Druck, Verformungsrate, Temperatur) gekennzeichnet ist. Doch wie ist diese Beziehung zu verstehen und als zuverlässig anzunehmen? Gibt es einen Pfad, der sich daraus ableiten lässt - oder keinen? Für diese Fragestellung wurde in dieser Arbeit das geomechanische Verhalten zweier Sandsteine durch triaxiale Kompressionsversuchen untersucht. Dabei wurde die lithologische Variabilität und das Anisotropie-Effekt berücksichtigt. Die untersuchten Sedimentgesteine sind die Trendelburger Schichten, ein quarz-zementgebundener subarkoser Buntsandstein der Solling-Folge (Trias) und der Rotliegend Sandstein, ein karbonat- und quarz-zementgebundener Sandstein des Perms, deutlich weniger porös und weniger durchlässig als der Buntsandstein. Trotz der Zufälligkeit der natürlichen Randbedingungen sind Strukturänderungsmuster entstanden, die mit lithologischen Parametern korreliert werden können. Beide Gesteine weisen ein ausgeprägt sprödes Verhalten und signifikante Anisotropie-Effekte auf, die durch die Bohrrichtung beeinflusst werden. Rotliegend und Buntsandstein haben jedoch ein inverses anisotropes Verhalten und unterschiedliche Verformungsmuster bei Porendruckänderungen gezeigt. An letzter Stelle wurde diese physikalisch-mechanische Wechselwirkung anhand anwendungsbezogener Aspekte der gesamten Prozesskette bei der CO<sub>2</sub>-Speicherung in geologischen Formationen veranschaulicht. Der Kontrast zwischen beiden Sandsteinen kann nicht nur mit ihren physikalischen Eigenschaften, wie Porosität oder Durchlässigkeit, in Verbindung gebracht werden, sondern auch mit ihrer unterschiedlich strukturierten Porenraumverteilung - sie nehmen Verformung unterschiedlich auf. Weiterhin soll die Strukturänderung von Sandsteinen als ein kontinuierlicher Prozess der Matrix- und Porenraumgestaltung abgebildet werden, statt einem festgelegten plastischen oder elastischen Bereich mit begrenzten Festigkeitseigenschaften. Demzufolge bietet diese Arbeit eine umfassende Darstellung der Auswirkung variierender Faktoren in die Strukturänderung von Gesteinen und ist damit von Bedeutung für diverse Fragestellungen zur Druckänderung in Gesteinsmassen.

# Inhaltsverzeichnis

Danksagung .....	3
Abstrakt .....	4
Zusammenfassung .....	5
<b>1. Einführung</b> .....	<b>7</b>
<b>2. Fachstudien</b> .....	<b>18</b>
Anisotropy of volume change and permeability evolution of hard sandstones under triaxial stress conditions .....	19
Introduction .....	19
Materials and Methods .....	22
Theory .....	24
Results and discussion .....	26
Conclusion .....	36
Acknowledgements .....	37
References .....	37
On the structural anisotropy of physical and mechanical properties of a Bunter Sandstone .....	38
Introduction .....	39
Materials and Methods .....	40
Results .....	42
Discussion .....	43
Conclusion .....	47
References .....	48
Geomechanical behavior changes of a Bunter Sandstone and a borehole cement due to scCO <sub>2</sub> injection effects .....	49
Introduction .....	50
Materials and Methods .....	50
Results and discussion .....	52
Conclusion .....	57
References .....	57
<b>3. Schlussfolgerung</b> .....	<b>58</b>
<b>4. Literatur- und Quellenangabe</b> .....	<b>64</b>
Lebenslauf .....	76

## 1. Einführung

Naturereignisse wie Erdbeben, Überschwemmungen, Vulkanausbrüche und sogar der Klimawandel werden von unzähligen Zufallsfaktoren beeinflusst, die aus unterschiedlichen Ereignissen bzw. Umständen hervorgehen und von entsprechenden Effekten geprägt sind.

Turcotte (1990) veranschaulicht diesen Zusammenhang anhand der Topographie. Diese wird hauptsächlich durch Erosion erzeugt, welche mit chemischen und mechanischen Verwitterungsprozessen verbunden ist. Allerdings wird die eigentliche Topographie von Entwässerungssystemen dominiert, welche hauptsächlich von großen Stürmen und Überschwemmungen beeinflusst werden. Diese folgen den Statistiken zufolge größeren Ereignissen, wie Erdbeben und Vulkanen, von denen sie letztendlich auch abhängig sind. In diesem Sinne lässt sich die Gebirgsverformung ebenfalls als bekanntes Beispiel für ein Naturereignis nennen, das durch die Wechselwirkung zwischen Gesteinen und variierenden Randbedingungen (z.B. lithostatischem Druck, Porendruckänderung, Verformungsrate) gekennzeichnet ist.

Die in verformtem Gestein resultierenden Strukturmuster sind kaum zufällig: Die Orientierung der Brüche, ihre Größe und ihre räumliche Verteilung weisen eine gewisse Ordnung auf, die auf ihre Entstehungsprozesse zurückzuführen ist (Healy et al. 2017). Im Folgenden werden deshalb zwei Arten von Rissen aufgeführt. Erstens, ein berühmtes Beispiel von Ramsay & Huber (1983) für die Beziehung zwischen Geometrie und Verschiebungssinn sind die berühmten en echelon Risse. En echelon sind gescherte Dehnungsfugen, die in einem halb-spröden Verformungsregime senkrecht zur Richtung der maximalen Dehnung entstehen. Dehnungsfugen lassen sich als Risse beschreiben, an denen wenig Bewegung stattgefunden hat, die im Allgemeinen durch das Anheben und Lösen von gespeicherter Spannung entstanden ist. Wenn während der anfänglichen Scherdeformation ein Dehnungsriss entsteht, dann bilden die Risse eine parallele Staffelung, die durch subsequente Verschiebungen in der Scherzone mitgerissen wird. Da sich die Scherzonen weit ausdehnen und die Verformungsfront sich nach außen bewegt, breiten sich die Risse in den Wänden der Scherzone aus. An zweiter Stelle wird die komplexe Kettenreaktion zur Entstehung von Scherbändern nach Scholz et al. (1993) betrachtet: Zunächst wird in der Nähe der Rissspitzen eine Reihe von Zugrissen erzeugt, deren Ausrichtung mit dem Spannungsfeld der Rissspitze übereinstimmt. Die weitere Scherung führt zur Entwicklung eines komplexen Gefüges, das sich in dieser spröden Prozesszone konzentriert und schließlich zu einem durchgehenden Riss entwickelt. Darüber hinaus kann die Entstehung unterschiedlicher Strukturmuster durch mehrere Faktoren verursacht werden und sogar innerhalb der gleichen lithologischen Einheit unterschiedlich entwickelt sein. Diese tief

einbezogene Variabilität von Randbedingungen (z.B. Korngrößenänderung, Lithifizierungskontrast, Wechsellagerungen) ruft physikalische Änderungen hervor, die letztendlich zu mechanischem Kontrast führen.

Angesichts der Maßstabsabhängigkeit vieler Ergebnisse sowie der Annahme von nötigen Randbedingungen, die in der Natur nur bedingt definierbar sind, ergibt sich die Überlegung, ob laborbestimmte Verhaltensmuster zu mindestens teilweise zu einer skaleninvarianten Strukturänderung gehören und deshalb mit großdimensionalen geologischen Prozessen direkter zu verknüpfen sind. Wenn ein kleiner Prozess skaleninvariant ist, dann sind die grundlegenden Prozesse, die für ihre Entstehung verantwortlich sind, auch skaleninvariant (Turcotte, 1990). Können zylindrische Gesteinskörper nach ihrem Bruchversagen im triaxialen Kompressionsversuch als Modell für das Gebirge mit seinen Trennflächen betrachtet werden? Mit dieser Frage soll in der vorliegenden Arbeit die Zufälligkeit der Randbedingungen im Detail hergeleitet werden und experimentell nachgewiesen werden, welche Faktoren eine besondere Rolle bei der Strukturänderung von Gesteinen spielen.

Die Beurteilung des Gesteinverhaltens erfolgt herkömmlicherweise durch die Ermittlung geomechanischer Parameter (z.B. Reibungskoeffizient, Kohäsion, einaxiale Druckfestigkeit, Verformungsmodul, Poissonzahl) und bestimmt so die Wahrscheinlichkeit, dass ein Rissvorgang entsteht und sich ausbreitet (Josh et al. 2012). Die Beziehung zwischen der Raumlage der Trennflächen und dem Spannungsfeld wird für Gesteine und Böden nach dem Mohr-Coulomb Bruchkriterium ermittelt. Alle relevanten Parameter werden aus sogenannten „repräsentativen Proben“ evaluiert und innerhalb der Kontinuumsmechanik betrachtet. Diese befasst sich mit der Deformation bzw. Bewegung kontinuierlicher Körper und ist als stetige, eindeutige Zuordnung der Körperteile auch unter einer neuen Konfiguration zu verstehen (Greve, 2003). Der kontinuierliche Körper bzw. das Kontinuum wird anschließend als eine zusammenhängende, kompakte aber unendliche Menge von Elementen „x“ in einem abstrakten Raum beschrieben und aufgrund des Mangels an Informationen über die Vielfalt der Geomaterie und deren Diskontinuitäten, hat sich die Kontinuumsmechanik etabliert (Wittke, 2004). Heute besteht eine gewisse Sicherheit in der geotechnischen Fraktion, das mechanische Verhalten eines Gesteines anhand traditioneller Betrachtung zu bewerten. Der Nachteil bei dieser Betrachtung besteht aber in der weitergehenden Vereinfachung der Komplexität der Geomaterie. Die Anwendung eines homogenen Modells erfordert die Schätzung eines sogenannten „repräsentativen Elementarvolumens“, in dem die Gesteinsmasse als statistisch homogen im Sinne einer Erhöhung ihres Volumens angesehen werden kann, die die mittleren Spannungen und Verschiebungen bei der Beschreibung der Gesteinsmasse als Kontinuum nicht

verändert (Wittke, 2004). Allerdings zeigen zweidimensionale Ebenen in den meisten geologischen Prozessen Flächenänderungen auf und auch Veränderungen in der dritten Dimension, die eine Nicht-Ebenen-Dehnung implizieren, welche wiederum eine Volumenänderung oder Dilatanz bedeuten kann (Ramsay & Huber, 1983). Unter Dilatanz versteht man hier eine Zunahme der volumetrischen Dehnung, im Vergleich zu dem, was zu erwarten wäre, wenn das Gestein linear elastisch wäre (Scholz, 1967). Gußmann (2018) exemplifiziert den Einfluss dilatanten Verhaltens anhand der finiten Elementmodellierung eines Erdwiderstandes. Seine Berechnungen des Erdwiderstandsfaktors mit und ohne Dilatanz unterscheiden sich um ca. 4. Interessant ist allerdings, dass die Ursache für die unterschiedlichen Ergebnisse in der Kinematik liegt: Durch die Dilatanz bewegt sich das Element nach oben und ohne Dilatanz nach unten. Interpretiert wird es so, dass sich durch die Annahme der Dilatanz der Reibungswinkel mobilisiert und somit das Richtungsvorzeichen von Scherstrukturen beeinflusst wird. Alle Strukturänderungen sind mit einer Volumenzunahme, also Dilatanz, verbunden, die auf ein Aufgleiten entlang der Rauheit der Rissoberfläche zurückzuführen ist (Pimentel, 2017).

Aufgrund des Auftretens von Klüften und Störungen in verschiedenen Maßstäben ist die Verformbarkeit von Gesteinsmassen im Allgemeinen anisotrop und ihre Eigenschaften sind nicht mit denen eines intakten Gesteins vergleichbar (Wittke, 2014). Hier stellt sich die Frage, wie eine intakte Gesteinsprobe definiert wird. Ab welcher Größe darf man über ein "Diskontinuum" reden und wie klein muss eine Probe sein, um sie als isotropen Körper bezeichnen zu können? Die Abhängigkeit der physikalischen und mechanischen Eigenschaften eines Gebirges wird auch als Maßstabseffekt bezeichnet (Pimentel, 2017). Aufgrund der Komplexität des Gebirges gilt im Allgemeinen: Je kleiner eine Probe ist, desto höher wird ihre Festigkeit sein. In dieser Dissertation wurde ein Maßstabseffekt an der Dichte von Buntsandsteinproben beobachtet (3. Publikation). Zum großen Teil wurden Sandsteinproben mit einem Volumen von ca. 540 cm<sup>3</sup> im Labor untersucht. Schon in diesem Maßstab hat sich eine beachtliche Variabilität der physikalischen und mechanischen Eigenschaften des Sandsteines gezeigt. Da es sich bei Gestein um ein polykristallines Aggregat aus einer oder mehreren Kristallphasen handelt, von denen viele in ihren physikalischen Eigenschaften anisotrop sind, sind die Spannungen im Gestein im Kornbereich heterogen. Deshalb existieren Unregelmäßigkeiten im Spannungsfeld, wodurch Mikrorisse nukleieren und propagieren (Anders et al. 2014). Bei der Verformung von Gestein unter Druck kommt es zur Entstehung kleinräumiger Risse, auch Mikrorisse genannt. Jedes Mikrorissereignis strahlt elastische Energie in analoger Weise zu Erdbeben ab (Scholz, 1967). Mikrorisse können physikalische

Eigenschaften wie Festigkeit, elastische Wellengeschwindigkeiten und Permeabilität beeinflussen. In Sedimentbecken liefern sie einen guten Beweis für die Prozesse der Verdichtung, Verfestigung und die Muster der Flüssigkeitsströmung (Anders et al. 2014). Sie liefern ausschließlich Informationen über das Wachstum und die Entwicklung von Scherzonen, die Entwicklung regionaler Stressfelder und den Erdbebenzyklus (Scholz, 1967).

Die Entwicklung experimentell induzierter Mikrofrakturen wurde zunächst dort gezeigt, wo Dilatanz (bzw. Volumenänderung) im triaxialen Druckversuch beobachtet wurde (Anders et al., 2014 apud Brace et al., 1966). Dilatanz ist der Ausdruck unelastischer Ausdehnung, der normal zur maximalen Spannungsrichtung orientiert ist, die durch das Wachstum und die Öffnung von Mikrorissen erzeugt wurde (Anders et al., 2014). Daher ist es notwendig, in einer modernen Betrachtung der Felsmechanik Aspekte der Volumenänderung der Geomaterie darzustellen. In diesem Sinne bemühen sich Forscher, Labor- und Simulationsergebnisse zu korrelieren. Bertrand et al. (2017) hat dafür sowohl Dilatanz in Form von Dilatanzwinkel als auch variierende elastische Parameter des Opalinuston angenommen, um die rechnerische Modellierung der elastischen und plastischen Zonen eines Tunnels den Ergebnissen von triaxialen Kompressionsversuchen anzupassen. Dabei konnte der Einfluss der Porendruckänderung nicht berücksichtigt werden – vermutlich aufgrund der Vielfalt der mechanischen Antwort eines hoch anisotropen Gesteins wie dem Opalinuston. Kluge et al. (2017) nutzte für die Berechnung der Durchlässigkeit von Klüften Korrekturfaktoren für die Breite der Kluft, die Oberflächenrauheit und die Scherverschiebungen entlang der Frakturen. In dieser Arbeit wurde die Volumenänderung anhand von negativen (Kontraktanz) und positiven (Dilatanz) relativen Änderungen bewertet. Dabei spielen die Porenkonnektivität, die Anisotropie und der effektive Druck eine bedeutende Rolle bei der Ab- oder Zunahme von Volumen unter triaxialen Spannungsbedingungen.

Um den Einfluss der Probenheterogenität zu minimieren, werden üblicherweise alle Testproben aus dem gleichen Gesteinsblock entnommen, wie bei Gehne & Beson (2017). In dieser Dissertation wurden mehrere Gesteinsblöcke untersucht und je nach Fragestellung wurden die Proben zu ihrem entsprechenden Block zugeordnet oder gemeinsam betrachtet. Ziel der durchgeführten experimentellen Untersuchungen war es, die Komplexität der zufälligen Strukturänderung echter diskontinuierlicher Geometrien zu analysieren, sowie die Verformungsneigung von Frakturen und ihre Durchlässigkeit bei variierenden Spannungsänderungen erkennen zu können.

Um die Strukturänderung eines Gesteins zu erklären, wird hier die bestehende Wechselwirkung zwischen Lithologie, Spannungsbedingungen und Anisotropie dargestellt. Im

Fokus dessen stehen der Einfluss struktureller Anisotropie, die Porenraumverteilung und deren Beschaffenheit. Wie Hobbs (1993) formulierte, ist zu erwarten, dass die Gesteine, denen wir bei technischen Untersuchungen begegnen auf eine oder mehrere verschiedene Arten verformt wurden, wodurch eine Vielzahl von verschiedenen Diskontinuitäten entsteht. Weiterhin hält Hobbs (1993) es für sinnvoll, zwei Arten von Strukturen in Felsmassen zu unterscheiden, die als durchdringende und nicht durchdringende Strukturen bezeichnet werden. Eine bestimmte Struktur gilt als durchdringend, wenn diese Struktur immer wieder wiederholt wird, mit weitgehend gleichen Abständen und Orientierungsmustern, wie die Lagerung von Sedimentgesteinen. Andererseits ist die Struktur nicht durchdringend, wenn sie in unterschiedlichen Abständen, Verteilungen und Orientierungen auftritt, wie z.B. bei Frakturen (diese Definition ist skalenabhängig). In dieser Dissertation wurde sowohl der Einfluss der Schichtungsanisotropie als durchdringende Struktur betrachtet, als auch die Entwicklung der relativen Permeabilität anhand unterschiedlicher Bruchsysteme analysiert. Die Anisotropie spielt eine wichtige Rolle bei der Entstehung von Bruchsystemen als solche, besonders bei schlecht (oder wenig) durchlässigen Sandsteinen wie dem Rotliegend.

In einer ähnlichen Fragestellung untersuchte Hecht et al. (2005) den Zusammenhang zwischen Struktur, mineralogischer Zusammensetzung und physikalischen Eigenschaften von Sedimentgesteinen aus der Karbon-Perm Zeit. Dabei wurden Parameter wie die Korngröße, Korngrößenverteilung, Zementierungsgrad, die Art von Zement und die Mikrorisse betrachtet. Gesteinseigenschaften wie Dichte und Porosität sind von der strukturellen Ordnung stärker abhängig, während die Festigkeitseigenschaften (einaxiale Druck- und Zugfestigkeit) zusätzlich von der Zusammensetzung des Gesteins abhängen. Die Ultraschallwellengeschwindigkeit reagiert sowohl auf strukturelle als auch auf kompositionelle Merkmale. Das geomechanische Verhalten ist kein unabhängiger Parameter, sondern eine variable Funktion von Struktur- oder Zusammensetzungsmerkmalen, die für Korrelationszwecke spezifiziert werden muss.

Ein wichtiger Faktor in der Untersuchung der Strukturänderung von Gesteinen ist die Anwesenheit von Fluiden in den Porenräumen des Gesteines. Porenfluide tragen einen Teil des Umgebungsdruckes und wirken diesem Druck gleichmäßig aus dem Porenraum entgegen. Dieser sogenannte Porendruck sorgt für eine „Abschwächung“ der Struktur des Gesteins und sogar für die Reaktivierung von Trennflächen. Wie beschrieben bei Wu et al. (2017), verschlechtert der Porendruck das Reibungsverhalten der Gesteinsprobe während der Rissausbreitung und fördert eine noch zufälligeren Ausbreitung in den späteren Phasen der Dilatanz. Jaegger & Cook (1979) erwähnen zwei Verbindungen der Gesteinsmechanik bei



denen Reibungseffekte von Bedeutung sind. Erstens, im sehr kleinen Maßstab, zwischen den Oberflächen von Griffith-Rissen. Zweitens, im großen Maßstab, zwischen den Oberflächen von Klüften oder Störungen. Diese Aussage, zusammen mit der oben zitierten Beobachtung von Gußman (2018), bedeuten indirekt, dass die Beziehung zwischen Dilatanz und Reibung durch den Porendruck stark beeinflusst wird. Obwohl ein volumetrisches Verhalten sich nicht anhand der Elastizitätstheorie erklären lässt, sind Reibungs- und Dilatanzwinkel spannungs- und materialabhängig, und werden besonders von der Porenzahl beeinflusst (Kolymbas & Herle, 2017). Mit Beispielen für assoziierte und nicht-assoziierte Fließregeln erklären Kolymbas & Herle (2017), dass für Sande ein höherer Reibungswinkel als Dilatanzwinkel gilt, und dass sich bei Tonen beide Winkel annähern dürften. Daraus folgt, dass ein Sandstein eine niedrigere Volumenänderung zeigt als ein Tonstein – ein volumentreues Verhalten ist für die Geomaterie jedenfalls ausgeschlossen. Das volumetrische Verhalten von harten Sandsteinen wird in dieser Arbeit nicht als einzelner, absoluter Beitrag aus Dilatanzwinkeln evaluiert, sondern durch die Änderung zweier Volumina. Die relative Volumenänderung der Probe wird entgegen der relativen Volumenänderung des Porendruckmediums aufgetragen. Ob eine Dilatanz (Auflockerung) oder eine Kontraktanz (Verdichtung) stattfindet, hängt von Sandsteintyp, effektivem Druck und Anisotropie ab.

Unter lithostatischen Spannungsbedingungen sind Volumen-, Porositäts- und Permeabilitätsänderung eng verknüpfte Prozesse. Wenn Spannungsänderungen das Volumen des Korngerüsts ändern, muss in wassergesättigten Gesteinsproben Porenwasser ab- oder zuströmen (von Soos & Engel, 2017). Porosität und Permeabilität neigen dazu, sich bei zunehmendem Manteldruck zu mindern – im Grunde wird das Gestein einer monotonen Verdichtung unterzogen (Iglauer et al. 2014; David et al. 2001). Nach Gehne & Benson (2017) wird die Permeabilität in den Gesteinen der oberen Kruste in erster Linie durch die damit verbundene Porosität, die Form und Ausrichtung von Mikrorissen, der bevorzugten Ausrichtung von Schrägschichtung und sedimentären Merkmalen wie Teilschichten gesteuert. Die Änderungen der Porosität infolge von Verformung werden durch Veränderungen der Korngröße, der Korngrößenverteilung und durch die Ausbreitung von Mikrostrukturen gesteuert, die die Porenkonnektivität verändern (Farrel et al., 2014). Dies führt zu einer signifikanten Permeabilitätsanisotropie. Weniger gut untersucht sind jedoch die Auswirkungen von Zeit und Wiederbelastung auf die Entwicklung der Permeabilität, die hinsichtlich der Fluidmigration immer wichtiger wird. In diesem Sinne berichteten Gehne & Benson (2017) über die Auswirkungen von Spannungshistorie und Anisotropie auf die Durchlässigkeit in einem gut zementierten, anisotropen Sandstein. Bei jedem Druckzyklus treten unwiderrufliche



und kumulative Veränderungen der Permeabilität, Porosität und Ultraschallgeschwindigkeit auf. Die experimentellen Ergebnisse dieser Dissertation hinsichtlich der Durchlässigkeitsänderung weisen eine ähnliche Feststellung auf: Nach der Wiederholung mehrerer Durchlässigkeitsversuche unter lithostatischen Bedingungen ist die Permeabilität der Proben gesunken. Dabei haben sich Porosität, Ultraschallgeschwindigkeit und Druckfestigkeit erhöht, Merkmale, die auf eine plastische Strukturänderung der Proben hinweisen (1. Publikation). Formänderungen können auf elastischem, plastischem oder rheologischem Weg stattfinden. Eine reversible, bzw. nicht dauerhafte Verformung wird als elastische Verformung bezeichnet. Unter plastischer Verformung versteht man die Fähigkeit eines Materials, sich unter einer Krafteinwirkung irreversibel zu verformen (Means, 1979). In dieser Arbeit konnte eine elastische Verformung experimentell nicht ermittelt werden.

Trennflächen beeinflussen die Qualität jedes Reservoirs, sei es durch Erhöhung der Speicherkapazität und des Fließverhaltens, der Entwicklung einer anisotropen Permeabilität, oder durch die Wirkung als undurchlässige Barriere (Watkins et al. 2018). Bei geringer primärer Porosität, wie z.B. in schlechten durchlässigen Sandsteinreservoirs, können Trennflächen entscheidend für das Fließverhalten der Fluide sein. Jeannin et al. (2018) untersuchte die relative Gasdurchlässigkeit von dichten und herkömmlichen Sandsteinen und stellte fest, dass die Durchlässigkeit dichter Sandsteine viel empfindlicher gegenüber Einschlüssen ist, als bei herkömmlichen Sandsteinen. Das zugrundeliegende Phänomen ist im mikroskopischen Maßstab das Auftreten eines Verschlusses der Verbindung durch Belastung in eng-porigen Sandsteinen, das neue Fließwege definiert. Umgekehrt zeigt sich, dass die relative Permeabilität bei konventionellen Sandsteinen nicht sehr empfindlich auf die Belastung reagiert, unter der Annahme, dass die Belastung nur die Porenradien verändert, ohne die Anbindung des Porennetzes zu verändern.

In dieser Dissertation haben die untersuchten Sandsteine zwar unterschiedliche Empfindlichkeiten gegenüber den Spannungsbedingungen gezeigt, sind aber vom Porendruck und von der effektiven Porosität abhängig. Ein beachtlicher Unterschied im Fließverhalten ergab sich erst nach Erreichen der maximalen Scherspannung, als Antwort auf eine ausgeprägte Beschädigung des Sandsteingefüges. Die Permeabilität eines Gesteins wird durch die Anwesenheit von Scherstrukturen nicht unbedingt erhöht, wie es von mehreren Forschern ebenfalls beobachtet wurde. Uehara & Takahashi (2013) untersuchten das mechanische Verhalten von Sedimentgesteinen anhand von mechanischen und micro-tomographischen Laborexperimenten. Im Fall von Tonsteinen hängt das Bruchkriterium fast ausschließlich von der maximalen Tiefe des Reservoirs ab. Wenn eine Störung in ähnlicher Tiefe während des

Hebungsprozesses bei Faltung und Verschiebung entsteht, wird diese Störung kompakt und die Durchlässigkeit ist im Vergleich zum Wirtsgestein nicht hoch. Wenn eine Störung unter weniger Beanspruchung entsteht, also flacher, kann die Permeabilität der Störungszone höher sein als das Wirtsgestein und es kann sich tatsächlich ein effektiver Fließweg bilden. Über die Permeabilitätsänderung in Kristallingesteinen berichtet Péres-Flores et al. (2017) anhand von intakten und verformten Proben aus dem vulkanischen Grundgebirge der südlichen Anden. In allen untersuchten Gesteinen wird sowohl die Permeabilität als auch deren Schwingungsverhalten durch die Erhöhung des effektiven Druckes verringert. Allerdings wird die Permeabilität, je nach Lithologie, durch Rissbildung bis zu 7-fach erhöht. Durch den ausgebildeten Fließweg kann die Permeabilität auch bei hohem Umlagerungsdruck unverändert bleiben. Fossen et al. (2011) wertete die Porositätsänderung durch Bildanalyse von Dünnschliffen aus, die aus der Scherzone der Kaibab (Grand Canyon) und deren Nebengesteinen hergestellt wurden. Alle Arten von Verformungsbändern in diesem Bereich verfügen über einen negativen Einfluss auf die Porosität und Permeabilität, und zwar ungefähr 4-fache im Vergleich zum unmittelbar umgebenden Wirtsgestein. Diese Unterschiede in der Porositätsreduktion spiegeln Variationen in der Intensität der mechanischen Beschädigung und Auflockerung innerhalb der Bänder wider.

Bei den Triaxialversuchen dieser Arbeit wird der Porendruck entweder durch Wassersättigung oder durch flüssiges CO<sub>2</sub> erzeugt. Um eine stationäre Strömung zu erzeugen, sind alle Proben im gesättigten Zustand zu belasten. Um den Einfluss der Porendruckänderung im Reservoir darzustellen, sind mehrere Poren- und Manteldruckstufen vorgesehen. Untersucht wurden zwei harte Sandsteine: Die Trendelburger Schichten, ein quarz-zementgebundener subarkoser Buntsandstein der Solling-Folge (Trias) und der Rotliegend Sandstein, ein karbonat- und quarz-zementgebundener Sandstein des Perms, deutlich weniger porös und weniger durchlässig als der Buntsandstein. Kreiszyindrische Prüfkörper (70 x 140 mm) mit planparallelen Endflächen und glatter Mantelfläche wurden aus verschiedenen Gesteinsblöcken des Rotliegend und des Buntsandsteins hergestellt, anhand dieser konnten die physikalischen Gesteinsparameter und die makroskopische Beschreibung des Sandsteines bestimmt werden. Gesteinsparameter wie effektive Porosität, Gesamtporosität, Korndichte, Trockendichte und Ultraschallgeschwindigkeit wurden für jede Sandsteinprobe vor jeder mechanischen Untersuchung bestimmt. Zur Charakterisierung des mechanischen Verhaltens wurden einaxiale Druck- und Zugfestigkeitsversuche durchgeführt, allerdings kommt der größte Teil der Ergebnisse aus triaxialen Kompressionsversuchen. Um Druckfestigkeit, Permeabilität und Volumenänderung von anisotropen Sandsteinen bestmöglich darzustellen, wurden drei

Varianten von weggesteuerten Druckversuchen durchgeführt. Mit der Auswertung wurden zwei spröde Bruchsysteme erkannt, die sich nicht nur anhand der Form, sondern auch anhand der mechanischen Eigenschaften unterscheiden. Deshalb wird angenommen, dass (1) ein einfacher Riss oder (2) ein Strukturmuster aus mehreren konjugierten Scherbändern jeweils unterschiedliche Entstehungsprozesse erfordert (Abb.01).



Abb. 1. Beispiele für unterschiedlich entwickelte Rissbildungen anhand von senkrecht zur Schichtung gebohrten Prüfkörpern aus dem Rotliegend (70 mm x 140 mm). Von links nach rechts: Verkeilte, isolierte und konjugierte Scherfläche.

David et al (2001) untersuchte ebenfalls die Strukturänderung von Sandsteinen mittels Triaxialkompressionsversuchen, allerdings mit extremen effektiven Manteldruckwerten: 5 und 165 MPa. Beide Proben zeigten zu Beginn des Versuches eine relativ lineare elastische Phase der Verformung, gefolgt von einer unelastischen Phase mit nach unten gerichteter Krümmung in den Spannungs-Dehnungs-Diagrammen. Die Probe bei 165 MPa wurde auf bis zu 20 % axiale Dehnung belastet und nach dem Entladen des Experiments konnte man keine Scherstruktur in der Probe erkennen. Umgekehrt zeigte die bei niedrigem effektiven Manteldruck (5 MPa) getestete Probe einen signifikanten Spannungsabfall nach Erreichen der maximalen Scherspannung: Ein solches Verhalten ist mit Bildung einer Scherstruktur verbunden, die die Probe vollständig durchquert. Im ersten Fall werden Reibungsprozesse

durch Scherspannung verursacht, wobei die Porosität und die Permeabilität bis zum Versuchsende abnehmen, weil die Porenstruktur durch Bildung von Abrieb verändert wird. Beim zweiten Fall wird eher die Dilatanz gefördert, bei der die Porosität rasant nach dem Spannungsabfall steigt. In einer ähnlichen Untersuchung fragten sich Ord und Hobbs (2010), „warum [sich] Bruchmuster [bilden], die letztendlich zum Wachstum von gut definierten Trennflächensystemen führen“. Daraus folgt die Vorstellung, dass die Strukturänderung von Trennflächen durch Konkurrenz zwischen Schäden (durch verschiedene Mechanismen) und Diffusion der Dichte dieser Schäden im Laufe der Verformung entsteht. Zur Entstehung von Trennflächen untersuchte Menéndez et al. (1995) den Einfluss von hydrostatischen und triaxialen Spannungsfeldern. Anisotrope Spannungsfelder besitzen eine höhere Verdichtungskapazität als hydrostatische Spannungsverhältnisse und fördern eine anisotrope Entstehung von Mikrorissen. Geologische Prozesse können gleichzeitig unterschiedliche Störungsstrukturen erzeugen, die allerdings miteinander verkoppelt sind und sich gegenseitig beeinflussen.

In dieser Dissertation werden sowohl zufällige naturbedingte Einflussfaktoren (z.B. Porenraumverteilung, Kluftscharen, Schichtung) als auch plangesteuerte Größen (z.B. effektiver Druck, Verformungsrate) betrachtet, die im Labor geregelt werden. Trotz der Zufälligkeit der naturbedingten Randbedingungen ergeben sich Verhaltensmuster, bei denen sich gewisse Parameter korrelieren lassen - z.B. die Abhängigkeit der Volumenänderung zum Porendruck und zur Gesteinsstruktur, der Einfluss lithologischer Eigenschaften bei zunehmendem effektivem Druck und die Wechselwirkung zwischen Durchlässigkeit, Spannungsverlauf und Strukturänderung. Diese Verhaltensmuster sind in den nachfolgenden Publikationen im Einzelnen erläutert.

An zweiter Stelle werden diese Ergebnisse auf gesellschaftliche Rahmenbedingung angewendet. Inwieweit spielen Trennflächen bzw. tektonische Störungen eine Rolle unter wirtschaftlich anwendungsbezogenen geologischen Aspekten? Können die bereits vorhandenen Diskontinuitäten in unterirdischen Reservoirs zielgerichtet genutzt werden, oder kommt es womöglich zu einer ungünstigen Reaktivierung bzw. sogar zur Erzeugung neuer Diskontinuitäten? Gesteine mit ausgeprägt sprödem Verhalten sind für die Erzeugung und Ausbreitung von hydraulischen Klüften nötig (Josh et al. 2012), wobei ihre Brüche und deren Gestalt einen wichtigen Einfluss auf die mechanischen und die Fluidtransport-Eigenschaften von Gesteinen ausüben (Healy et al. 2017). Ein weiteres Beispiel ist die im Rahmen der Gas- und Wassergewinnung statistische Quantifizierung und qualitative Beschreibung von Strukturmustern aus Aufschlüssen und Bohrkernen, wo sie zur Ursachenermittlung von

Anomalien eingesetzt wurde (Li et al. 2018). Die Injektion großer Mengen Kohlendioxid in tiefliegenden geologischen Formationen sorgt für spontane Druckänderungen und hat dadurch ein beachtliches Potenzial, Erdbeben auszulösen (Verdon & Stork, 2016). Andere Energieanwendungen wie Geothermie, saisonale Erdgasspeicherung und unterirdische Energiespeicherung implizieren eine Einspeisung bzw. Extraktion, die Veränderungen im effektiven Spannungsfeld bewirkt und (Mikro-) Seismizität hervorruft (Vilarrasa et al. 2018). In allen diesen Fällen ist die Auswertung von Strukturmustern eine wesentliche Vorstufe, um die physikalischen Grundprinzipien ihrer Entstehung nachvollziehen zu können (Healy et al. 2017). Dies dient sowohl der Abschätzung der Festigkeit als auch der Verformbarkeit und ermöglicht somit die Standsicherheitsberechnung eines typischen Gebirges mit Trennflächen.

Zur Darstellung eines anwendungsbezogenen Aspekts der geomechanischen Untersuchung wird hier der Einfluss einer langfristigen Einwirkung von CO<sub>2</sub> auf die physikalischen Eigenschaften des ausgewählten Buntsandsteines untersucht, wobei die Vielfalt der Meßergebnisse die lithologische Variabilität und die Struktur des Gesteins widerspiegelt. In diesem Kontext können die hier präsentierten Ergebnisse als ein Beitrag zur Abhängigkeit zwischen mechanischem Verhalten und Porendruckänderung betrachtet werden.

Die wissenschaftlichen Beiträge dieser Arbeit zeigen Einzelheiten in der Fragestellung, Methodik und Versuchsdurchführung. Wie Jaeger & Cook (1979) bereits erwähnten, kann jede Gesteinsart ein breites Spektrum an mechanischen Eigenschaften aufweisen, so dass eine geologische Beschreibung alleine keine zufriedenstellenden Informationen über diese Eigenschaften liefert. Daher wird in dieser Dissertation keine Vorhersage über das mechanische Verhalten von anisotropen Sandsteinen abgeleitet, sondern es werden vielmehr die Einflussfaktoren für die Verhaltenstendenzen der „chaotischen Ergebnisse“ erklärt und mit der Entstehung unterschiedlicher Strukturen korreliert. Nach der Betrachtung einzelner Publikationen werden deren Verknüpfungspunkte in einer kurzen Schlussfolgerung dargestellt - dies verdeutlicht erneut den Zusammenhang zwischen Lithologie, Spannungsbedingung und Anisotropie.



## 2. Fachstudien

Diese kumulative Dissertation besteht aus drei Publikationen. In der ersten Arbeit wird die Wechselwirkung zwischen physikalischen Eigenschaften und der mechanischen Antwort am Beispiel von zwei Sandsteinen dargestellt. Der Sandstein aus dem Rotliegend und die Trendelburger Schichten aus dem Buntsandstein sind kompakte, überwiegend silikatisch gebundene Sandsteine, die eine ähnliche und allgemeine Tendenz zeigen: Sprödigkeit und Festigkeit erhöhen sich bei zunehmenden effektiven Druck. Allerdings weisen beide Gesteine ein umgekehrtes anisotropes Verhalten auf, sowie unterschiedliche Reaktionen auf den Einfluss des Porendruckes. Für diese Arbeit wurden die Ergebnisse hinsichtlich der Volumenänderung, Permeabilität und Bruchfigur berücksichtigt. Diese Arbeit wurde bei der 2. Young Researchers in Structural Geology (YORSGET 2018, in Montgenèvre) vorgestellt und ist als Publikation unter dem folgenden Link zu finden:

<https://www.sciencedirect.com/science/article/abs/pii/S0920410518310751>



# Anisotropy of volume change and permeability evolution of hard sandstones under triaxial stress conditions

Flora Feitosa Menezes

Engineering Geology, Martin-Luther-University Halle Wittenberg, Germany

## ARTICLE INFO

### Keywords:

Triaxial testing  
Volume change  
Fracture pattern  
Permeability  
Bunter Sandstone  
Rotliegend

## ABSTRACT

Volumetric strain and permeability are strictly interconnected properties and important controlling parameters for deformation patterns in rock masses. Under reservoir conditions, stresses may be highly inhomogeneous and anisotropic, leading to porosity changes and consequently affecting fluid flow. Therefore, it turns out to be a challenging issue in rock mechanics to evaluate volume change based on traditional soil mechanics background, originally intended for soft materials under low and mostly isotropic pressures. In this respect, triaxial compression tests were carried out to describe the interplay between physical properties, volume change and permeability of two hard sandstones by quantifying porefluid volume change with fully water saturated rock specimens (14 cm length and 7 cm radius). The investigated sedimentary rocks are (1) the greyish Trendelburg beds, a silica cemented subarkose Bunter Sandstone of Triassic age (porosity of ca. 12%), and (2) the red-brownish Rotliegend Sandstone (Bebertal), a carbonate and silica cemented sandstone of Permian age, clearly less porous (ca. 6% of effective porosity) and less permeable ( $3.5 \times 10^{-10}$  m/s) than the Bunter Sandstone. Both materials present a pronounced brittle behaviour influenced by coring direction: permeability, volumetric strain and fracture pattern are direction-dependent. Effective porosity and pore pressure level affect the fracturing development, which therefore influences the permeability after stress fall. For the Bunter Sandstone, increasing porefluid pressure leads to an earlier microcracking stage, which shortens the forerun of compaction and induces a more pronounced dilatant behaviour with decreased compressive strength. For the Rotliegend, the increase of pore fluid pressure enhances compaction. Altogether, this examination is valuable to understand the combined effects of pore pressure change and pore space quality on the mechanical behaviour of rock masses.

## 1. Introduction

Volume change and permeability are strictly interconnected properties. As exemplified by Ord (1990), dilatancy or an increase in volume represents porosity increase, and therefore enhances the possibility of a fluid flow if permeability increases with porosity. This interplay can also be conceptually summarized as dilatancy-induced permeability (Alkan, 2009). Understanding the interaction between volume change and permeability in rock masses has turned into a widely used tool for geological engineering purposes: to ensure the stability of underground structures, to assess risks from geological carbon storage or from the exploration of natural resources, as well as to predict rock bursts and seismicity (Tan et al., 1989; Alkan, 2009; Alejano et al., 2017). Many studies have focused on the interaction between deformation and fluid flow, either in an experimental approach or through numerical modelling (David et al., 2001; Sheldon et al., 2006; Zhao and Cai, 2010; Farrel et al., 2014). In this study, the interaction among physical properties, pore pressure and bedding anisotropy are evaluated to

describe the interplay between the evolution of permeability and volume change.

Primarily, volume change (or volumetric strain) of a rock undergoing compression is a continuous process with successive stages of deformation, which are grouped into domains of either volume decrease (compaction) or volume increase (dilatancy). In conclusion, the process of volume change begins with fissure closing and elastic compression, followed by pore structure collapse and increasing the microcrack density up to the yield strength (Cook, 1965; Goodman, 1989). The turnover point between the stages of compaction and dilatancy is commonly denominated as dilatancy boundary. The dilatancy boundary of a rock is dependent on its mechanical and hydraulic properties, which can be changed due to a disturbance of the original stress distribution, e.g. excavations of the underground repositories and caverns for disposing waste or storing gas (Alkan, 2009). Considering these geological settings, temperature and time are also important factors in the development of dilatancy. Dilatancy tends to increase with temperature, as the increase of vapor and gas pressure increases

E-mail addresses: [floramenezes@gmx.de](mailto:floramenezes@gmx.de), [flora.menezes@student.uni-halle.de](mailto:flora.menezes@student.uni-halle.de).

<https://doi.org/10.1016/j.petrol.2018.11.079>

Received 5 September 2018; Received in revised form 5 November 2018; Accepted 28 November 2018

Available online 29 November 2018

0920-4105/© 2018 Elsevier B.V. All rights reserved.

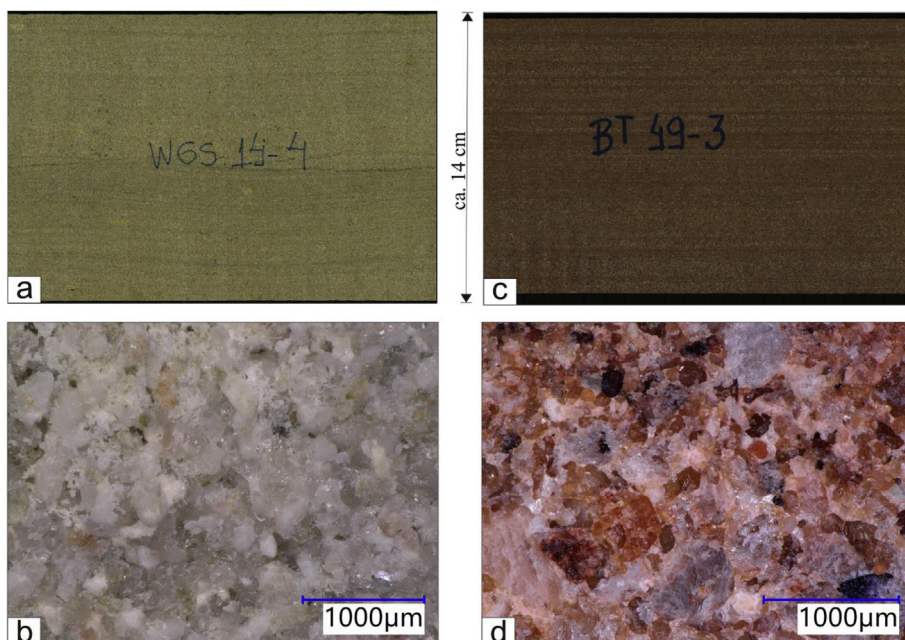


Fig. 1. Pictures in different scales for the Trendelburg beds (WG 14–1) and Rotliegend (BT 49–3) sandstones. The lateral surface of cylinder specimens were firstly photographed by using a borehole scanner (a, c) and after under reflected light on a 3D-Digital microscope (b, d).

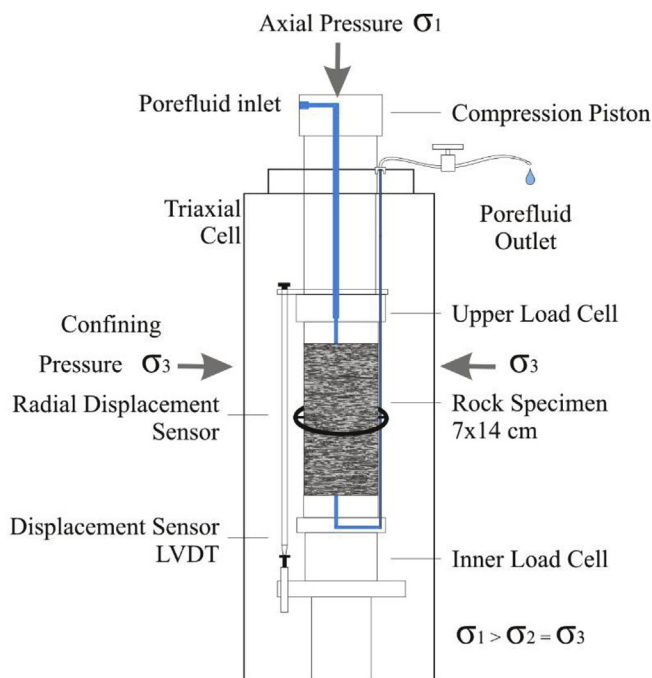
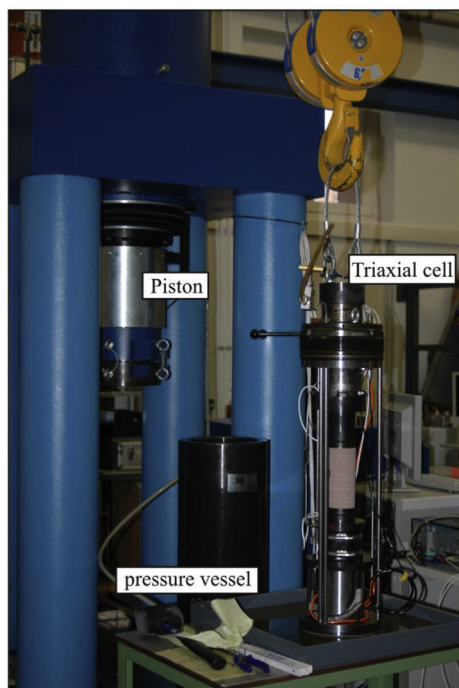


Fig. 2. Triaxial set up consist of servo-controlled testing with 3 independent unit pumps - confining pressure, pore fluid pressure and axial loading. Displacements are measured in axial direction through a LDVT, and in the radial direction with a sensor ring. Changes in water and oil volumes are registered in. This equipment was used to carry out traditional deformation tests (closed system) as well as for flow tests with lithostatic pressure conditions (open system). Rock specimens.

the tensile stresses at the crack tip and favors the crack opening, whereas a time-dependent effect is characterized by an apparent quiescent period of deformation, leading to sudden energy release and stress fall (Tan et al., 1989; Li et al., 2017).

A consequence of this mechanical dilation during fault slip events is the generation of porosity, whose amount and distribution within fault zones is highly variable, depending on factors such as rock type and rheology, stress regime, thermal history, and displacement (Sheldon and Ord, 2005). As permeability linearly increases with crack

volumetric strain (Xu and Yang, 2016), there is a direct association between volume change, porosity and permeability. Some laboratory works have been conducted to estimate the permeability behavior of rocks. Oda et al. (2002) carried out permeability tests with the transient pulse method on damaged granite samples and concluded that rocks under stress can be roughly idealized as isotropic porous media, in spite of the fact that cracks grow preferentially. Mitchell and Faulkner (2008) investigated the permeability evolution of two intact, low porosity crystalline rocks by means of conventional triaxial deformation



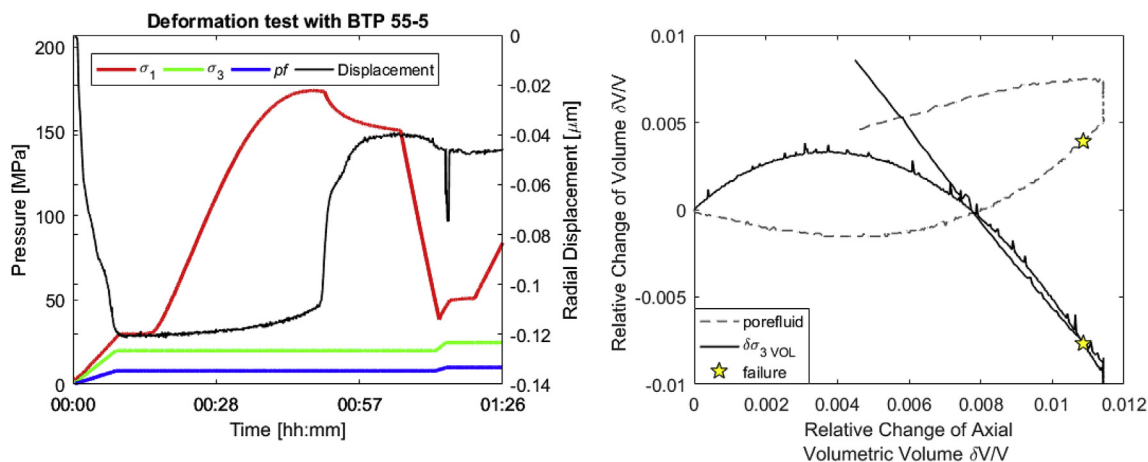


Fig. 3. Pressure and displacement curves of a traditional triaxial compression test carried out with constant confining- and pore pressures (20 MPa and 8 MPa, respectively). On the right side (b), volume change during triaxial loading is represented as relative changes of axial volumetric strain (x axis) and of porefluid volume (y axis). The yellow star signs mechanical failure. (For interpretation of the references to color in this figure legend, the reader is referred to the Web version of this article.)

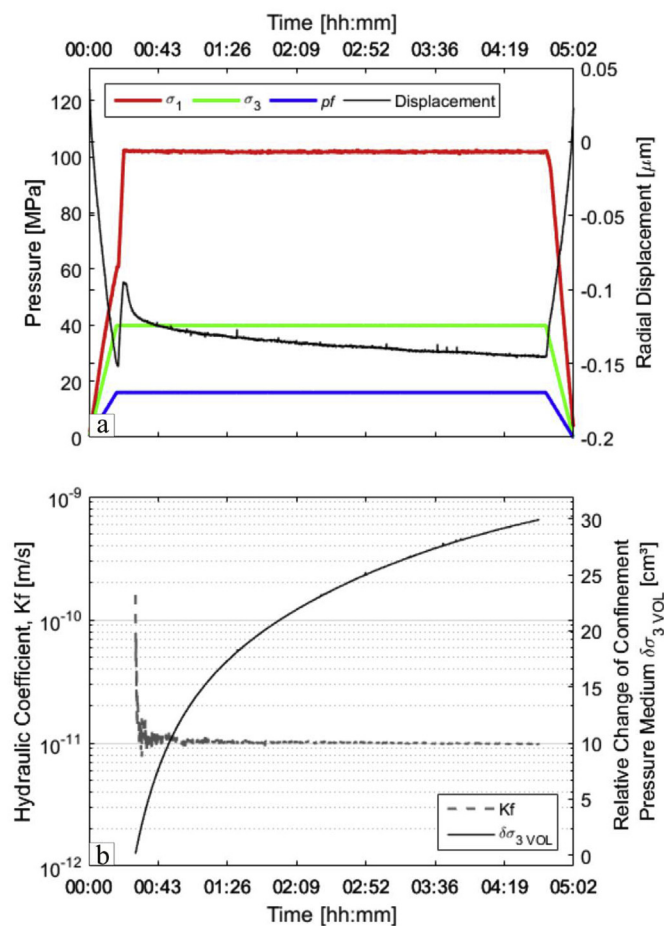


Fig. 4. Alternatives to the traditional triaxial compression test with porefluid flow during loading. In (a), a flow test carried out with constant stress conditions and anisotropic stress field ( $odif = 60$  MPa). The evaluation of this kind of test is presented in (b), by means of volume change of the confinement pressure medium (oil) and hydraulic coefficient (Kf) as a function of time.

experiments, with a continuous monitoring of permeability and pore volume. They stated a positive relationship between permeability and strain, in which permeability increases with differential stress and strain by up to and over 2 orders of magnitude up to stress fall.

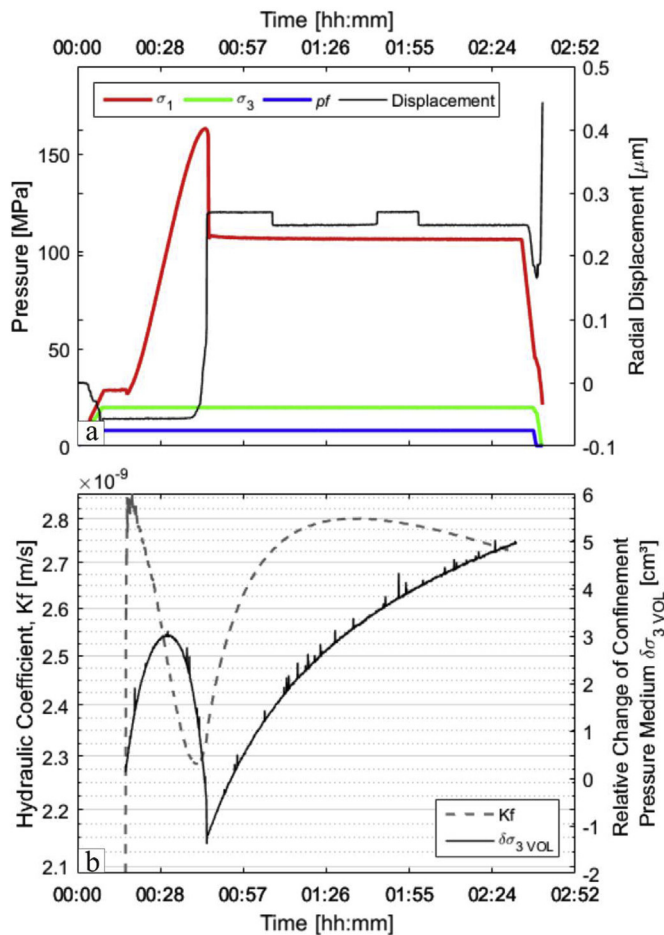


Fig. 5. The third test variant is a deformation-flow-through test with constant pore- and confining pressures (a), but with variable pore- and confining volume (b). Volume change of confinement pressure and porefluid are presented as a function of time (b), where Kf means hydraulic coefficient and  $\Delta\sigma_3$  corresponds to the volume change of the confinement pressure medium.

The interaction between dilatancy and permeability can also be considerably influenced by planar anisotropic rock fabric, e.g. joints, bedding, foliation and cleavage. Naumann et al. (2007) carried out true triaxial compression tests to detect the onset of dilatancy on cubic

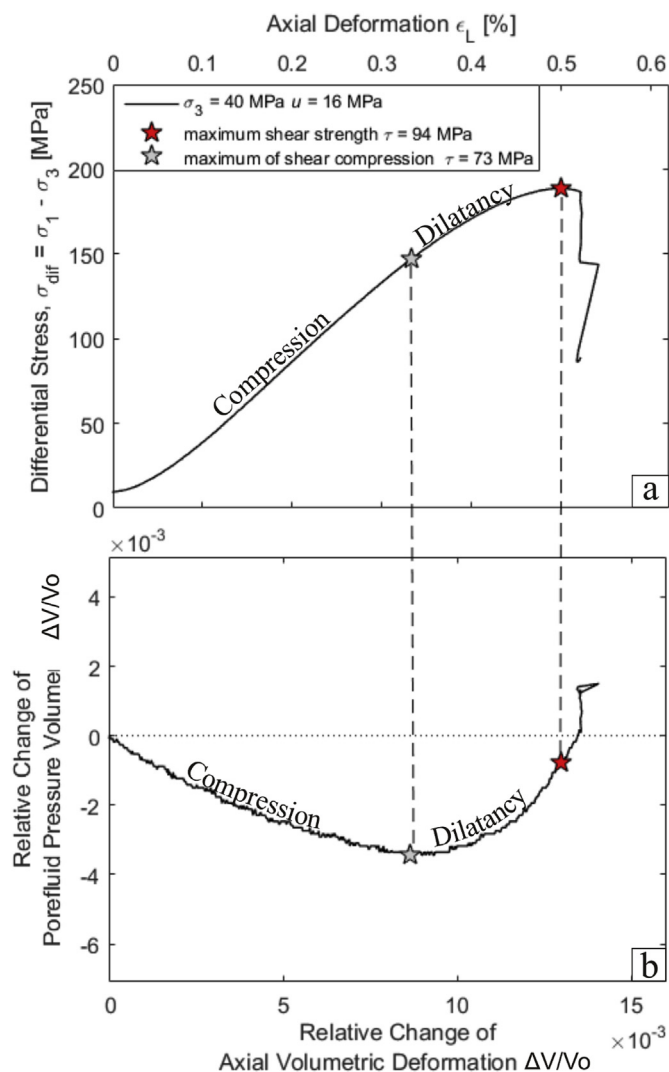


Fig. 6. Stress-strain (a) and volumetric strain (b) curves of a traditional triaxial compression test carried out with a Bunter Sandstone sample by 40 MPa of confining pressure and 16 MPa of pore pressure. The maximum of shear compression (grey star) signs the limit between compression (volume decrease) and dilatancy (volume increase) stages of volume change. The maximum of shear strength corresponds to failure (red star). (For interpretation of the references to color in this figure legend, the reader is referred to the Web version of this article.)

samples of Opalinus Clay with two different bedding orientations. They stated that short term strength and dilatancy are direction dependent. However, the failure strength has a more pronounced anisotropic mechanical answer than the dilatancy behavior. By applying the major stress normal to the bedding planes, the dilatancy boundary moves closer to the failure boundary, therefore shortening the dilatancy phase. Anisotropy in dilatancy can also be parameterized in terms of dilation angle. With this method, Kim et al. (2018) described the dilation behavior of coal for four cleats orientation. They found that coal behaves anisotropic and sensitive to confining stress, where the peak dilation decreases most rapidly at an included angle of 30° between cleat orientation and major stress. For metamorphic rocks, Rawling et al. (2002) determined that both the onset of dilatancy and ultimate strength attain minimum values at intermediate foliation angles.

However, no experimental investigation has considered the relationship between volume change, permeability and fracture pattern with different levels of pore pressure and the influence of bedding angle in sandstones. The volume change of a porous solid material under

compressional stress is related to a progressive development of a permanent, plastic fabric reaction, which is expressed in terms of permeability, evolution and cracking. In the following, by comparing two hard sandstones with slightly different physical properties (Rotliegend and Bunter Sandstone), this study presents a pressure-dependent interaction between volumetric strain and permeability based on three different triaxial compression test procedures. Later, the interplay among physical properties, pore pressure level and fracture pattern are discussed considering the lithological varieties of the investigated sandstones.

## 2. Materials and methods

Two sandstones were chosen for this investigation; the Trendelburg Beds, a Bunter Sandstone from the Lower Solling Formation, and the Bebertal Sandstone from the Upper Rotliegend sequences. Firstly, rock blocks of the greyish Trendelburg Beds (WG) were collected at the quarry Bunk in Bad Karlshafen, Center of Germany. The Trendelburg Beds correspond to a sandy, braided river deposit of the Triassic age, placed in the center of the Reinhardswald Basin (Weber and Ricken, 2005). Neumann et al. (2018) analyzed the mineralogy of 16 varieties of Trendelburg Beds and stated a quartz to feldspar ratio of 73.33 wt.% to 26.67 wt.%, which classifies this material as a subarkose with a certain homogeneous composition. The Trendelburg Beds is a fine to medium grained subarkose with pronounced anisotropic layers with different volume of pore spaces, which range from a few millimeters up to 2 cm (Fig. 1a and Fig. 1b). The complete mineralogy and a description of the pore space of the Trendelburg Beds are given by Pöllmann et al. (2017) and Neumann et al. (2018).

Secondly, the red-brownish Rotliegend Sandstone (BT) is a carbonate and silica cemented sandstone of Permian age, considerably less porous (ca. 6% of effective porosity) and less permeable ( $3.5 \times 10^{-10}$  m/s) than the Bunter Sandstone. This variety of Rotliegend consists of a fine to medium grained, red-brownish sandstone, solid and mostly horizontally stratified (Fig. 1c and d). A very characteristic feature of this sandstone is the well disseminated red colored ferruginous layer that originated mainly from iron-bearing hematite in the hematitic-illite cutans (Pludo et al., 2011). Joints and layers of clays or fine gravels were often observed in core samples. Rock specimens show a weak bubbling release when in contact with hydrochloric acid (10 mol-%). The Rotliegend Sandstone is classified into the lower Permian clastic sediments sequence and correlates with aeolian-fluvial facies from the North German Basin (Henningsten and Katzung, 2006; Fischer et al., 2012). Rock blocks of BT were collected in a quarry at Bebertal, ca. 28 km northwest from Magdeburg, Germany.

### 2.1. Preliminary investigation

In order to characterize physical and mechanical properties of both geological materials, cylinder specimens with edge lengths of about 140 mm and a diameter of 70 mm were drilled out of layered rock blocks of Rotliegend and Bunter Sandstone. As both sandstones are clearly layered, we considered the bedding as a plane of anisotropy and treated it by drilling in parallel and perpendicular directions. According to German standards (DIN EN, 1936:2007–02), the effective porosity can be evaluated through the difference between dry and fully water saturated densities in respect to the sample volume (ca. 540 cm<sup>3</sup>). Effective porosity will here be referred to as the amount of the sample's interconnected pore spaces that are capable to be filled with fluid, whereas total porosity means the entire pore space in a rock sample. To evaluate total porosity, the dry density of a rock sample is divided through its grain density. The latter was ascertained with a helium injection (gas pycnometer) by using dry rock powder, which is an indirect method to determine the gas volume through pressure measurement between sample and reference chambers, as described by Farrel et al. (2014).

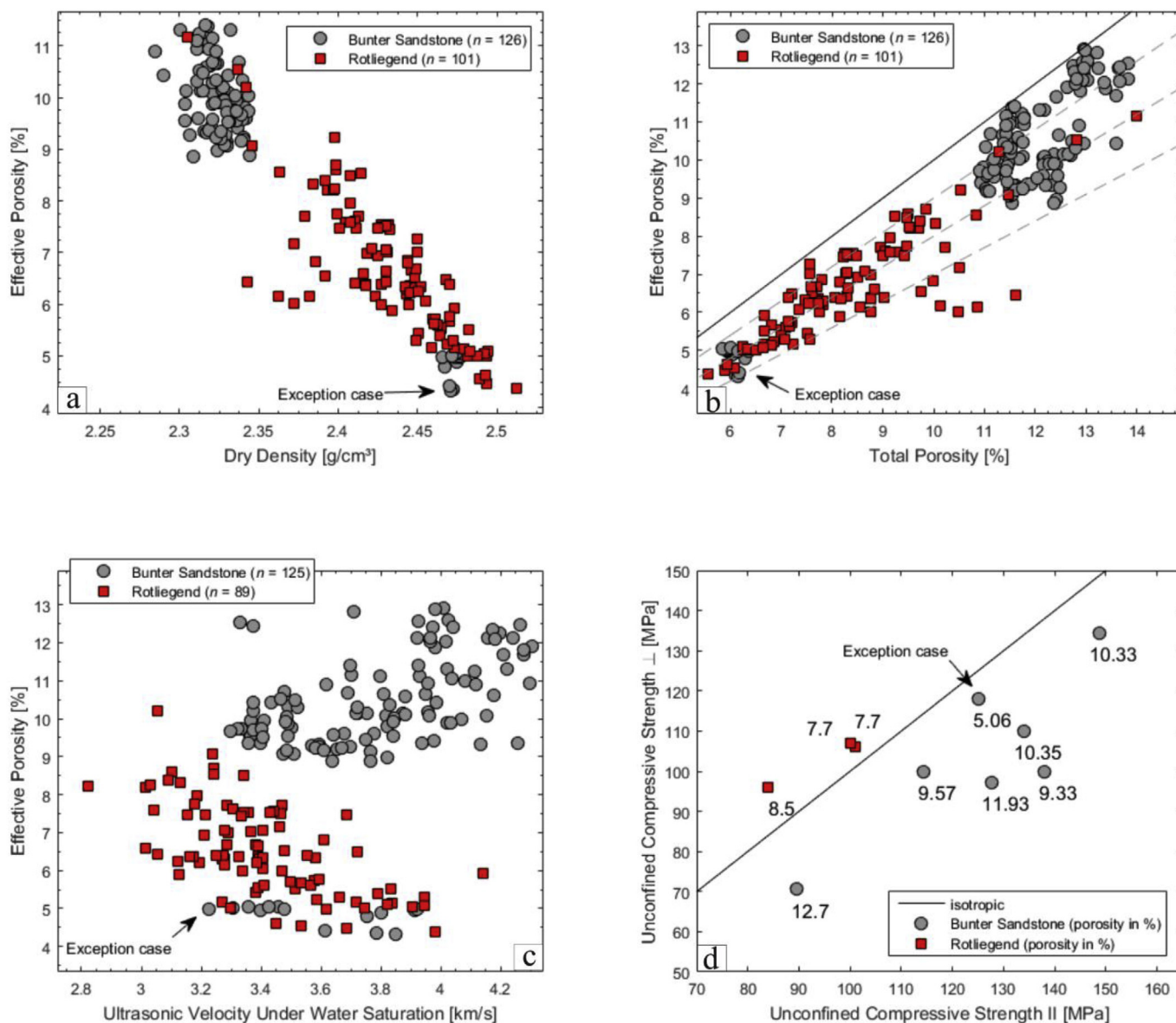


Fig. 7. Physical properties determined under atmospheric conditions for Rotliegend and Bunter Sandstones samples (diameter = 7 cm, length = 14 cm). Clusters are recognized for both materials by plotting effective porosity as a function of either dry density (a), total porosity (b) or ultrasonic wave velocity (c). In (d), the anisotropy is presented through uniaxial compression strength values measured parallel and transverse to bedding, with regard to the effective porosity. N means the number of samples.

## 2.2. Geomechanical tests

The geomechanical tests for the present investigation were conducted at the geomechanical laboratory of the Martin-Luther-University, in Halle (Germany), by using an electric hydraulic servo-controlled rock mechanics testing system for brittle materials. Details of the triaxial cell are shown in Fig. 2. This apparatus can perform pore and confining pressures of up to 70 MPa, with a maximal axial loading of 1500 kN (or 5000 kN under uniaxial stress conditions). The volume change of pore- and confining pressure fluids are recorded during the entire test with a precision of 0.01 cm<sup>3</sup>. Axial displacement is measured twice, once externally and once by the LVDT, and the axial load is recorded directly at the sample. A radial displacement sensor is placed as a ring around the sample. The experimental approach of this study consists of three kinds of triaxial compression tests:

1. The first procedure is a conventional triaxial compression test, in which pore- and confining pressures are held steady and the axial

pressure increases with a controlled rate of deformation ( $\dot{\epsilon} = 5.7 \times 10^{-6} \text{s}^{-1}$ ) (Fig. 3a). This kind of test has been widely applied to evaluate strength and deformability properties of geological materials (Mitchell and Faulkner, 2008; Menezes and Lempp, 2018) and will here be referred to as a deformation test. Overall, 52 deformation tests were carried out with Bunter Sandstone (WGS 2-2, WGS 2-9, WGS 2-8, WGS 2-10, WGS 6-2, WGS 6-3, WGS 6-4, WGS 6-12, WGS 6-13, WGS 6-14, WGS 11-4, WGS 11-5, WGS 11-8, WGS 15-4, WGP 2-1, WGP 2-2, WGP 2-3, WGP 2-4, WGP 2-6, WGP 5-3, WGP 5-9, WGP 6-4, WGP 7-2, WGP 9-3, WGP 10-3, WGP 11-3, WGP 14-1, WGP 14-2) and Rotliegend (BT 30-1, BT 30-5, BT 30-8, BT 30-9, BT 30-11, BT 31-11, BT 31-12, BT 48-1, BT 48-2, BT 49-1, BT 49-2, BT 49-3, BT 49-4, BT 53-1, BT 53-3, BT 58-1, BT 58-3, BTP BT 50-1, BTP 51-1, BTP 55-4, BTP 55-5, BTP 57-4, BTP 58-2, BTP 58-3).

2. The second test procedure consists of a flow-through test, intended to estimate the coefficient of water permeability during short-time triaxial loading. The advantage of determining permeability in the



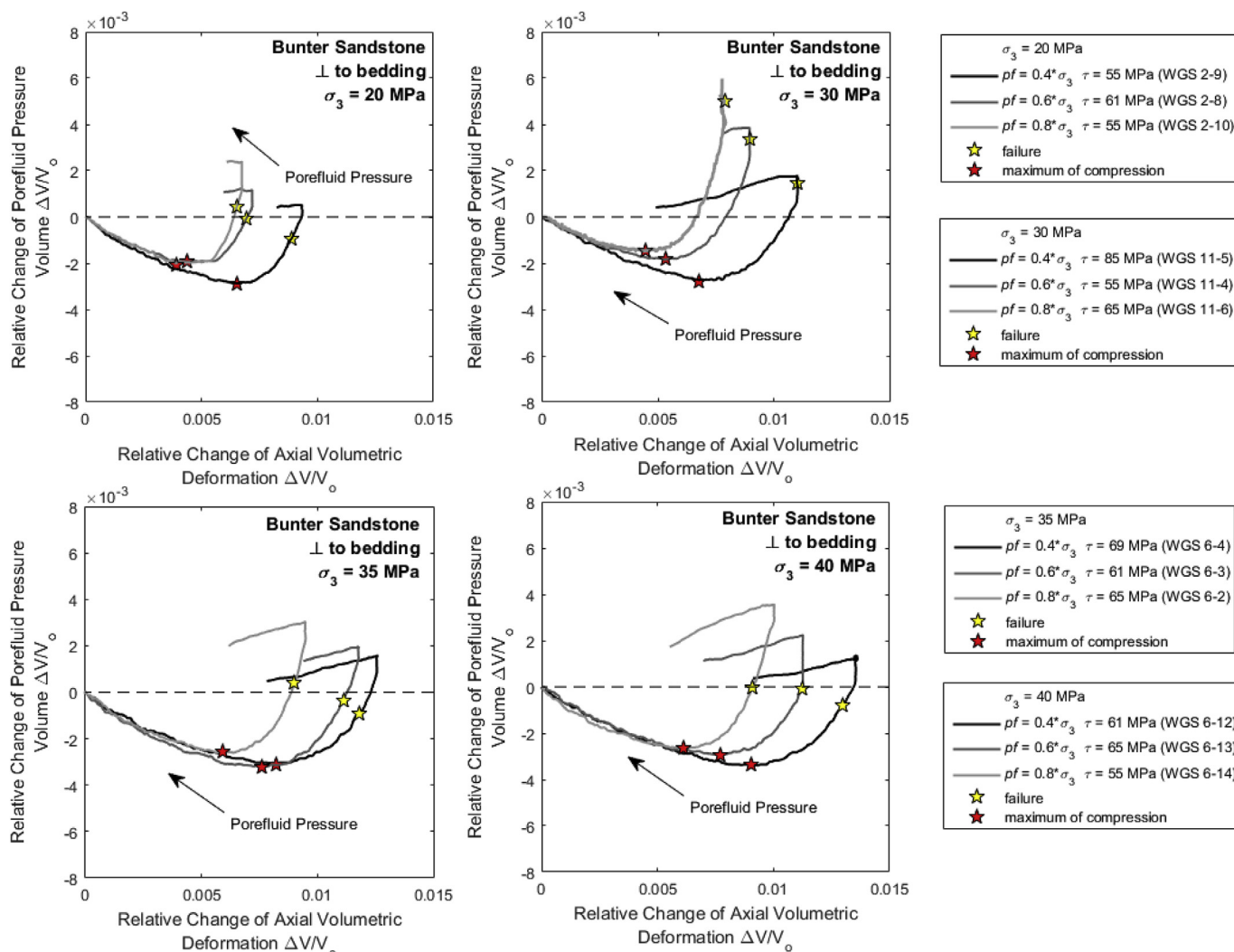


Fig. 8. Volumetric strain curve for 12 samples of Bunter sandstone drilled transverse to bedding. Samples are grouped after confining pressure: 20 MPa (a), 30 MPa (b), 35 MPa (c) and 40 MPa (d).

triaxial cell is seeing its relative performance with representative reservoir pressure conditions. In this case, axial, confinement and pore pressures are maintained steadily, whereas deformation (axial and lateral) and volume change of oil (saturating fluid of confining pressure, in the cell) and water (saturating fluid of pore pressure, in the sample) are continuously measured (Fig. 4a). The water supply from the pump unit remains connected to the triaxial cell through a cable and an always open inlet valve. After reaching the launching test conditions, an open water flow system can be created within the triaxial cell by opening the outlet porefluid valve. As the outlet pressure corresponds to the atmospheric pressure, a pressure gradient is established within the sample, and therefore, water streamed from the top to the bottom of the specimen. The maximal volume of water corresponds to 700 cm<sup>3</sup>. Similar test procedures are known in the literature as water seepage test (e.g. Luo et al., 2011; Xu and Yang, 2016), however the restriction in the present approach is to measure the pressure difference within the sample. Overall, 28 flow-through tests were carried out with Bunter Sandstone (WGP 14-1 and WGS 14-1) and Rotliegend (BT 58-1 and BTP 58-2).

3. The last test procedure is a compound between deformation and flow tests. A deformation test is carried out with drained conditions, i.e. the outlet porefluid valve is open (Fig. 5a). Therefore, deformation and water flow are related during triaxial loading. This procedure will be cited in this work as deformation-flow-test.

Overall, 6 deformation-flow-through tests were carried out with Bunter Sandstone (WGS 15-1, WGS 15-3, WGS 15-4) and Rotliegend (BT 53-2, BT 53-3, BT 53-4).

All varieties of tests were conducted under room temperature and with fully distilled water saturated rock specimens. Succeeding the test, rock specimens were photographed by using a core sample scanner, in a similar approach as by Menezes and Lempp (2018).

### 3. Theory

#### 3.1. Volume change

Volume change under increasing stress is referred to as volumetric strain, which can be calculated through the ratio between volume changes to initial volume (Means, 1976). To specify volumetric strain, it is necessary to consider the geometrical properties of the material. For cylinder specimens, it can be evaluated through the addition of axial and lateral strains, regarding the Poisson Constant of Proportionality (Goodman, 1989; Alejano and Alonso, 2005). However, the Rotliegend and the Bunter Sandstone are hardly stretched under triaxial stress conditions (in order from 10<sup>-4</sup> μm) and therefore their Poisson ratio is nearly zero. As proposed by Goodman (1989), Arzúa and Alejano (2013) measured volumetric strain directly by monitoring the oil flow

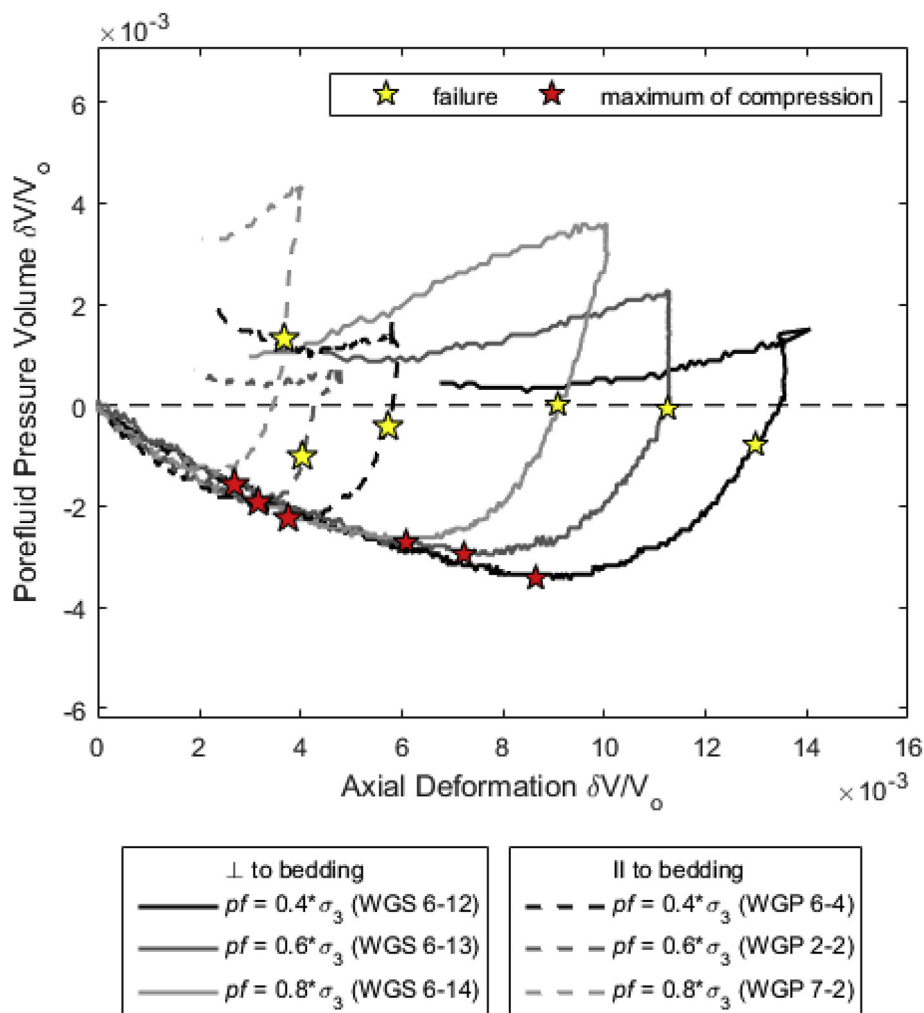


Fig. 9. Volume Change of six Bunter sandstone samples in regard of porefluid pressure variability (40, 60 or 80% of confining pressure,  $\sigma_3 = 40$  MPa) and of structural anisotropy. Dashed lines represent samples drilled parallel to bedding (II), and continuous lines transverse ( $\perp$ ) to bedding. Failure is represented by yellow stars and the maximum of compression by red stars. (For interpretation of the references to color in this figure legend, the reader is referred to the Web version of this article.)

into or out of the confining vessel as the confining pressure was held constant by a servomechanism. This is an appropriate approach to estimate dilatancy and compaction stages for hard materials without direct mentioning of axial or lateral strain. In this work, volumetric strain was measured on the basis of traditional, triaxial deformation tests, by evaluating the water volume supply into and out of the sample. As mentioned before, the volume change of a porous solid material under compressional stress is related to a progressive development of a permanent, plastic fabric reaction. Therefore, to keep a controlled pore pressure in the sample, the amount of water volume (porefluid) will continually change. This approach is only possible because the triaxial cell is intended to be a closed system, meaning the volume between cell and pressure cycles remains constant during all tests. Volume change ( $\Delta V$ ) was calculated from the launching condition until unloading, as a difference between the n-water-volume ( $V_n$ ) to the first-water-volume ( $V_1$ ), as following:

$$\frac{\Delta V}{V_0} = \frac{V_n - V_1}{V_0}$$

Considering the effect of sample size and scale, the volume change was normalized to the geometrical initial volume of the sample ( $V_0$ ), which corresponds to a right circular cylinder with 14 cm length and 7 cm radius (ca. 540 cm<sup>3</sup>). Fig. 6 illustrates a triaxial compression test in terms of stress-strain curve (Fig. 6a) and volumetric strain (Fig. 6b). In

this example, volume change corresponds to two stages of deformation. The first one is called compaction, which means a volume decreasing by closing pre-existing fissures. The point of maximal compaction (grey star) is also the maximum of void ratio which is characterized by the maximal quantity of confining fluid in the cell, in order to balance with the smallest pore space volume (maximum void ratio) in the sample. This turnover point is also known as dilatancy boundary.

After reaching the maximum of compaction (or dilatancy boundary), grain boundaries start to dislocate due to an energy release (Alkan, 2009) and the sample experienced a volume increase resulting from the shear distortion in the material (Alejano and Alonso, 2005). This is related to the formation and extension of open microcracks in a rock specimen undergoing compression, briefly before reaching its mechanical strength (Jaegger and Cook, 1979; Goodman, 1989). The reason for this inelastic stress-strain behavior originates in the rock's inherent inhomogeneity, which produces fluctuations in the stress field sufficient to arrest cracks shortly after they have been initiated (Scholz, 1968). Considering different scales of observation, dilatancy can be represented from the sliding of grains over one another to macroscopic fracturing (Sheldon and Ord, 2005), which explains its pervasive nature (Cook, 1965). Nonetheless, even after reaching the yield strength, the rock may continue to shorten through the joining and consequently sliding of microcracks (Goodman, 1989). In most studies, a dilatant behavior is represented in meanings of dilation angle associated to the

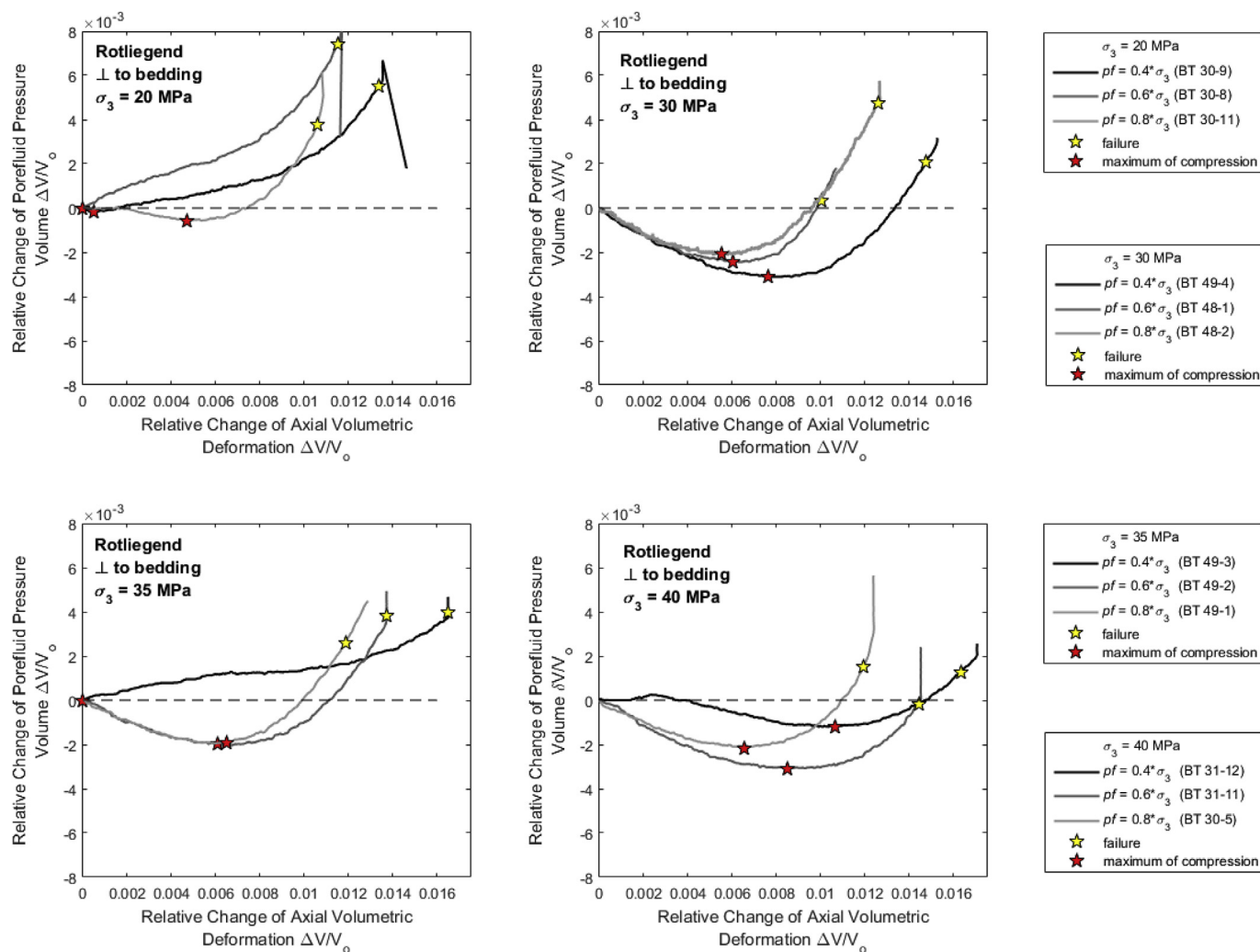


Fig. 10. Volumetric strain curve for 12 samples of Rotliegend drilled transverse to bedding. Samples are grouped after confining pressure: 20 MPa (a), 30 MPa (b), 35 MPa (c) and 40 MPa (d). Note that some samples do not show any compression stage before increasing volume (BT 30–9, BT 30–8, BT 49–3 and BT 31–12).

confining pressure (Ord, 1991; Alejano and Alonso, 2005; Zhao and Cai, 2010; Arzúa and Alejano, 2013). In this work, volume change will not be presented through a rate or an absolute modulus of plastic deformation, but rather as a continuous process of permanent deformation in terms of porefluid volume change as a function of axial deformation (Fig. 6b).

### 3.2. Permeability

Permeability was evaluated in terms of hydraulic head based on the laminar flow regime of Darcy's statement. The rate of fluid flow at a point is defined as the volume of fluid (Q) crossing unit area per unit time (A) and is proportional to the gradient of pore pressure at that point (Jaegger and Cook, 1979). One is aware of the effects of pressure gradient within the sample, of the difficulty of measuring this gradient under triaxial test conditions and especially to express this change in an equation. Therefore, permeability in terms of hydraulic coefficient should be considered cautiously. The pressure gradient (g) was evaluated as the ratio between hydraulic high difference and sample length (L), and the hydraulic high difference is the proportion from pore pressure to weight of water. Additionally, a variant to illustrate flow evolution is offered by the filter velocity, which despite not taking into account the pressure gradient and sample length, allows the results to be compared to each other, as the rock specimens were prepared with the same dimensions of length and sectional area. Filter velocity (F, in

m/s) and permeability (Kf, in m/s) were evaluated as following:

$$F = \frac{Q}{A}$$

and

$$Kf = \frac{F}{g}$$

## 4. Results and discussion

A preliminary investigation with Bunter Sandstone and Rotliegend samples was carried out to determine their physical properties and lithological variation. This includes the evaluation of porosity, density, ultrasonic velocity and uniaxial compression strength (Fig. 7). Physical properties for the investigated Rotliegend samples are presented here for the first time. However, the data of 94 out of 126 samples of Bunter Sandstone were collected from previous works related to this research (Menezes and Lempp, 2018). Overall, samples from 12 different rock blocks of Trendelburg Beds and from 18 rock blocks of Rotliegend were investigated and the corresponding results will be analyzed in the following.

The grain density of the Bunter Sandstone varies from 2.62 to 2.65 g/cm<sup>3</sup>, which is mainly associated to a feldspathic-quartziferous mineralogical composition and therefore matches its petrological

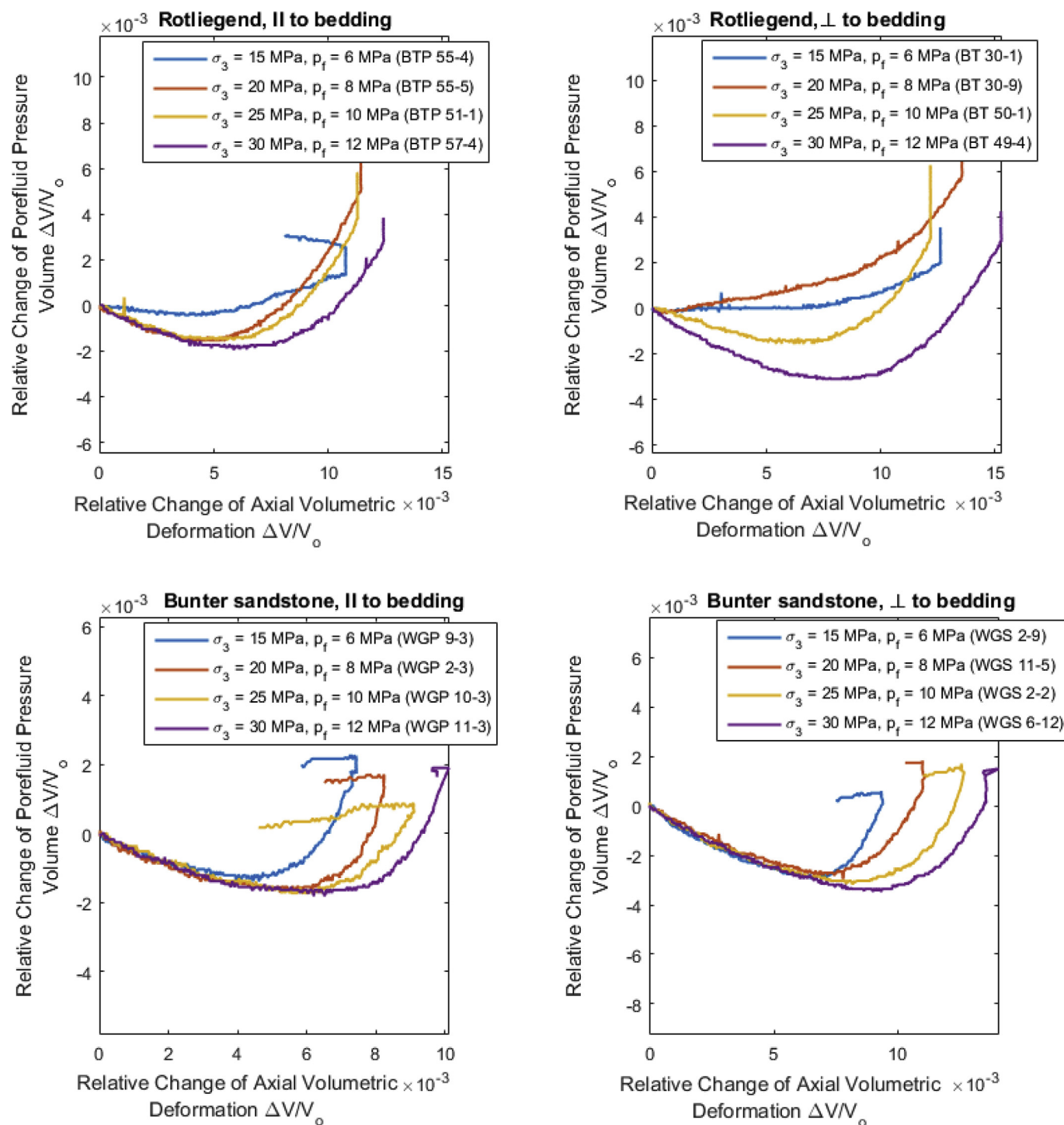


Fig. 11. The development of volume change after confining pressure for Rotliegend and Bunter sandstone, in regard of bedding angle. Tests were carried out with 15, 20, 25 and 30 MPa of confining pressure and a pore fluid pressure rate of 40%.

classification as subarkose, according to Weber and Ricken (2005). It is important to note that this singular value of grain density is related to a certain mineralogical composition (e.g. quartz, feldspar, mica) and should represent all solid material of a rock block. Both sandstones are recognizably structured according to layers of different mineralogical composition, grain size and thickness. Therefore, the grain density represents solely a weighted average of all those materials and should be interpreted as an approximate value which can vary within a geological formation. The grain density of Rotliegend rock blocks is to be found on an interval slightly above the Bunter Sandstone, between 2.67 and

2.78 g/cm<sup>3</sup>, which is associated to an apparent influence of micaceous and argillaceous components present in the Rotliegend facies as mentioned earlier. Furthermore, both materials have a similar ultrasonic velocity under water saturation (Fig. 7c), but they scatter in at least two major groups when comparing porosity and density values (Fig. 7a). Rotliegend samples are rather concentrated between 2.36 and 2.5 g/cm<sup>3</sup> and the Bunter Sandstone between 2.30 and 2.34 g/cm<sup>3</sup>. However, in all charts there are exceptions from both materials. Particularly noticeable is a rock block of Bunter Sandstone (Block No. 17, signed with an arrow as “exceptional case”), which distanced itself considerably

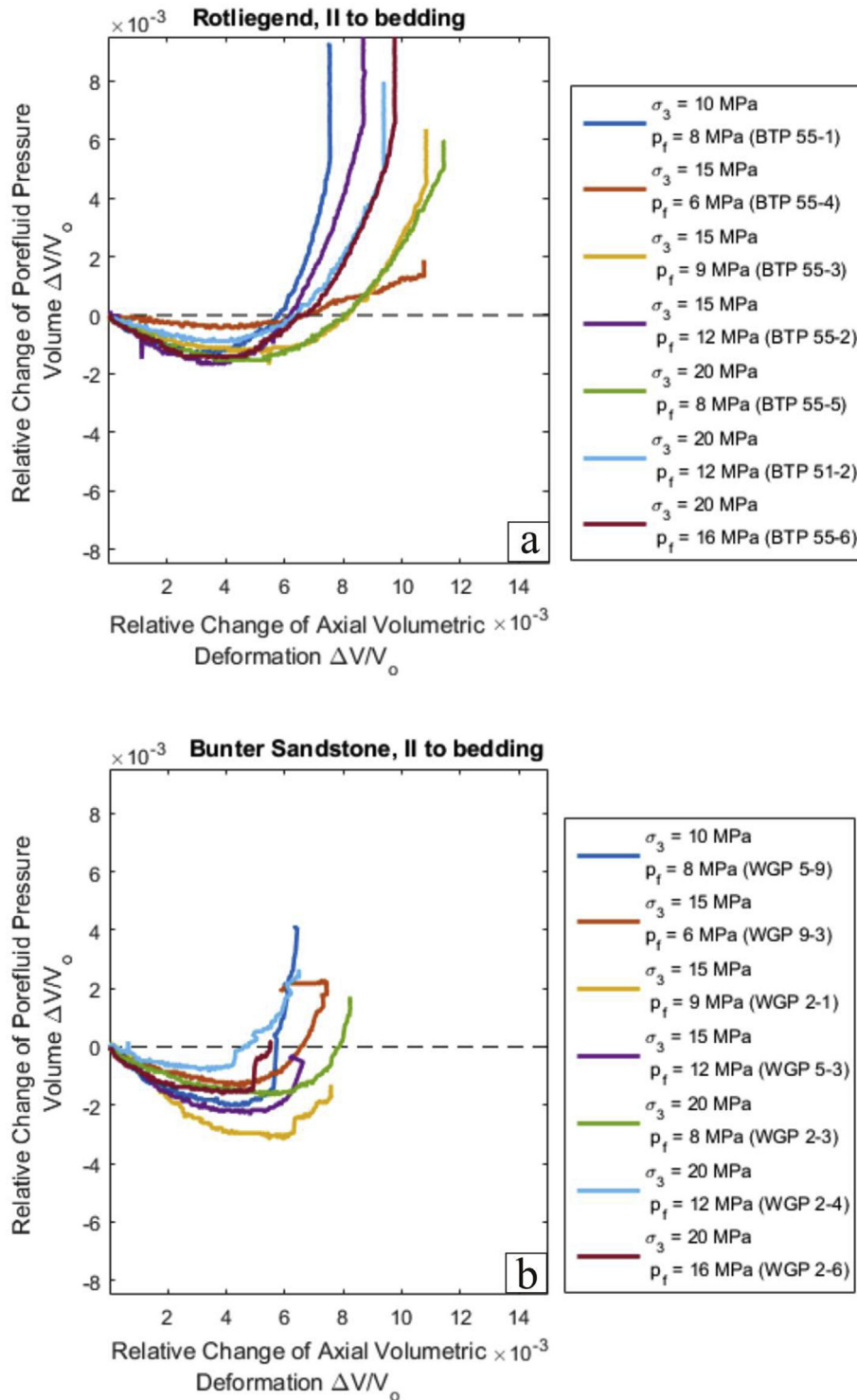


Fig. 12. The development of volume change after pore- and confining pressures for Rotliegend (a) and Bunter sandstone (b) samples drilled parallel to bedding. Tests were carried out with 10, 15 and 20 MPa of confining pressure and variable pore fluid pressure.

from the other Bunter Sandstone samples.

Fig. 7d shows the lithological variability of Rotliegend and Bunter Sandstone in terms of strength anisotropy, a mechanical property displaying the variation of strength according to the angle between major normal stress (axial pressure) and bedding (plane of anisotropy). In this chart, each point matches two values of maximal compressive uniaxial strength of one particular rock block. The first one (on the x axis) was obtained by testing the sample with the bedding angle transverse to the major stress component, and the second one parallel to bedding.

Strength anisotropy was observed in both materials, however in different ways. For the Bunter Sandstone on the one hand (grey circles), the maximal compressive strength was reached by applying the major stress component parallel to the plane of anisotropy, as all points are located below the line of isotropy (uniformity in all directions, 1:1). There is an approximate trend between effective porosity and compressive strength, indicating that the more porous the medium is, the weaker is its strength. The Rotliegend on the other hand is a low anisotropic material, however with an inverted anisotropic behavior





Fig. 13. Fracture pattern of Rotliegend core specimens drilled either parallel (upper row) or transverse (lower row) to bedding. The samples correspond to the deformation tests from Fig. 11a and b. Pictures taken with a core sample scanner.

unlike the Bunter Sandstone. For the Rotliegend, the maximal compressive strength is obtained by applying loading transverse to bedding, and the strength contrast due to bedding orientation is lower (UCS parallel/UCS transverse ca. 0.9). Comparing these results may raise questions concerning the cause of structural anisotropy – is this due to the lithological contrast between layers, the different physical properties, or due to the distribution of pores within the bedding? The influence of effective porosity, as an absolute value only, can be questionable if we analyze the unusual rock block of Bunter Sandstone (No. 17). Despite of a low effective porosity (ca. 4%) and high density (ca. 2.47 g/cm<sup>3</sup>), this rock block is showing similar values of uniaxial strength to other Bunter Sandstone samples and the same anisotropic tendency. Therefore, the influence of other microstructural features on the anisotropic behavior of these materials must be assumed. The effects of structural anisotropy in the Bunter Sandstone (Trendelburg Beds) have already been explained by Menezes and Lempp (2018), therefore the focus of this work will be on the Rotliegend and correspondingly on the difference between both materials.

As we can observe, both sandstones have a singular mineralogical composition, unique pore-matrix structure and present a range of physical properties. Describing both materials based on average values (e.g. typical density or effective porosity) will not satisfy the natural, lithological variation of any geo-matter. Accordingly, samples and test conditions were carefully matched, prioritizing the comparison

between similar samples or among samples from the same rock block.

#### 4.1. Volume change under triaxial stress conditions

Listed below, volumetric strain is presented in Fig. 8 with relative changes of porefluid pressure volume (y axis) and axial volume deformation (x axis) for 12 Bunter Sandstone samples, drilled transverse to bedding. Each chart represents a series of three triaxial tests carried out with the same confining pressure (20, 30, 35 or 40 MPa), where the samples were compressed up to stress fall (signed by yellow stars). Additionally, the maximum of compaction, marked by red stars, limits the border between compaction and dilatancy stages.

In all graphs the same sequence of results sorted by pore pressure level (relative to the confining pressure) can be observed. From left to right, firstly we have samples with high pore pressure level (80%, lines in lighter grey), followed by samples with medium pore pressure level (60%, lines in grey) and lastly samples with low pressure level (40%, black lines). The higher the porefluid pressure level, the earlier an increase of volume (dilatancy) occurs. In other words, increasing the porefluid pressure enhances an earlier fracturing, which corroborates the statement of a pore weakening effect. Considering the development of compaction and dilatancy stages of these curves, it can be stated that a lower porefluid pressure rate allows a more pronounced volume change in the sample.

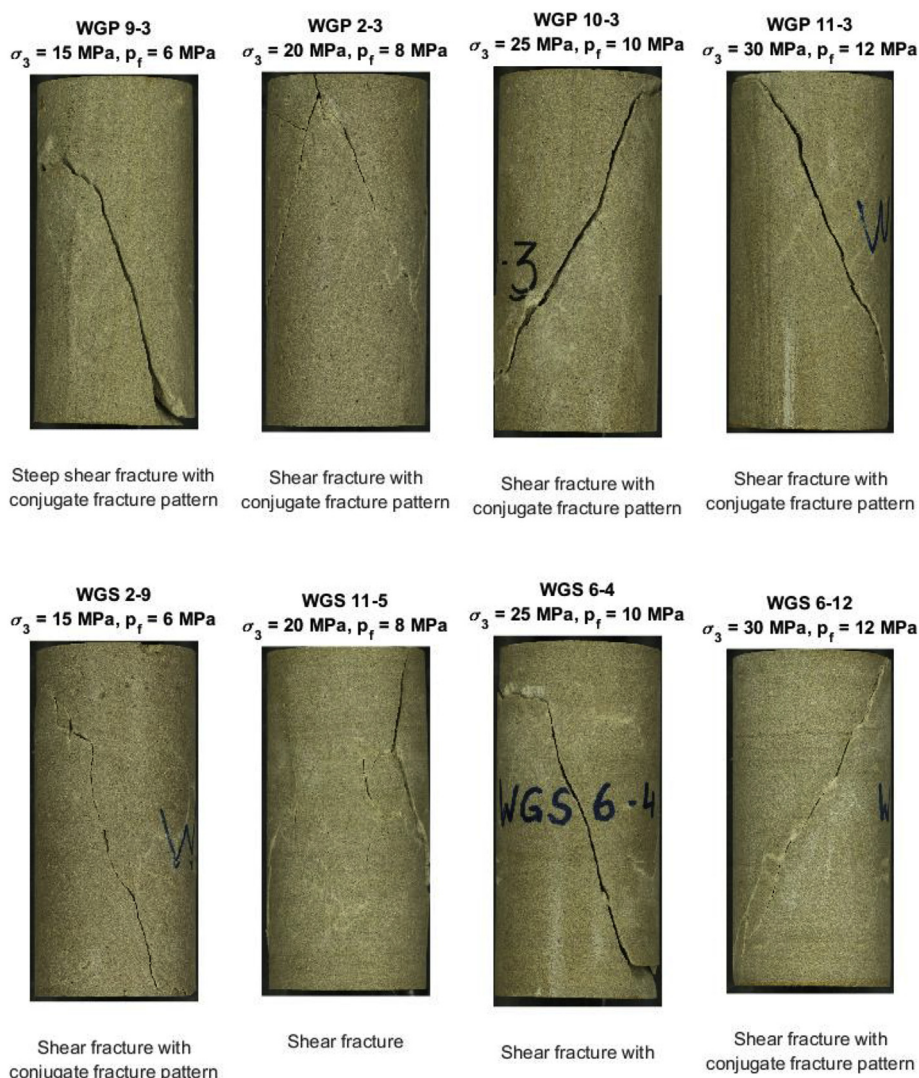


Fig. 14. Profile pictures of Bunter sandstone specimens after triaxial testing. The samples correspond to the deformation tests of Fig. 11c and d. Pictures taken with a core sample scanner.

Another important factor affecting volumetric strain is the bedding angle. As presented in Fig. 9, both stages of compaction and dilatancy have been shortened if the major stress component is applied parallel to the bedding (dashed lines). The maximum of compaction (or the starting point of volume increase) is brought decently forward at all pore pressure levels. Nonetheless, both directions of anisotropy still respect the sequence of porefluid pressure. The displacement of the dilatancy boundary (or maximum of compaction) could be associated to improved flow capacity favored by the bedding.

The relationship among volume change, porefluid pressure and structural anisotropy was clearly visualized for Bunter Sandstones samples. In contrast, by repeating the same test procedure with Rotliegend samples, there are some exceptions to be recognized (Fig. 10). In this material, the pore weakening effect is not sufficiently clear in 3 of 4 charts (Fig. 10a, c and 10d.), as the curves do not follow the sequence of pore pressure levels. Four of these samples (BT 31–12, BT 30–9, BT 30–8 and BT 49–3) have not shown any compaction stage before performing dilatancy. If the curves show a compaction stage, the sequence of porefluid pressure is respected, as observed in Fig. 10b. Nevertheless, the black lines representing the lowest porefluid pressure level occasionally do not express any compaction stage before increasing volume, meaning that volume change entirely corresponds to dilatancy. These exceptions in volume change make it difficult to

compare volumetric strain between different bedding angles, meaning if the major stress component is applied parallel to bedding, a compaction stage will take place regardless of pressure conditions (Fig. 11a, Rotliegend samples and Fig. 12).

To illustrate this situation better, the development of volumetric strain of Rotliegend and Bunter Sandstone is presented in Fig. 11 as a function of confining pressure, for both directions of anisotropy. In Fig. 12, volumetric strain is presented for different pore pressure with varied confinement stress. Tests were carried out with 15, 20, 25 and 30 MPa of confining pressure with a porefluid pressure level of 40% (6, 8, 10 and 12 MPa, respectively). Considering the influence of pressure, it needs to be pointed out that dilation has a more pronounced expression under low confining pressure, as described in the literature. On a laboratorial data basis from 7 different lithologies, Zhao and Cai (2010) created an empirical approach to describe the dilation behavior in a non-associated, Mohr-Coulomb strain-hardening model. They stated that at low confining pressure, the material demonstrates relatively higher volumetric dilation. However, dilation decreases drastically if the confining pressure increases. This statement will not be contradicted here - nevertheless, the development of a compaction stage is actually the only one directly affected by the increase of either pore- or confining pressure. Compaction is usually a preliminary stage of dilatancy and of course, it would affect the later stage of volume



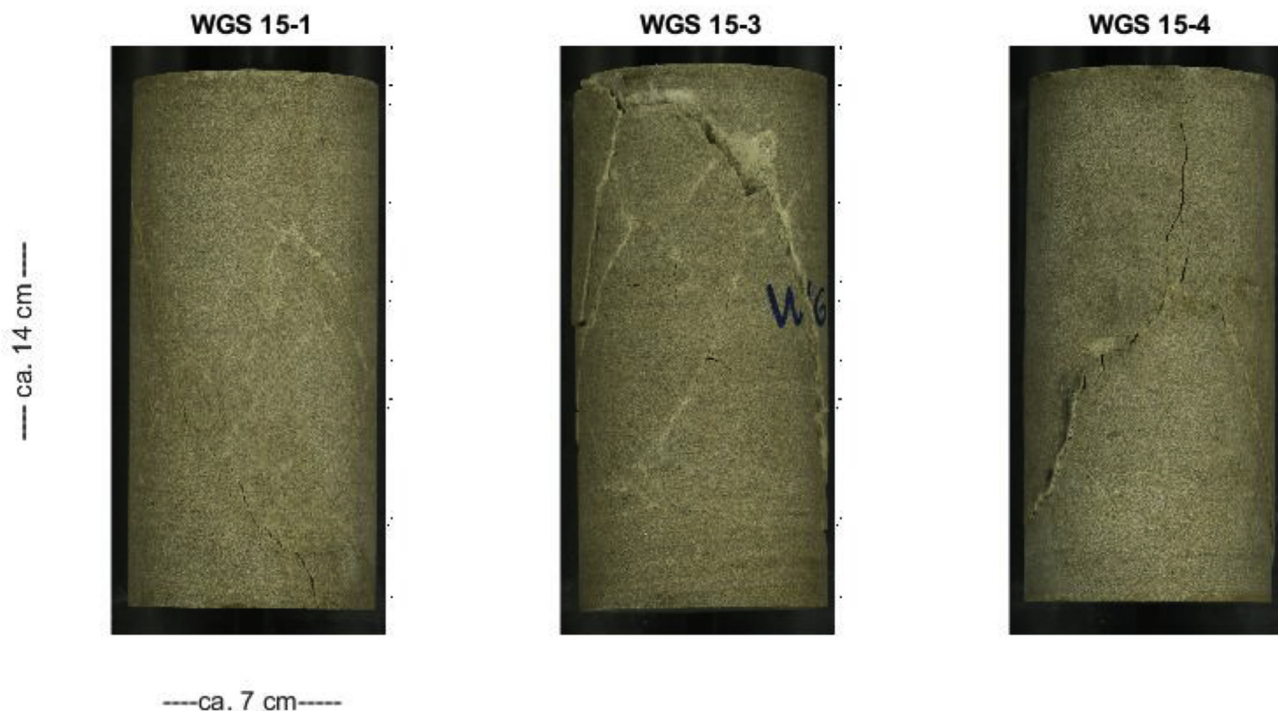
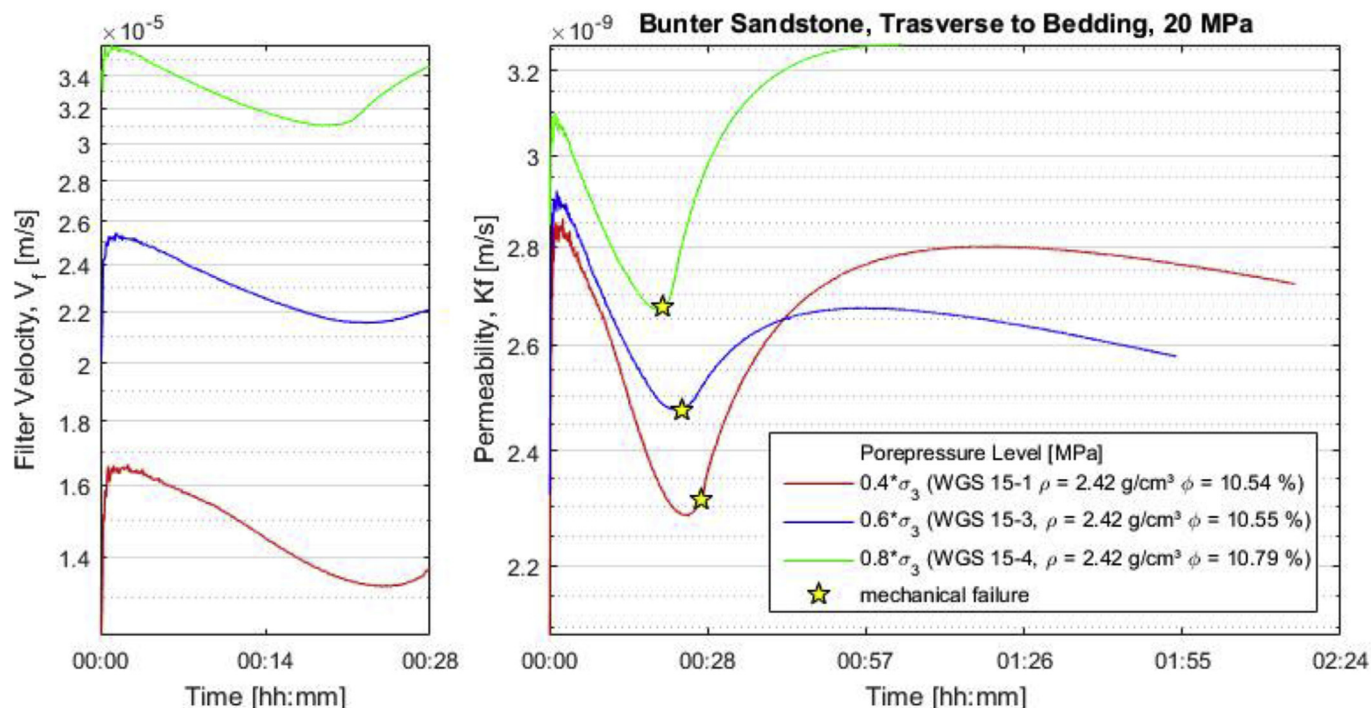


Fig. 15. Permeability development for three Bunter sandstone samples under triaxial stress conditions. Permeability curves obtained from deformation-flow tests carried out with 20 MPa of confining pressure and variable pore pressure levels: 40% (WGS 15-1), 60% (WGS 15-3) and 80% (WGS 15-4).

increase. However, a compaction stage is not mandatory for a material undergoing triaxial compression.

It is important to highlight that exceptions in volume change (= dilatancy) were observed for Rotliegend samples drilled transverse to bedding only, and that all Bunter sandstone samples (in both directions of anisotropy) have performed a typical compaction-dilatant volume behavior under triaxial stress. Considering the particularly low

porosities (~6%) and high densities (~2.44 g/cm<sup>3</sup>) of the Rotliegend samples, we can assume that physical properties and bedding anisotropy exert an influence on the development of exceptional volumetric strain under triaxial stress. This statement on the dependency of volume change on physical properties can be supported by comparing the sandstone behavior with the findings of Naumann et al. (2007), where anisotropy in volume change was investigated by using Opalinus Clay.

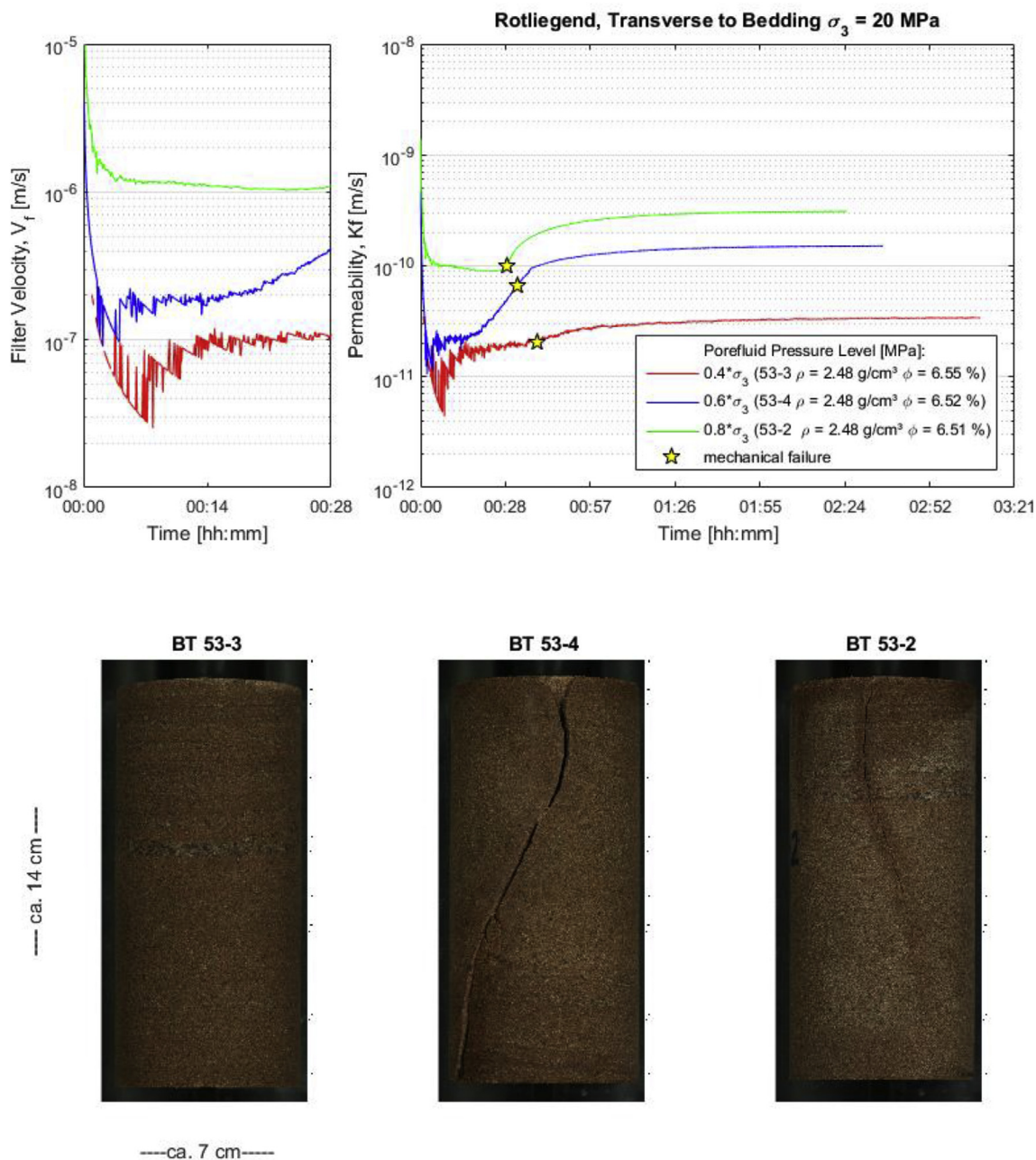


Fig. 16. Permeability development for three Rotliegend samples under triaxial stress conditions. Permeability curves obtained from deformation-flow tests carried out with 20 MPa of confining pressure and variable pore pressure levels: 40% (BT 53–3), 60% (BT 53–4) and 80% (BT 53–2).

Opalinus is a very fine sedimentary rock with a mean water content of ca. 6.7% and with a pronounced capability of self-healing. For samples drilled transverse to bedding, they detected the onset of dilatancy prior to but close to failure, which means that volume change is mostly constituted by the compaction stage.

Furthermore, a second aspect concerning pressure was already observed in Fig. 8, namely that low pore pressure levels tend to shift volume increase. Therefore, the fact that some Rotliegend samples did not express a decrease in volume (compaction stage) before microcracking may be traced back to the anisotropy (transverse to bedding), specific pressure conditions (low confining and pore pressure levels) and material properties (low effective porosity, poorly permeable and bad pore space connectivity). Due to the low volume of pore spaces available, there are not enough vacancies that can be closed, therefore “skipping” the compaction stage. This process may additionally be intensified through low pore pressure, leading to a low internal resistance

and high effective pressure, as well as if the porefluid flow is not favored by the bedding angle.

At this point, it is worthwhile to recall the contrary anisotropy behavior between Rotliegend and Bunter Sandstone illustrated with uniaxial compression strength values (Fig. 7d). The Rotliegend is a low anisotropic rock (~0.9), in which the maximal strength will be reached by applying the major component of stress transverse to bedding, the opposite to the Bunter Sandstone. Matching these observations about strength anisotropy and deformability, they raise questions about the influence of different microstructures on the deformation of these materials. Which component plays the major role in the deformation of Rotliegend and Bunter Sandstone? Förster and Lempp (2014) quantified the amount of plastic deformation in three different sedimentary rock types tested under uniaxial compression. By evaluating the vector displacement of grains in core photographs, by means of the intercept-method, they found a correlation between the particle to the matrix-

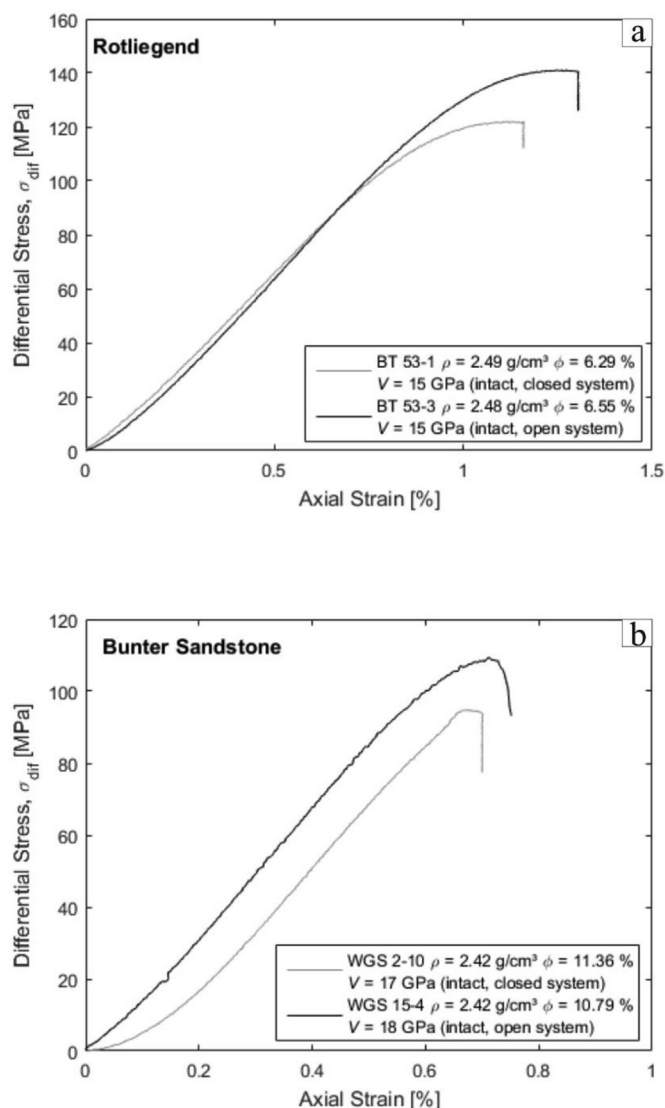


**Fig. 17.** Comparison of stress-strain curves and modulus of deformation ( $V$ ) for Rotliegend samples tested under 20 MPa of confining pressure and 8 MPa of pore pressure, either in a closed system (black line) or in an open system (grey dashed line). Density ( $\rho$ ) and porosity ( $\phi$ ) for the investigated samples are given.

ratio and the shape of the deformation. Matrix-supported limestones and sandstones showed significantly higher ellipticity values than the grain-supported conglomerate. It is likely that the matrix-supported microstructure of the samples distributes the stress more effectively (Förster and Lempp, 2014).

Based on this knowledge, one of the aims of this study is to estimate the influence of porefluid pressure and anisotropy on the distribution of stress and strain in sedimentary rocks, while keeping focus on the macroscopic scale. A further element that helps us understand deformation trends is the fracture pattern observed in rock specimens. Examples are displayed in Fig. 13 for Rotliegend samples and in Fig. 14 for Bunter Sandstone samples. In this study, fracture patterns were visually classified and characterized by the quantity of fissures, their steepness, and ultimately by the geometry or the appearance of conjugated fissures. They were divided into two groups: the first one corresponds to a simple fracture pattern (1), with one penetrative shear fracture sometimes attended by tensile or wedged joints, and the second one corresponds to a complex fracture pattern (2), with numerous conjugated fractures.

#### 4.2. Permeability evolution as a function of porefluid pressure

The development of permeability during stages of compaction, dilatancy and after failure (better: maximal differential stress) is represented in the graphs below as a function of porefluid pressure for Bunter Sandstone (Fig. 15) and Rotliegend (Fig. 16) samples. Filter velocity and permeability depend on the volume of water and on the flow time, therefore they are expected to rise by increasing porefluid pressure. This tendency was observed in both sandstones, where filter velocity and permeability curves agree with the hierarchy of pore pressure level (related to the confining pressure). Permeability and filter velocity tend to decrease as differential stress and strain increase, and near sample failure an increase of permeability is notable.

The second noteworthy aspect to analyze is the development of permeability after stress fall. Unfortunately, some flow tests were not carried out up to the steady flow because of limited water supply (700 cm<sup>3</sup>). However, after ca. 1 h of water flowing after reaching the maximal differential stress, it is possible to observe a clear downward trend of permeability. This trend could reflect a new period of compaction, characterized by the enclosure of fissures (collapse of pore space) and the development of a residual strength. However, the fracture permeability of Bunter Sandstone samples does not seem to agree with the hierarchy of pore pressure level, because of the influence of a new arrangement of pore spaces and matrix due to fracturing. Therefore, permeability does not necessarily increase after reaching the maximal differential stress. Instead, the new pore spaces created during the dilatancy stage may collapse at the maximal differential stress due to the loss of cohesion. Along the fissure surface, grains could get reduced in size due to shear friction, communed as grain-powder (cataclastic material) that may fill vacancies, thus preventing flow across the fissure. Therefore, the sample could become less permeable after stress fall than during the dilatancy stage. This observation leads us to consider permeability as a strain-sensitive parameter, which means dependence on the fracture pattern, especially if a high porous sandstone is considered. Bauer et al. (2015) describe that fracture induced permeability depends mainly on fracture aperture and connectivity, and the latter is relative to the length, orientation and density of the fracture. Comparing the fracture development of both materials, at the lowest pore pressure level (40% of confining pressure, samples BT 53–3, WGS 15–1) there is a fracture pattern which does not correspond to a penetrative, continuous shear surface, but rather to dispersedly distributed pairs of shear fracture. As we can observe in the profile pictures of the rock specimens and with the development of permeability during the test, the porefluid pressure seems to have an influence on the fracture development, and the fracture pattern affects the development of permeability after stress fall. The fracture permeability depends (1) on the fracture pattern, which is influenced by the porefluid pressure level and (2) on the initial porosity of the rock, which affects its reduced strength after stress fall. Similar processes have been observed in the literature. Wong et al. (1997) stated that dilatant brittle failure may result in increased or decreased permeability, depending on the porosity of the initial rock. Sheldon et al. (2006) verified this statement by using log permeability as a function of porosity and demonstrated that permeability decreases with increasing porosity of a high porosity sandstone. In this case, their example is based on the Rothbach Sandstone, which has an effective porosity of ca. 20% and mainly consists of quartz (68%), feldspar (16%) and clay (12%).

Initially, during the first 20 min of the experiment, a certain flow instability characterized by a zigzag pattern or wavering of the permeability curve was observed. Comparing both sandstones, this instability seems to be more likely to occur in the Rotliegend than in the Bunter Sandstones and is more pronounced at low porefluid pressure levels. Therefore, one of the reasons for this behavior may be the properties of the material, e.g. the magnitude of effective porosity and the quality of the pore spaces connectivity, as well as the pressure conditions. This is also a sign for a non-laminar fluid flow rate.



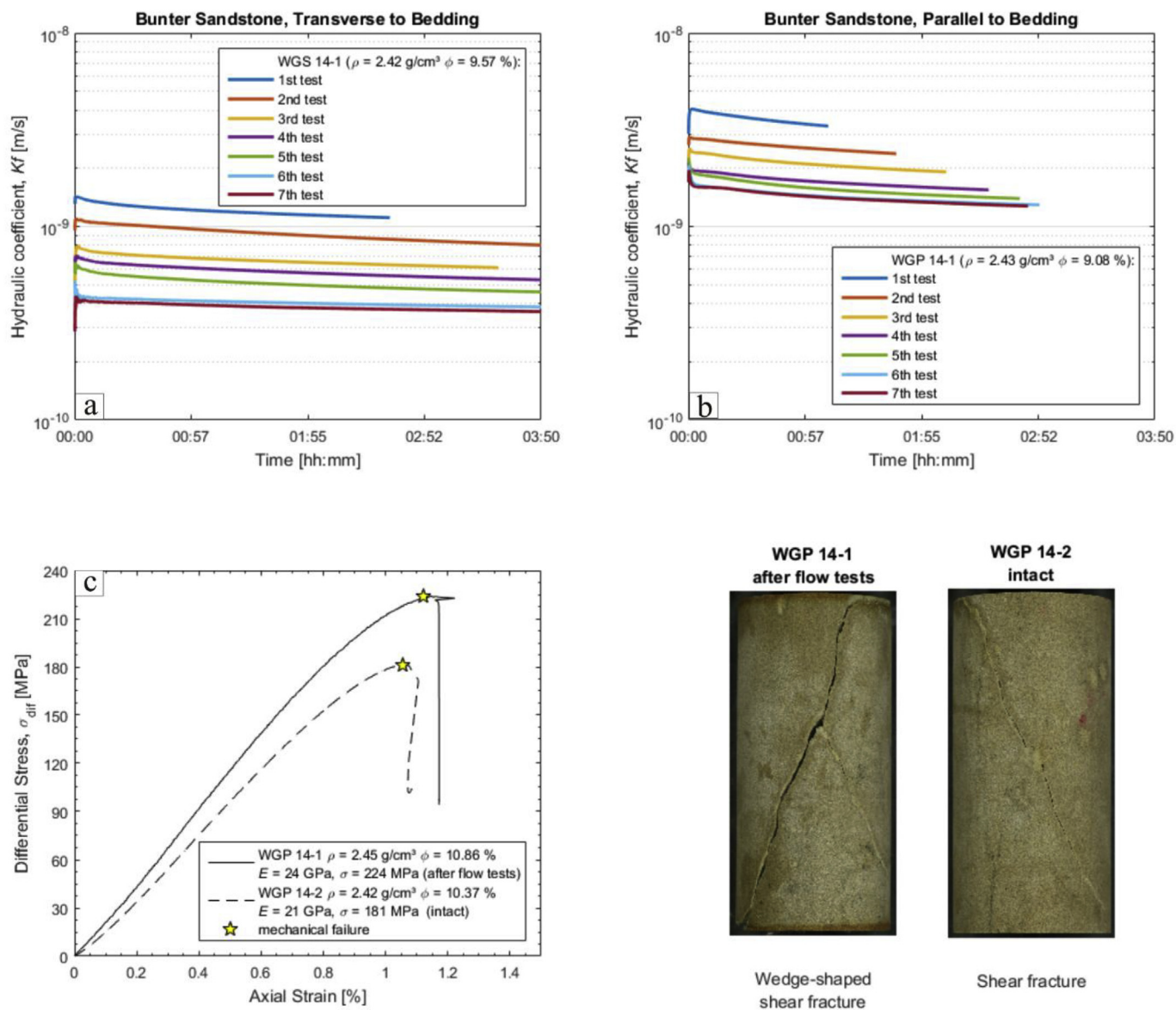


Fig. 18. In (a) and (b), permeability curves of Bunter sandstone samples considering a parallel (WGP 14–1) or a transverse (WGS 14–1) water flow to the bedding. Afterwards, the streamed sample WGP 14–1 was tested up to mechanical failure and compared with an intact rock specimen (c).

Additionally, performing a deformation test with an open fluid flow system enhances the stiffness of the material, due to the inconsistent porefluid pressure within the sample. This means that a pressure gradient is produced between the steered porefluid pressure of the pump unit and the atmospheric pressure. The pressure gradient itself has a clear effect on the brittleness of the sample, as we observed with stress-strain curves for deformation (closed system) and deformation-flow (open system) tests presented in Fig. 17.

### 4.3. Permeability under anisotropic stress conditions

Furthermore, in order to estimate the variation of permeability under triaxial stress conditions, experiments with high lithostatic pressure ( $\sigma_3 = 40 \text{ MPa}$ ) and a porefluid pressure rate of 40% ( $p_f = 16 \text{ MPa}$ ) were successively repeated. With differential stress ( $\sigma_{diff}$ ) of ca. 60 MPa ( $\tau = 30 \text{ MPa}$ ), an anisotropic stress field well below the maximum of compaction ( $\tau = 73 \text{ MPa}$ ) and far from the critical failure stress ( $\tau = 94 \text{ MPa}$ ) was reproduced. Under these conditions, tests should theoretically have taken place within the elastic deformation behavior, which allowed us to repeat this procedure seven times by

using the same rock specimen.

Permeability curves for each of the 7 tests are subsequently shown as a function of time for Bunter Sandstone (Fig. 18) and Rotliegend (Fig. 19 and Fig. 20) samples. The first remark on these graphs is the effect of anisotropy on permeability, showing that the flow is favored when applied parallel to bedding. The Bunter Sandstone has higher permeability coefficients than the Rotliegend, which preliminary investigation under atmospheric conditions shows. Furthermore, the permeability tends to decrease as the test was repeated, in both directions of anisotropy. After the 7th test, the water-saturated weight of the streamed samples (WGP 14–1, BTP 58–2 and BT 58–1) was controlled and the ultrasonic run time was measured (once more). For example, an increase of ca. 20% in the effective porosity (from 9.08 to 10.86%) and of ca. 5% in the ultrasonic velocity (from 3.39 to 3.58 km/s) was detected in the sample WGP 14–1. These small but effective physical changes in the streamed samples allow us to consider a rearrangement of the sandstone’s framework, such as the connection (or collapse) of isolated pore spaces or the compaction of grains in the matrix. This adjustment of elements in the sandstone’s fabric due to an anisotropic stress field can also be understood as plastic deformation, which leads

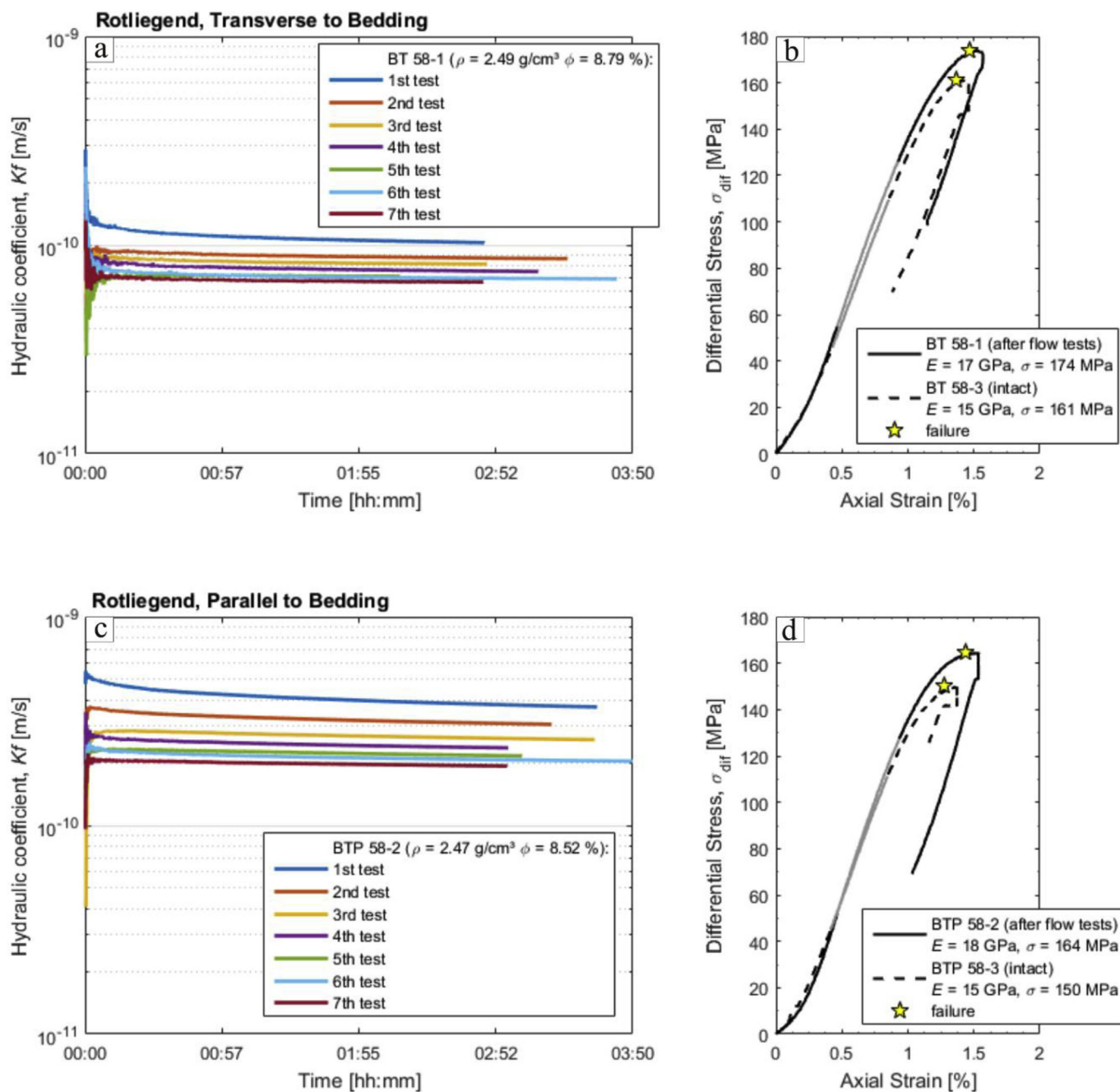


Fig. 19. Permeability curves for Rotliegend samples tested under 40 MPa of confining pressure and 16 MPa of pore pressure, with flow direction perpendicular (a) or parallel (c) to bedding. After the last test, the water-saturated weight and the ultrasonic run time of the streamed samples (BT 58–1 and BTP 58–2) were measured once more. These values are presented on b (BT 58–1) and d (BTP 58–2).

to an increase in porosity and decrease in permeability. Therefore, the linear relationship between effective porosity and permeability commonly observed for experiments under atmospheric conditions cannot be applied when considering pressure changes in the magnitudes of lithostatic stress conditions.

In order to investigate the influence of physical changes (effective porosity, density and ultrasonic velocity) on streamed samples, we carried out deformation tests up to stress fall under the same stress conditions as the flow tests ( $\sigma_3 = 40 \text{ MPa}$  and  $p_f = 16 \text{ MPa}$ ). Subsequently we compared these results to an intact sample from the same rock block, as presented in Figs. 18c, 19b and d. Streamed samples are deformed samples and have shown a higher modulus of deformability and maximal strength than intact rock specimens, which

suggests a more pronounced brittle behavior. The reason for this could be a consolidation effect caused during and by repeated loading in the sample. Moreover, this effect seems to act differently according to the bedding angle, as we can observe in the fracture pictures of the Rotliegend samples (Fig. 20). It is necessary to recall the radial displacement taking place during flow tests (Fig. 4a, black line), which reinforced the idea of a continuous process of deformation during non-critical, homogeneous triaxial stress conditions and doubted the limits of the classical elastic deformation theory for rocks.

As mentioned before, fracture patterns were visually evaluated considering the quantity of fissures and its geometry. As described by Healy et al. (2017), fractures and their pattern exert a fundamental influence on the mechanical and transport properties of rocks. As the

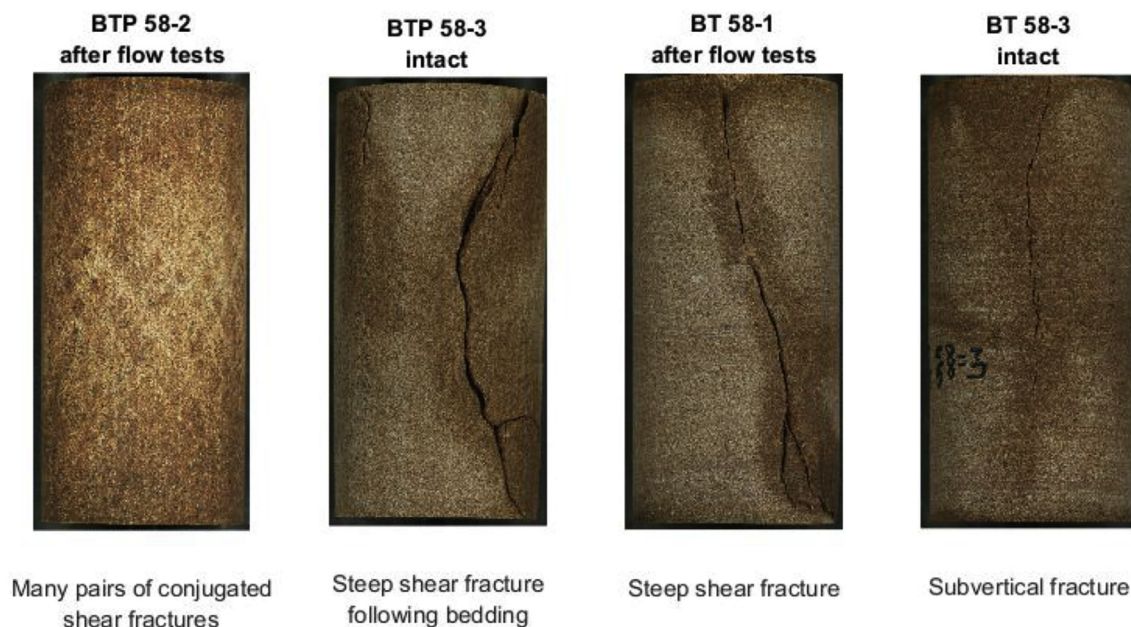


**Fig. 20.** Comparison of fracture pattern from streamed (BTP 58–2 and BT 58–1) and intact (BTP 58–3 and BT 58–3) Rotliegend rock specimens. Samples were drilled either transverse (BT) or parallel (BTP) to bedding. Test conditions are 40 MPa of confining pressure and 16 MPa of porefluid pressure.

development of fracture patterns is rarely random, an explanation for the two groups of figure patterns observed in Rotliegend samples is proposed. As observed in the charts of Figs. 8 and 10, a high level of porefluid pressure enhances fracturing. Why does a higher porefluid pressure level (e.g. 80%) enhance the development of a penetrative shear fracture, while a lower level (e.g. 40%) tends to form well-distributed, conjugated pairs of shear bands?

To answer this question, the following is listed. Connecting the relation between volume change, pore pressure level and their corresponding fracture pattern, it is to deduce that volumetric deformation driven by low pore pressure levels is more likely to be evenly distributed within the sample - especially in the matrix, leading to a parallel development of related shear planes, especially if a material with low effective porosity is considered. Samples investigated under low pore pressure compensate a more pronounced volumetric strain (Figs. 8 and 10, black lines). Increasing the porefluid pressure leads to a higher internal resistance, which counteracts to the compression pressure from the matrix and anticipates the dilatancy stage - and again dilatancy occurs earlier in rocks with low porosity values. In this case, the volumetric strain tends to settle on the main shear plane within the sample, leading to development of one penetrative steep shear fracture. For the Bunter Sandstone, the link between fracture pattern and pore pressure level is not easily discernible because of its high effective porosity (ca. 12%, Fig. 7a). Due to the mechanical contrast between matrix and pore spaces, the latter is considered a zone of weakness in which strain easily disseminates. Therefore, the fracture pattern observed in the Bunter Sandstone is often constituted by one main shear fracture with many smaller subordinate shear pairs. Considering the observations of Wong et al. (1997), the transition between different developments of failure may depend on the grain size and on critical effective pressure. Therefore, the reported findings are solely related to the here investigated materials.

However, there is the possibility of a continuous deformation process between both fracture developments, relatively similar to the diffuse bifurcation approach presented by Vardoulakis and Mühlhaus (1986). For rocks tested under uniaxial stress conditions, splitting would turn to shear bands due to the tensile stresses originated by diffuse bifurcation. The theory of diffuse bifurcation would explain the joint occurrence of a penetrative fissure with subordinate small pairs of

shear fracture, as observed in the samples WGP 11–3, BTP 55–5, BTP 55–1, BTP 57–4, BTP 55–4. However, the sequence of failure development is not clear enough for the Rotliegend samples tested under triaxial stress conditions. If both failure processes are related to each other, the turning point may depend on the dilatancy boundary, which, in turn, depends on the pore pressure level, anisotropy angle and on the physical properties of the medium.

## 5. Conclusion

In this study, three variants of triaxial compression tests were carried out in order to describe the dilatancy-induced permeability behavior of two hard sandstones: the grey Trendelburg Beds, a silica cemented subarkose Bunter Sandstone of Triassic Age (porosity of ca. 12%), and the red-brownish Rotliegend Sandstone (Bebertal), a carbonate and silica cemented sandstone of Permian Age, considerably less porous (ca. 6% of effective porosity) and less permeable ( $3.5 \times 10^{-10}$  m/s) than the Bunter Sandstone. As a conclusion of this study, the role of different pore pressure levels on the permeability evolution, fracture pattern and volume change for the investigated materials can be described, as well as some aspects on the relationship among permeability evolution, volumetric strain and physical properties. These findings are listed in the following:

- Anisotropy effects could be observed for both materials under atmospheric and lithostatic conditions. However, Bunter Sandstone and Rotliegend have an inverse anisotropic strength behavior, which may be caused by the differing influence of pore structure and matrix on the deformation.
- A compaction stage before increasing volume is not mandatory for a material undergoing triaxial compression. For a relatively porous medium, such as the Bunter Sandstone, porefluid pressure enhances dilatancy. For the low porosity Rotliegend, increasing pore pressure enhances a higher internal resistance, which favors the development of a compaction stage.
- The volume change in a porous medium is strain-sensitive and, similar to the permeability and filter velocity, can be favored or inhibited due to bedding angle. For both materials compaction and dilatancy stages were observed when applying the axial load parallel



to bedding. For the Bunter Sandstone, the dilatancy boundary is decently brought forward due to the anisotropy. Accordingly, increasing the confining pressure leads to an increase of both compaction and dilatancy stages.

- Increasing the pore pressure level leads to higher permeability and filter velocity. An open fluid flow system enhances the stiffness of the materials due to the development of a pressure gradient within the sample. The fracture permeability will vary according to the new arrangement of pore spaces and matrix accommodation of strain. At this point, Bunter Sandstone as well as Rotliegend differ from each other, again due to their inverted anisotropic behavior: they accommodate strain differently.
- Every pressure change will lead to a rearrangement of matrix and pore structure, changing the previous framework of the material. Deformation should be considered as a continuous process with different intensities of cracking, rather than to be classified under the concepts of elastic and plastic domains.
- Fracture patterns observed especially in the Rotliegend associate their development strongly with effective pressure. Low levels of pore pressure promote a more widely distribution of strain within the sample and build a network of many related shear bands. For the Bunter Sandstone, high levels of pore pressure anticipate the dilatancy boundary, therefore shortening the compaction stage and leading to a canalization of deformation on a main shear surface of the sample.

Altogether, this examination showed results about the volume change and on the permeability evolution of two hard sandstones and will be valuable due to its understanding of the combined effects of pore pressure change and pore space quality on the mechanical behavior of brittle rock masses. Further alternatives to pursue this investigation are e.g. a fourth experimental approach of flow anisotropy under hydrostatic conditions, and numerical modelling to find the porefluid pressure gradient within the sample during flow tests, regarding its structural anisotropy. Due to time limitations, an evaluation of microstructural crack damage is beyond the scope of the present study, although this is an interesting topic to be considered in future studies. Further investigations are being carried out to examine permeability evolution after consecutive events of fracturing.

## Acknowledgements

A special thank you goes to Professor Dr. Christof Lempp for his extremely positive collaboration and encouragement throughout this project. I am also pleased to acknowledge Dr. John Maximilian Köhne for his technical expertise and contribution to the permeability equation. Comments and discussion from Kristoff Svensson and Tom Huber were also much appreciated.

## Appendix A. Supplementary data

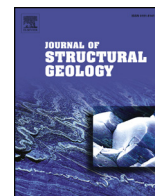
Supplementary data to this article can be found online at <https://doi.org/10.1016/j.petrol.2018.11.079>.

## References

- Alejano, L.R., Alonso, E., 2005. Considerations of the dilatancy angle in rocks and rock masses. *Int. J. Rock Mech. Min. Sci.* 42, 481–507.
- Alejano, L.R., Arzúa, J., Bozorgzadeh, N., Harrison, J.P., 2017. Triaxial strength and deformability of intact and increasingly jointed granite samples. *Int. J. Rocks Mech. Min. Sci.* 95, 87–103.
- Alkan, H., 2009. Percolation model for dilatancy-induced permeability of the excavation damaged zone in rock salt. *Int. J. Rock Mech. Min. Sci.* 46, 716–724.
- Arzúa, J., Alejano, L.R., 2013. Dilatation in granite during servo-controlled triaxial strength tests. *Int. J. Rock Mech. Min. Sci.* 61, 43–56.
- Bauer, J.F., Meier, S., Philipp, S.L., 2015. Architecture, fracture system, mechanical properties and permeability structure of a fault zone in Lower Triassic sandstone, Upper Rhine Graben. *Tectonophysics* 647–648, 132–145.
- Cook, N.G.W., 1965. The failure of rock. *Int. J. Rock Mech. Min. Sci.* 2, 389–403.
- David, C., Menendez, B., Zhu, W., Wong, T-f., 2001. Mechanical compaction, microstructures and permeability evolution in sandstones. *Phys. Chem. Earth Solid Earth Geodes.* 26, 45–51.
- DIN EN 1936 2007-02. Natural Stone Test Method – Determination of Real Density and Apparent Density, and of Total and Open Porosity. German version EN 1936, pp. 2006.
- Farrel, N.J.C., Healy, D., Taylor, C.W., 2014. Anisotropy of permeability in faulted porous sandstones. *J. Struct. Geol.* 63, 50–67.
- Fischer, C., Dunkl, I., von Eynatten, H., Wijbrans, J.R., Gaupp, R., 2012. Products and timing of diagenetic processes in upper Rotliegend sandstones from bebental (North German basin, parichim, formation, flechtingen high, Germany). *Geol. Mag.* 149 (5), 827–840.
- Förster, A., Lempp, C., 2014. Determination of states of stress in hard rocks: results of laboratory conducted finite deformation analysis. In: Perucho, Olalla, Jiménez (Eds.), *Rock Engineering and Rock Mechanics: Structures in and on Rock Masses – Alejano*. Taylor & Francis group, London 978-1-138-00149-7.
- Goodman, R.E., 1989. *Introduction to Rock Mechanics*, second ed. John Wiley & Sons, USA.
- Healy, D., Rizzo, R.E., Cornwell, D.G., Farrell, N.J.C., Watkins, H., Timms, N.E., Gomes-Rivas, E., Smith, M., 2017. FracPaQ: a MATLAB toolbox for the quantification of fracture patterns. *J. Struct. Geol.* 95, 1–16.
- Henningsen, D., Katzung, G., 2006. *Einführung in die Geologie Deutschlands*, vol. 6 Spektrum Verlag, Auflage.
- Jaegger, J.C., Cook, N.G.W., 1979. *Fundamentals of Rock Mechanics*, third ed. Chapman and Hall, London.
- Kim, B.-H., Walton, G., Larson, M.K., Berry, S., 2018. Experimental study on the confinement-dependent characteristics of a Utah coal considering the anisotropy by cleats. *Int. J. Rock Mech. Min. Sci.* 105, 182–191.
- Li, J., Wang, M., Xia, K., Zhang, N., Huang, H., 2017. Time-dependent dilatancy for brittle rocks. *J. Rock Mech. Geotech. Eng.* 9, 1054–1070.
- Luo, W., Qin, Y-p., Zhang, M-m., Wang, C-x., Wang, Y-r., 2011. Test study on permeability properties of the sandstone specimen under triaxial stress conditions. First international symposium on mine safety science and engineering. *Proc. Eng.* 26, 173–178.
- Means, W.D., 1976. *Stress and Strain*. Springer-Verlag, New York.
- Menezes, F.F., Lempp, C., 2018. On the structural anisotropy of physical and mechanical properties of a Bunter sandstone. *J. Struct. Geol.* 114, 196–205.
- Mitchell, T.M., Faulkner, D.R., 2008. Experimental measurements of permeability evolution during triaxial compression of initially intact crystalline rocks and implications for fluid flow in fault zones. *J. Geophys. Res.* 113.
- Naumann, M., Hunsche, U., Schulze, O., 2007. Experimental investigation on anisotropy in dilatancy, failure and creep of Opalinus Clay. *Phys. Chem. Earth* 32, 889–895.
- Neumann, A., Svensson, K., Menezes, F., Lempp, C., Pöllmann, H., 2018. Mineralogical Analyses of the Impact of CO<sub>2</sub> and Associated Compounds on Sandstone in the Presence of Formation Waters at Non-ambient Conditions.
- Oda, M., Takemura, T., Aoki, T., 2002. Damage growth and permeability change in triaxial compression tests of Inada granite. *Mech. Mater.* 34, 313–331.
- Ord, A., 1990. Mechanical Controls on dilatant shear zones. *Geol. Soc. Lond. Spec. Publ.* 54 (1), 183–192.
- Ord, A., 1991. Deformation of rock: a pressure-sensitive, dilatant material. *Pageoph* 137 N° 4.
- Pludo, D., Albrecht, D., Ganzer, L., Gaupp, R., Kohlhepp, B., Meyer, R., Reitenbach, V., Wienand, J., 2011. Petrophysical, Facies and mineralogical-geochemical investigations of Rotliegend sandstones from the Altmark natural gas field in central Germany. *Energy procedia* 4, 4648–4655.
- Pöllmann, H., Neumann, A., Menezes, F., Svensson, K., Lempp, C., Göske, J., Winter, S., 2017. Quartz habits and secondary pseudomorphs from secondary filled lenses in Triassic grey Wesersandstein. *Boletim do Museu de Geociências da Amazônia*(3) Ano 4.
- Rawling, G.C., Baud, P., Wong, T-f., 2002. Dilatancy, brittle strength, and anisotropy of foliated rocks: experimental deformation and micromechanical modelling. *J. Geophys. Res.* 107.
- Scholz, C.H., 1968. Microfracturing and the inelastic deformation of rock in compression. *J. Geophys. Res.* 73 (4).
- Sheldon, H.A., Ord, A., 2005. Evolution of porosity, permeability and fluid pressure in dilatant fault post-failure: implications for fluid flow and mineralization. *Geofluids* 5, 272–288.
- Sheldon, H.A., Barnicoat, A.C., Ord, A., 2006. Numerical modelling of faulting and fluid flow in porous rocks: an approach based on critical state soil mechanics. *J. Struct. Geol.* 28, 1468–1482.
- Tan, T.K., Shi, Z.Q., Yu, Z.H., Yang, W.X., 1989. Dilatancy, creep and relaxation of brittle rocks measured with the 8000 kN multipurpose triaxial apparatus. *Phys. Earth Planet. In.* 55, 335–352.
- Vardoulakis, I., Mühlhaus, H.B., 1986. Technical note: local rock surface instabilities. *Int. J. Rock Mech. Min. Sci.* 23 (5), 379–383.
- Weber, J., Ricken, W., 2005. Quartz cementation and related sedimentary architecture of the triassic Solling Formation, Reinhardswald Basin, Germany. *Sediment. Geol.* 175, 459–477.
- Wong, T.F., David, C., Zhu, W.L., 1997. The transition from brittle faulting to cataclastic flow in porous sandstones: mechanical deformation. *J. Geophys. Res.* 102, 3009–3025.
- Xu, P., Yang, S.-Q., 2016. Permeability evolution of sandstone under short-term and long-term triaxial compression. *Int. J. Rocks Mech. Min. Sci.* 85, 152–164.
- Zhao, X.C., Cai, M., 2010. A mobilized dilation angle model for rocks. *Int. J. Rock Mech. Min. Sci.* 47, 368–384.

Die zweite Arbeit bietet eine Einführung in das Thema „Anisotropie“ am Beispiel der Trendelburger Schichten aus der Sollingfolge des Buntsandsteines. Dieser Sandstein war auch gemeinsamer Untersuchungsgegenstand und Speichervertreter der am BMWi-CLUSTER-Projekt beteiligten Untersuchungspartner. Im aktuellen Manuskript wurde jedoch noch nicht auf die Wirkungen des CO<sub>2</sub>-Stroms eingegangen, vielmehr werden die möglichen Ursachen für die Entstehung anisotroper Effekte erläutert, sowie deren Entwicklung unter Berücksichtigung des effektiven Drucks und der Auswirkungen des Porenwasserdrucks. Für diese Arbeit wurden die Ergebnisse hinsichtlich Bruchfigur, Festigkeit (Scherparameter), Arbeit und Verformungsmodul betrachtet. Der Mitautor war durch fortgesetzte Diskussionen über Fragstellung und inhaltliche Abgrenzung beteiligt. Diese Arbeit wurde bei der 21. International Conference on the Deformation Mechanisms, Rheology and Tectonics (DRT 2017 in Inverness) vorgestellt und ist veröffentlicht unter dem folgenden Link zu finden:

<https://www.sciencedirect.com/science/article/pii/S0191814117303152>



# On the structural anisotropy of physical and mechanical properties of a Bunter Sandstone

Flora Feitosa Menezes\*, Christof Lempp

Engineering Geology, Institute for Geosciences and Geography, Martin-Luther-University Halle-Wittenberg, Halle, Germany



## ARTICLE INFO

### Keywords:

Anisotropic rocks  
Bunter Sandstone  
Triaxial testing  
Mechanical behaviour  
Fracture pattern  
Mohr-Coulomb failure criterion

## ABSTRACT

Studies of structural anisotropy of rocks contribute to the understanding of their mechanical behaviour variation in a broad spectrum of geological settings. In this work we characterise the lithological variation and the mechanical behaviour of the Trendelburg beds, a fine-grained subarkose from the Bunter Sandstone, with moderate effective porosity (10%) and low permeability (0.5 mD). Traditional triaxial compression tests were carried out with varying confining- and pore pressures in water saturated specimens (7 cm diameter × 14 cm length). Ultrasonic velocity, permeability, deformability, compressive strength, mechanical work and fracture pattern were determined in two directions of anisotropy (0° and 90°) with respect to bedding. Changing the angle of anisotropy leads to different reactions to the influence of lithological heterogeneities, which reaches a maximum when arranged parallel to  $\sigma_1$ . The Trendelburg beds has significant anisotropy effects, which tend to increase with effective pressure. The effects of a structural anisotropy due to bedding are associated with an anisotropy of physical properties, stress state, pore pressure and likely pore space distribution. Mechanical properties are direction dependent, however, the influence of lithological factors may diverge between both directions of anisotropy as pressure increases.

## 1. Introduction

Structural anisotropy due to bedding can be considered as a scale-invariant geological feature, on which deformation is strongly dependent. Anisotropic rocks are classified as such after the concept of strength anisotropy, meaning the variation of compressive strength according to the direction of the principal stresses (Goodman, 1989). This variation occurs due to parallel arrangements of minerals or cracks in crystalline igneous and metamorphic rocks, bedding in sedimentary rocks, or regularly interlayered materials, which are considered as planes of weakness within the rock (Ramsay and Huber, 1983; Rawling et al., 2002; Geng et al., 2016). Some well-known factors that may aggravate the strength anisotropy effect consist of layers of differing composition, the preferred alignment of inequant voids and pore fabric shape – all these factors enhance different degrees of compaction, competences and lead to mechanical instability (Ramsay and Huber, 1983; Louis et al., 2003; Benson et al., 2005; Baud et al., 2005; Bubeck et al., 2017; Heap et al., 2017; Griffiths et al., 2017). Former studies have shown a trend for peak stresses with a minimum between 30° and 60° of bedding orientation, and a maximum at 0° and 90° (Broch, 1983; Rawling et al., 2002; Baud et al., 2005). Considering the directions normal (0°) and parallel (90°) to the weakness planes as the most

important anisotropies, there is no convention in the literature where the strength should be the greatest.

Anisotropy in rocks is a well investigated issue in rock mechanics and has been a widely applied tool in geological environments. Vishnu et al. (2018) investigated the anisotropy of metabasalts emplaced by veins by means of uniaxial compression strength, point load test and magnetic susceptibility. They conclude that the variation in strength of the metabasalts has played an important role in channelizing fluids for emplacement of veins and mineralization. With regards to stability assessments of rock engineering: Bigdoli and Jing (2014) compared the anisotropy of joint clusters to intact core samples. They emphasized the scale effect in the anisotropy and concluded that for fractured rocks, properties obtained in a laboratory are not adequate for proper evaluation and design engineering projects, due to the irregular fracture system geometry of rock masses. Farrel et al. (2014) investigated permeability anisotropy in three orientations in faulted porous sandstones, considering them as an analogue material for water and hydrocarbon reservoirs. They observed that the maximum permeability is often parallel to a fault dip. Through the expansion of X-ray computerized tomography and modelling, the microanalysis of pore space geometry has been gaining much attention to evaluate anisotropy effects, as they are able to qualify geometrical attributes and spatial distribution of the

\* Corresponding author. Martin-Luther-Universität Halle-Wittenberg, Institut für Geowissenschaften und Geographie, Von-Seckendorff-Platz 3, 06120 Halle/Saale, Germany.  
E-mail addresses: [flora.menezes@geo.uni-halle.de](mailto:flora.menezes@geo.uni-halle.de), [flora.menezes@student.uni-halle.de](mailto:flora.menezes@student.uni-halle.de) (F.F. Menezes).

<https://doi.org/10.1016/j.jsg.2018.06.010>

Received 24 January 2018; Received in revised form 9 June 2018; Accepted 11 June 2018  
Available online 21 June 2018

0191-8141/ © 2018 Elsevier Ltd. All rights reserved.

pore space in a more detailed scale (Bubeck et al., 2017; Heap et al., 2017; Griffiths et al., 2017). In this work, we decided to investigate anisotropy effects on the mesoscale of the specimen, as an analogue procedure to evaluate interactions among matrix, pore space and saturating fluid in rock masses. No study so far has incorporated a characterization of the anisotropy effect in a mesoscale, by matching physical and mechanical properties of intact rock samples. Then we start this study by describing the Trendelburg beds, a greyish, subarkosic Bunter Sandstone of the Lower Solling Formation, in terms of ultrasonic p-wave velocity, hydraulic gradient of water permeability and unconfined compressive strength. Further, we carried out a systematic series of triaxial compression tests by considering the Bunter Sandstone as an analogue, host sedimentary rock in a compressional tectonic setting. We consider the two principal directions of anisotropy, normal ( $0^\circ$ ) and transverse ( $90^\circ$ ) to bedding. Modulus of deformation, shear parameters and mechanical work are presented as functions of anisotropy, effective porosity and effective pressure. The Trendelburg bed is markedly directional in its physical and mechanical behaviour, however, with different degrees of anisotropy. By increasing effective pressure, the influence of lithological variation on the mechanical response diverge between both directions of anisotropy. Anisotropy due to bedding is more likely to be related to an anisotropic pore space distribution rather than to a change in physical properties (e.g., absolute porosity and density values). Moreover, anisotropy is influenced by pore pressure and therefore affects deformation patterns.

## 2. Materials and methods

The Trendelburger bed belongs to the Lower Solling Formation, one of the most characteristic formations of Middle Bunter Sandstone exposed in the Reinholdswald Basin in Germany (Weber and Ricken, 2005). This sandstone is a greyish, fine-grained subarkose distinguished

by parallel bedding planes and distinctly porous layers (Fig. 1a). Pöllmann et al. (2017) described the Trendelburg beds as a typical triassic feldspathic sandstone containing secondary modified lenses with lower density, which are related to a replacement of halite by albite during diagenetic processes (Fig. 1b and c). Rock blocks were collected at the Fa. Bunk quarry, located in Bad Karlshafen (Germany).

A summary of densities and effective porosities of 94 rock samples drilled from 10 different blocks of Trendelburg beds (WG) are presented below (Fig. 2a). These properties were evaluated through dry and water-saturated masses of rock samples with a defined volume (ca.  $540\text{ cm}^3$ ), as suggested in German standards (DIN EN, 1936:2007-02). Regarding this chart, we recognize some blocks with a cloudy distribution of their samples (WG 1, 2 and 5), and other blocks with a positive linear tendency among their samples (WG 11, 12). Effective porosity and density could not be considered as a directionally influenced parameter, but in contrast to that, water permeability determined under room temperature and at low radial pressures (6 bar) displays a clear dependency towards structural anisotropy. Falling head permeability tests were carried out with a hydrostatic pressure of 0.6 MPa, at room temperature with a pressure difference of 2 bar between the top and bottom of the sample (German standards DIN-18130-1, 1998). Coefficients of water permeability (Kf) are presented as a function of porosity in Fig. 2b with respect to anisotropy angle. At the same effective porosity, permeability can be twice as much higher if the water flows parallel to bedding instead of transverse to it.

### 2.1. Preliminary investigation

In order to investigate directional anisotropy of the Trendelburger beds, rock specimens with 7 cm diameter and 14 cm length were drilled parallel ( $\parallel$ ) and perpendicular ( $\perp$ ) with respect to the bedding (Fig. 3). Due to the small size of the rock blocks obtained for this investigation,

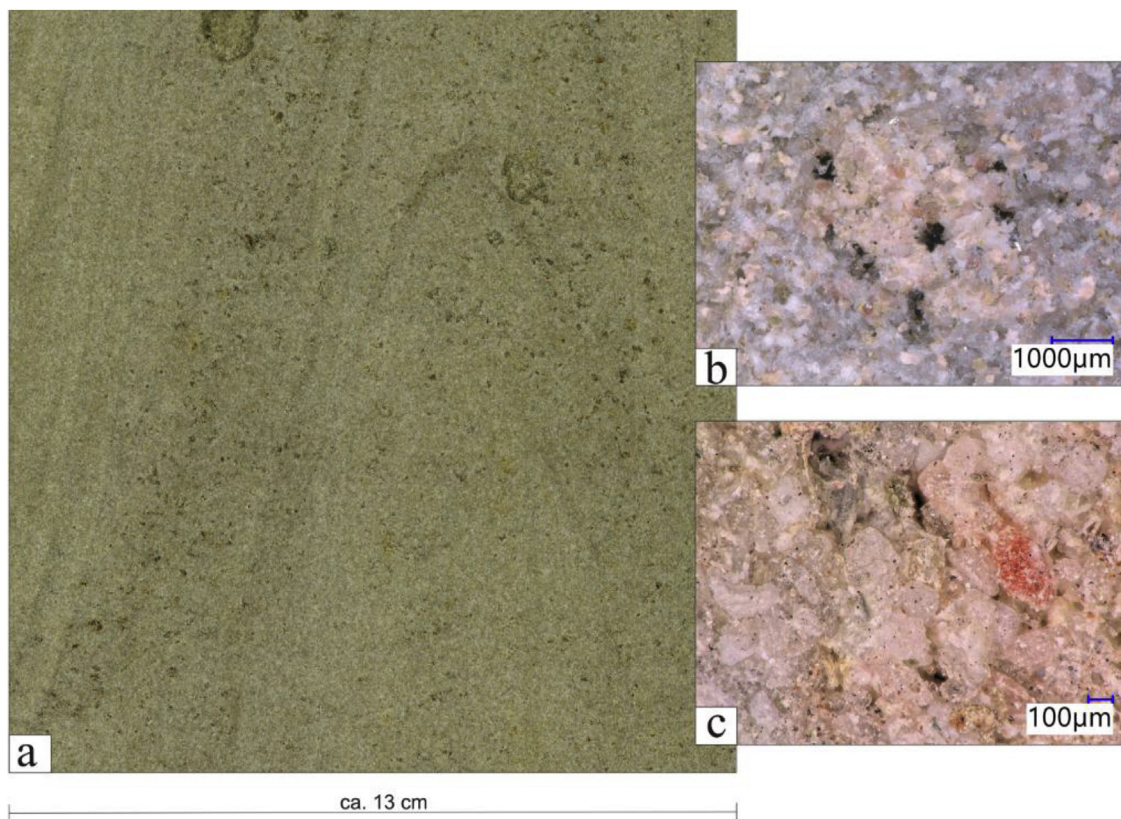


Fig. 1. The Trendelburg beds are a layered, fine-grained subarkose with different spatial distributions of pore spaces. A very characteristic feature of this material is the presence of half-filled elliptical pore spaces or lenses from variable sizes, shown here at core specimen scale (a) and under microscopic resolution (b). The matrix is siliciclastically cemented and consists mainly of sub-rounded grains (c). Pictures b and c were taken with a 3D microscope under reflected light.



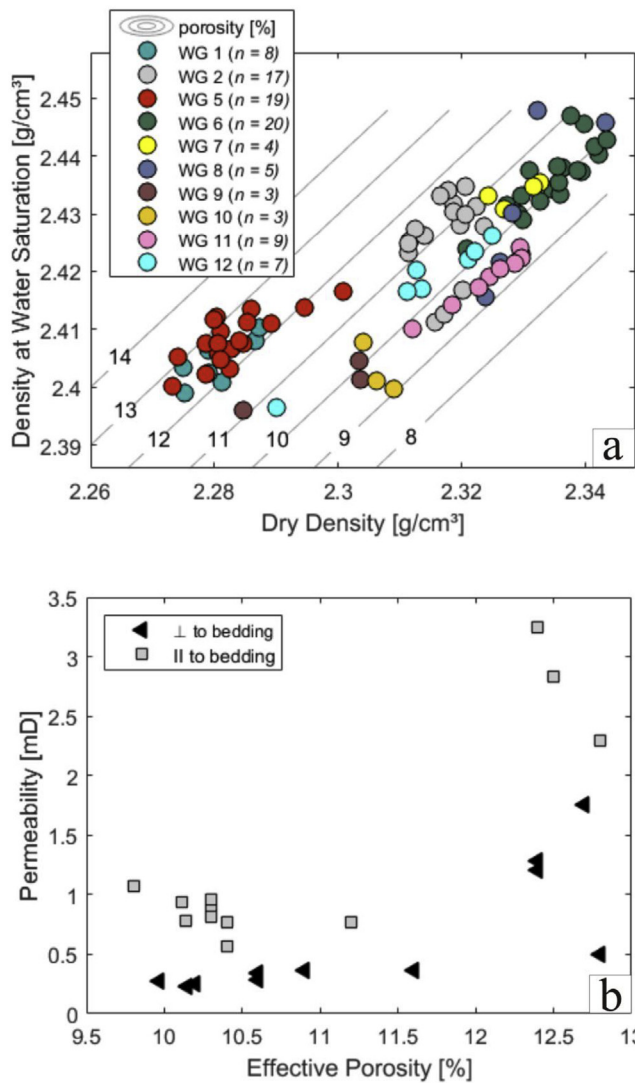


Fig. 2. In (a), density at water saturation is plotted against dry density for 94 samples from 10 different rock blocks of Trendelburg beds (WG). Effective porosity is represented as grey lines, which varies between 9 and 13.4%. In (b), permeability coefficient is a function of effective porosity with respect to the anisotropy angle: parallel (grey squares) and transverse (black triangles) to bedding.

core samples were just drilled for the two most important and easily to detect directions of bedding anisotropy (0 and 90°). Before carrying out any geomechanical experiments, the transmission time for P waves was measured for each sample with a low frequency ultrasound device, under room conditions (USME-C, resolution: 0.1 μs). The longitudinal ultrasonic wave velocity ( $V_p$  in km/s) could be evaluated along the sample's length, under dry and saturated conditions. Uniaxial compression tests were executed with 12 dry samples by using the same loading frame for triaxial tests, which is described below. For this test, six rock blocks of Trendelburger beds were investigated and for each block, two specimens for each orientation were tested.

### 2.2. Triaxial compression tests

Traditional triaxial compression tests were performed using a compression test machine for brittle materials, consisting of two pump units (for confining and pore pressures) and a loading frame with a maximal axial load of 5000 kN. The confining pressure is considered as the minor stress component, which is horizontally equal ( $\sigma_2 = \sigma_3$ ), and

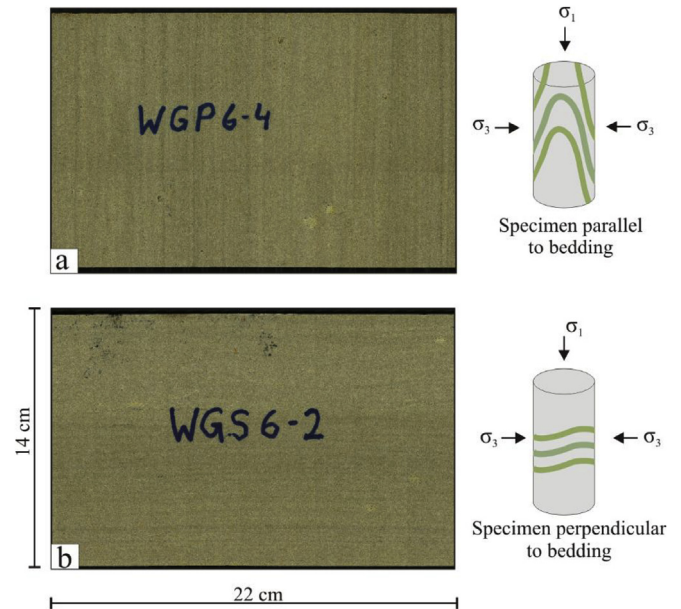


Fig. 3. Lateral surface of a cylindrical sandstone specimen drilled either perpendicular (WGP, in a) or transverse (WGS, in b) to bedding. Core samples have a diameter of 7 cm and length of 14 cm. Sketches on the right side illustrate the orientation of the axis of compression of a traditional triaxial compression test ( $\sigma_1 > \sigma_3$  and  $\sigma_3 = \sigma_2$ ) and the spatial representation of bedding (bold green lines). Pictures taken with a core sample scanner. (For interpretation of the references to colour in this figure legend, the reader is referred to the Web version of this article.)

the axial pressure corresponds to the major normal stress component ( $\sigma_1$ ). In addition to that, an internal and constant pore fluid pressure (pf) is applied in pore spaces of the rock specimen, by using distilled water as saturating fluid. Nineteen conventional triaxial experiments were carried out, with a constant confining pressure of 10, 15, 20, 25, 30, 35 or 40 MPa and a pore pressure of 6, 8, 9, 10, 12, 14, 15, 16, 18, 20, 21, 24, 28 or 32 MPa. Pore pressure was defined as “levels”, which are 40, 60 and 80% of  $\sigma_3$ . Each experiment was executed with both directions of anisotropy.

Before starting the test, the intact rock specimen had been fully water saturated. Tests were started under hydrostatic conditions by gradually increasing all pressures until the desired values of pore and confining pressures were reached. After pressure stabilization, the triaxial loading was initiated by increasing the axial pressure using a controlled rate of deformation ( $\dot{\epsilon} = 5.7 \times 10^{-6} \text{s}^{-1}$ ) up to peak stress. After reaching this point, a relaxation phase is carried out by controlling and hindering the displacement. Finally, mechanical loading is released back to isostatic conditions. These compression tests are described as continuous-failure-state-tests (multi-stage), which follow the recommendation procedures of the German Geotechnical Society (DGGT, 1987). After the experiment, specimens were photographed by using a core sample scanner (SmartCis 1000 E) to analyse the fracture pattern.

### 2.3. Evaluation of mechanical properties

From the data obtained from triaxial compression tests it was possible to evaluate the modulus of deformation, shear parameters (after Mohr-Coulomb failure criterion) and the mechanical work done up to failure. Modulus of deformation (or Young's modulus,  $E$ ) could be evaluated after Hooke's law as the elastic proportionality factor between differential stress and axial strain during loading. As suggested in the literature and recommended by the ISRM, the modulus of deformation was assessed between 30% and 60% of the stress peak of the stress-strain curve to avoid the influence of test start and early failure

behaviour (Marbler et al., 2015; Erickson et al., 2015; Alejano et al., 2017). Due to sandstones pronounced brittle behaviour, there was no considerable elastic lateral deformation during loading, which has made it impossible to evaluate the Poisson's ratio. Considering the deformation of sandstone in the domain of brittle deformation, it is usual to apply the Mohr-Coulomb failure criterion with effective pressures to evaluate effective shear parameters, namely cohesion ( $c'$ ) and friction angle ( $\phi'$ ). Results of stress peaks could be grouped by pore pressure level and presented on shear stress ( $q$ ) and effective middle or mean stress ( $p'$ ) space. Equations to calculate shear parameters by using shear and middle stress are presented in the literature (Bauch and Lempp, 2004; Alejano et al., 2017). For a better comparison between shear parameters obtained in different stress states, the uniaxial compressive strengths were recalculated by using effective cohesion and friction angle and presented as  $\beta_d$  (in MPa) (Eq. (1)).

$$\beta_d = \frac{2 \cdot c'}{\tan\left(45 - \frac{\phi'}{2}\right)} \quad (1)$$

Besides conventional mechanical rock properties, as the modulus of deformation and the uniaxial strength, we chose to evaluate mechanical work ( $W$ ). Mechanical work is defined as the amount of energy required from external forces to drive the deformation in a body of rock (Means, 1976). Thuro (1997) defines destruction work as a measurement for the quantity of energy, required for destruction of a rock sample, or the work necessary to build new cracks in rock. Therefore, it is a property which joins force and displacement by considering the deformation rate between them, and represents the work of shaping alteration. Mechanical work was evaluated as the area below the force-displacement or stress-strain curve, which could be evaluated using the trapezoidal method of surface measurement (Thuro, 1997; Reyer and Philipp, 2004).

### 3. Results

The physical and mechanical properties presented below were determined in laboratory, either in ambient or under triaxial stress conditions, considering two angles of anisotropy (parallel and transverse to bedding). Geomechanical experiments were carried out by using at least 50 intact rock specimens from eleven different rock blocks. In order to properly evaluate the influence of lithological variation and anisotropy, we executed a systematic series of triaxial tests with three levels of porefluid pressure (40, 60 and 80%). For evaluation purposes results were considered as an ensemble, a factor that could contribute to scattering of results. However, such lithological variation is very likely to occur even in the same rock block and therefore should be more representative when comparing the mechanical behaviour at different scales.

#### 3.1. Anisotropy under atmospheric conditions

Relationships between ultrasonic wave velocities and effective porosity are plotted for 94 samples on Fig. 4, with respect to the anisotropy angle (transverse as black triangles and parallel as grey squares). As mentioned before, each sample was measured twice, once in dry condition and afterwards under water saturation. The longitudinal wave velocity varies from 3.3 to 4.3 km/s under water saturation, and from 3.0 to 3.8 km/s under dry conditions (Fig. 4d). Louis et al. (2003) distinguish between matrix-related and void-related anisotropy by comparing dry and saturated acoustic measurements. Following this example, effective porosity is presented as a function of ultrasonic velocities (Fig. 4a and b). Here we observe a more clearly delimited cluster of anisotropy under dry conditions than under water saturation. However, a linear dependency between porosity and ultrasonic velocity is easily discernible under water saturation. In 3 charts of Fig. 4, in which all samples are shortened by the angle of anisotropy

(4a, 4b and 4c), we recognize the influence of the angle of anisotropy and of the lithological variation. A possibility to dissolve the effects of the anisotropy angle is to apply a ratio between both ultrasonic velocities ( $V_p \text{ max}/V_p \text{ min}$ ). This ratio makes it easier to compare different anisotropic samples with each other, and therefore to focus on the influence of the lithological variation of the different rock blocks (Fig. 4d).

Results of unconfined compression tests carried out on 12 dry samples from six different rock blocks are presented on Fig. 5. A considerable variation in the uniaxial compressive strength (UCS) can be observed either if the mean stress is applied parallel (from 89 to 149 MPa) or transverse (from 70 to 134 MPa) to bedding (Fig. 5a). Similarly, the modulus of deformation ( $E$ ) ranges from 20 to 24 GPa (grey squares) and from 16 to 20 GPa (black triangles), depending on the direction of anisotropy (Fig. 5d). To quantify the anisotropy of each block, an anisotropy ratio by means of uniaxial strength was evaluated (i.e., the ratio of strength parallel to perpendicular, under dry conditions). This ratio “ $r$ ” varies from 1.11 to 1.38 and can be considered as a low to middle anisotropic value, compared to the dry ratio of other sedimentary rocks presented by Broch (1983) (limestone 1.24; sandstone 1.09, arkosic sandstone 2.78, black shale 1.03). A last question to take into consideration is the relation between modulus of deformation ( $E$ ), mechanical work ( $W$ ) and strength to the effective porosity (Fig. 5c, d and 5e, respectively). As mentioned by Griffiths et al. (2017), porosity is known to exert a first-order control on the physical properties of rocks.

#### 3.2. Anisotropy under lithostatic conditions

Effective compressive strength ( $\sigma_1'$ ), mechanical work ( $W$ ) and work ratio of 38 samples (19  $\parallel$ , 19  $\perp$ ) are presented as a function of effective confining pressure ( $\sigma_3'$ ) in Fig. 6, with respect to the pore pressure level and anisotropy angle. Total and effective mechanical work were calculated by using the axial displacement recorded directly on the specimen through LVDT displacement transducers. The only difference between them originates in the effective mechanical work being evaluated with effective pressure. Therefore, the ratio between total and effective mechanical work shows us to what extent the pore pressure level is effective. In Fig. 6e and f, ratios below 1.15 are related to a low pore pressure level ( $0.4 \cdot \sigma_3$ ), whereas ratios between 1.15 and 1.35 are to mid and high pore pressure level ( $0.6 \cdot \sigma_3$  and  $0.8 \cdot \sigma_3$ ). Another remark to be included on these figures is the different slopes of the pore pressure levels. Although they increase linearly, the higher the level is, the more steep the slope gets.

Strain-stress curves, modulus of deformation and mechanical work are presented for selected experiments in Fig. 7, for both directions of anisotropy. In general, the Trendelburg beds have shown a strain-softening behaviour and typical brittle failure, as is usual for siliciclastic sandstones (Wong et al., 1997; Baud et al., 2015). Note that experiments carried out under the same effective confining pressure do not necessarily have to show similar results (Fig. 7a and e). In regard to the anisotropy, worth noting is not only the differing slope of both stress-strain curves, which is represented as modulus of deformation, but also the straightness (parallel to bedding) or the initial concave curvature (transverse to bedding) of the curve (Fig. 7d).

The mechanical behaviour of the Trendelburg beds is summarised in Fig. 8 in terms of strength (after Mohr-Coulomb failure criterion) and deformation (modulus of deformation), for both directions of anisotropy. Effective shear parameters (cohesion and friction angle) were evaluated according to pore pressure levels (40, 60 and 80%) and for comparison purposes, strength is represented as  $\beta_d$  (Fig. 8a and b). Transverse to bedding, a negative trend is observed between strength and pore pressure level, however no correlation can be established parallel to bedding. Fig. 8c displays effective deviator ratio ( $\sigma_1'/\sigma_3'$ ) as a function of effective confining pressure ( $\sigma_3'$ ), where both directions of anisotropy show an inverse relation to the effective pressure. Due to a

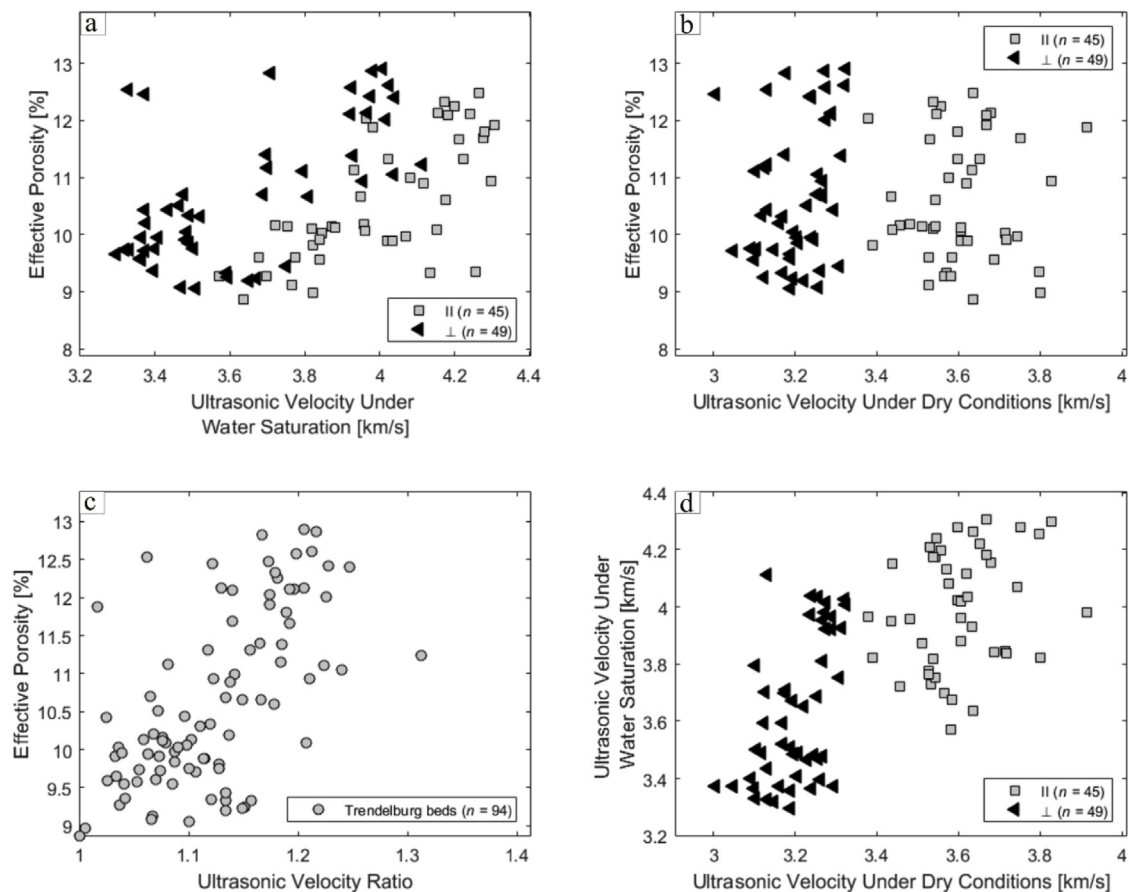


**Fig. 4.** Effective porosity and ultrasonic velocity of 94 rock specimens of Trendelburg beds with respect to the anisotropy angle; parallel (gray squares) or transverse (black triangles) to bedding ( $n$  is the number of samples). Effective porosity against ultrasonic velocity wave measured at water saturation (a) and under dry conditions (b). In (c), effective porosity is plotted as a function of ultrasonic velocity ratio, meaning the ratio between water-saturated and dry-wave velocities. In (d), the samples are compared to each other by means of ultrasonic velocities.

pore pressure increase, or more specifically by decreasing the effective pressure, the deviator ratio increases and the trends of parallel and transverse diverge from each other. In the next chart, modulus of deformation is presented as a function of shear stress in respect to the anisotropy angle (Fig. 8d). In general, samples drilled parallel to bedding have shown a more brittle behaviour (higher modulus of deformation) than samples drilled transverse to bedding.

### 3.3. Fracture pattern as a function of structural and lithological anisotropy

Materials tested under triaxial stress are expected to show a shear fracture that lies ca.  $45^\circ$  to  $\sigma_1$ . Pictures of the lateral surface of a specimen, taken with a core sample scanner, show how the fracture's geometry follows the bedding's boundaries (Fig. 9). For specimens drilled parallel to bedding, the fracture is well defined and penetrative along the bedding surface (Fig. 9 WGP 5–9), but for specimens drilled transverse to bedding the fracture is dispersive and spreads out of the bedding border (Fig. 9 WGS 5-5). Furthermore, a change of porosity due to bedding influences fracture patterns as well. In high porous layers – compared to its surroundings – the fracture density is higher than in the layers below and above (Fig. 9 WGS 6–11).

## 4. Discussion

Although many investigations have been already carried out about the effects of anisotropy in many types of rocks, there is not possible to find a general tendency or predictable behaviour about anisotropy effects in rocks. Anisotropy is strongly dependent on the physical

properties of the material, such as porosity and permeability, as well as on its framework, matrix and pore structure. Therefore we decided to delimit ourselves by investigating a certain type of sandstone (Trendelburg beds) with the two more important directions of anisotropy (parallel and transverse to bedding). Regarding our results concerning ultrasonic velocity and porosity, we can conclude that ultrasonic p-waves can travel up to 24% faster under water saturation than under dry conditions, as well as propagating up to 10% faster when applied parallel to bedding (Fig. 4a, b and 4d). We could point out a dependency between ultrasonic velocity ratio and effective porosity, so that the higher the effective porosity, the more permeable the specimen and the higher the difference between dry and water saturated conditions (Fig. 4c). These tendencies in terms of anisotropy coincide with previous studies on sandstones (Bentheim sandstone in Louis et al., 2003; Bunter sandstone in Heap et al., 2017). Under uniaxial stress conditions, the Trendelburg beds show a significant anisotropy in its behaviour despite its low anisotropy ratio (from  $\sim 1.1$  to  $\sim 1.4$ , Fig. 5a). Anisotropy of compressive strength (from 4 to 24%) and of modulus of deformation (from 13 to ca. 60%) has been higher when the bedding gets parallel to the major normal stress component (Fig. 5e and d). One possibility to explain strength and deformation anisotropy in porous media could be linked to the explanations from Bubeck et al. (2017), who describe the influence of pore shape on rock strength by means of uniaxial compression tests and found, that the strongest samples have spherical or oblate pores with the major axis parallel to the axis of applied compression.

Furthermore, a positive correlation was observed between modulus of deformation and uniaxial compressive strength (Fig. 5b), meaning

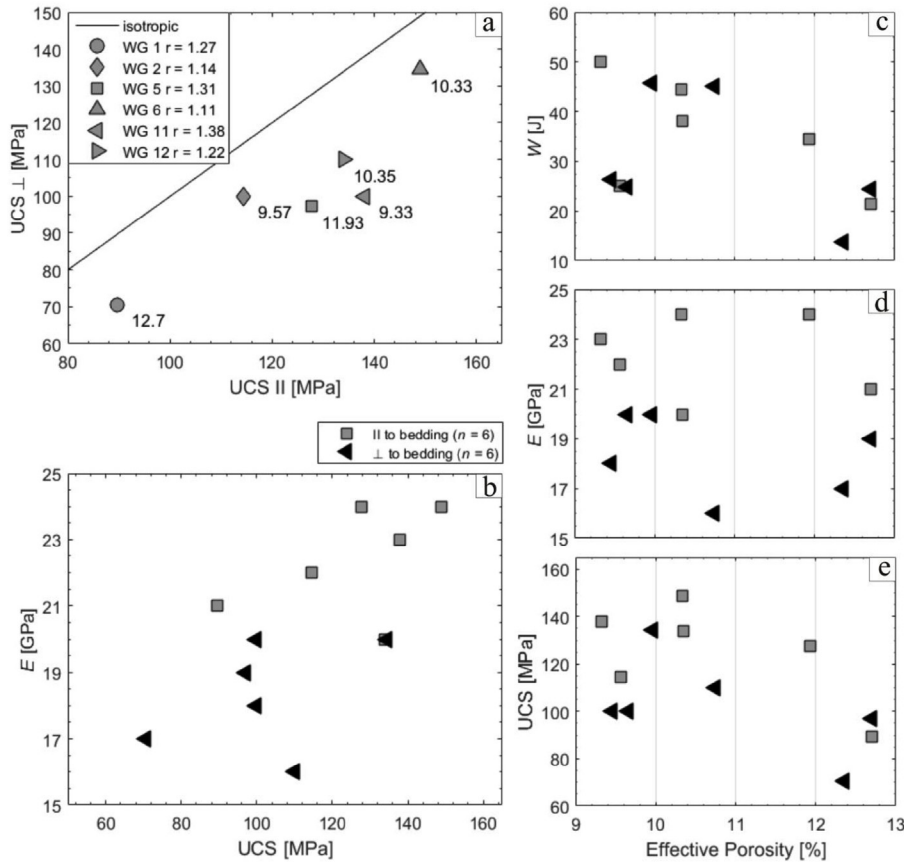


**Fig. 5.** Uniaxial compression strength (UCS), modulus of deformation ( $E$ ), mechanical work ( $W$ ), anisotropy ratio ( $r$ ) and effective porosity determined with 12 dry samples from 6 different rock blocks of Trendelburg beds. Anisotropy angle is represented either as gray squares (parallel to bedding) or as black triangles (transverse to bedding).

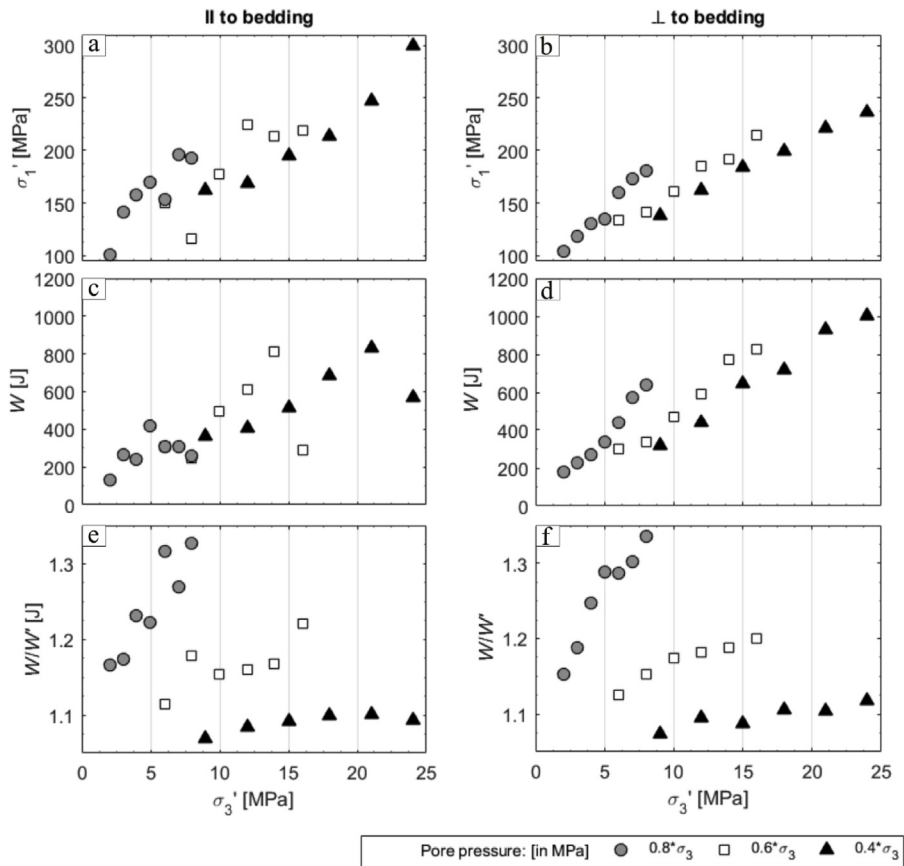


**Fig. 6.** Effective peak strength ( $\sigma_1'$ ), mechanical work ( $W$ ) and work ratio as a function of effective confining pressure ( $\sigma_3'$ ) for two directions of anisotropy (parallel on the left and perpendicular on the right). In all charts we recognize positive linear tendencies with different slopes clustered after the pore pressure level. Pore pressure level (in MPa) means 0.8, 0.6 or 0.4 times the value of total confining pressure ( $\sigma_3$ ).



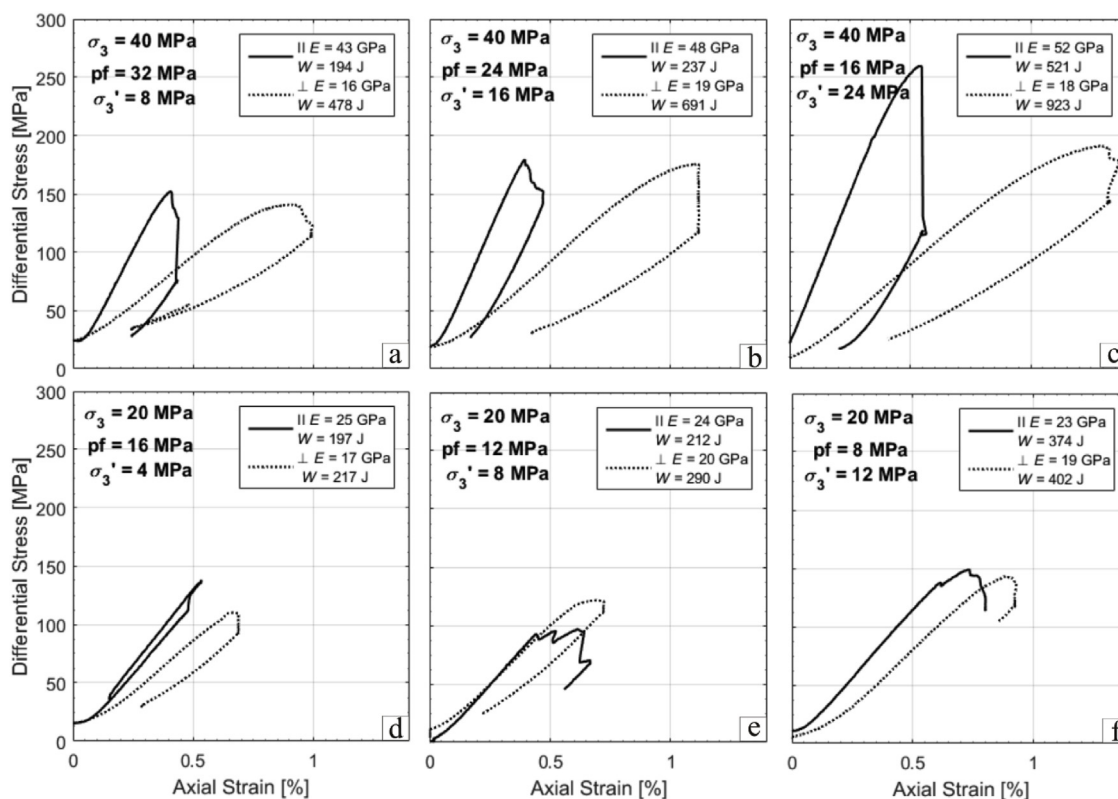


Fig. 7. Comparison of brittle behavior for samples tested under 40 MPa of confining pressure (a, b, c) or under 20 MPa (d, e, f). Pore pressure levels consist of 40% (c, f), 60% (b, e) and 80% (a, d). Modulus of deformation (E) and mechanical work (W) are given for both directions of anisotropy.

that the Trendelburg beds show a general tendency of increasing brittleness with strength. Porosity also seems to have an influence on these results, as a negative trend was observed for both directions of anisotropy by plotting mechanical work and strength as a function of effective porosity (Fig. 5c and e, respectively). These inverse correlations can be assigned to previous findings in the literature for e.g., volcanic rocks (Zhu et al., 2011), limestones and sandstones (Baud et al., 2014). Considering increasing porosity enhances crack spreading and dilatation, mechanical failure (or collapse) would be anticipated. However, there is a weak or non-existent relation between modulus of deformation and porosity (Fig. 5d), which could be a reason to believe in a restricted influence of porosity - or rather in a combined influence of voids and matrix on mechanical properties. Nevertheless, Thuro (1997) has shown a positive correlation of work and uniaxial compressive strength to porosity for hard rocks from the middle to upper Bunter sandstone, contradictory to the results present here. Ultrasonic velocity, uniaxial strength and modulus of deformation determined at atmospheric conditions have shown a large scattering, which can be associated to the differing occurrence of mineralogical or structural details in the various rock blocks. There may be layers of different thickness or porosity, the occurrence of cracks or veins of opaque minerals. Those contrasts are related to diagenetic processes and changes of boundary conditions during sedimentation and are typical for sedimentary rocks. As mentioned by Thuro (1997), this variety of geological phenomena cannot be put into figures and rock properties.

Under triaxial stress conditions, we are able to give general statements for both directions of anisotropy. Due to the strengthening effect of confining pressure (Jaeger and Cook, 1979), work, strength and modulus of deformation tend to increase with pressure (Figs. 6 and 7). Increasing pore pressure leads to earlier failure and decrease on strength and work, which illustrates the adverse interaction between pore- and confining pressures (Means, 1976). However, pore pressure level and work ratio have shown similar tendencies over effective

pressure and have equivalent effects on the mechanical properties. A lower strength requires less mechanical work exerted up to failure, so the difference between total and effective work increases (work ratio, Fig. 6a and f). The higher the work ratio, the higher is the influence of pore pressure on the mechanical properties, accordingly confirming the statement of a pore weakening effect (Zhu et al., 2011). In general, results obtained from samples drilled transverse to bedding are better correlated with effective pressure and mechanical properties, despite the fact that samples derived from different rock blocks (Figs. 6b, d, f and 8a). In this case, deformation due to triaxial stress seems to overcome the influence of lithological anisotropic agents. However, samples drilled parallel to bedding have shown bad correlations with states of stress (Figs. 6a, c, e and 8b). The reason for the different degrees of correlation between both directions of anisotropy may be due to the influence of lithologic particularities that enhance anisotropy effects (such as cracks, veins, pore space distribution and geometry). Such particularities may maximise their influence when arranged parallel to the major stress component ( $\sigma_1$ ).

Regarding anisotropy, the modulus of deformation and mechanical work have shown contrary tendencies (Fig. 7). Similar to uniaxial stress conditions, modulus of deformation has been higher when the major normal stress component was applied parallel to bedding, although considerably less mechanical work had been exerted in that direction (Fig. 7). This is compatible considering time being an implicit factor in the relationship between stress and strain. It is essential to note that our triaxial compression tests were displacement-controlled, carried out with the same rate of deformation. This implies that the axial strain on the x-axis is also a temporal-related parameter. Compared the axial strain needing to reach the peak stress in both directions, there is a faster stress-strain performance when applying loading parallel to bedding (Fig. 7). In this regard, modulus of deformation and mechanical work can be considered as linked properties to describe mechanical anisotropy. If we consider the increase of anisotropy in the modulus of

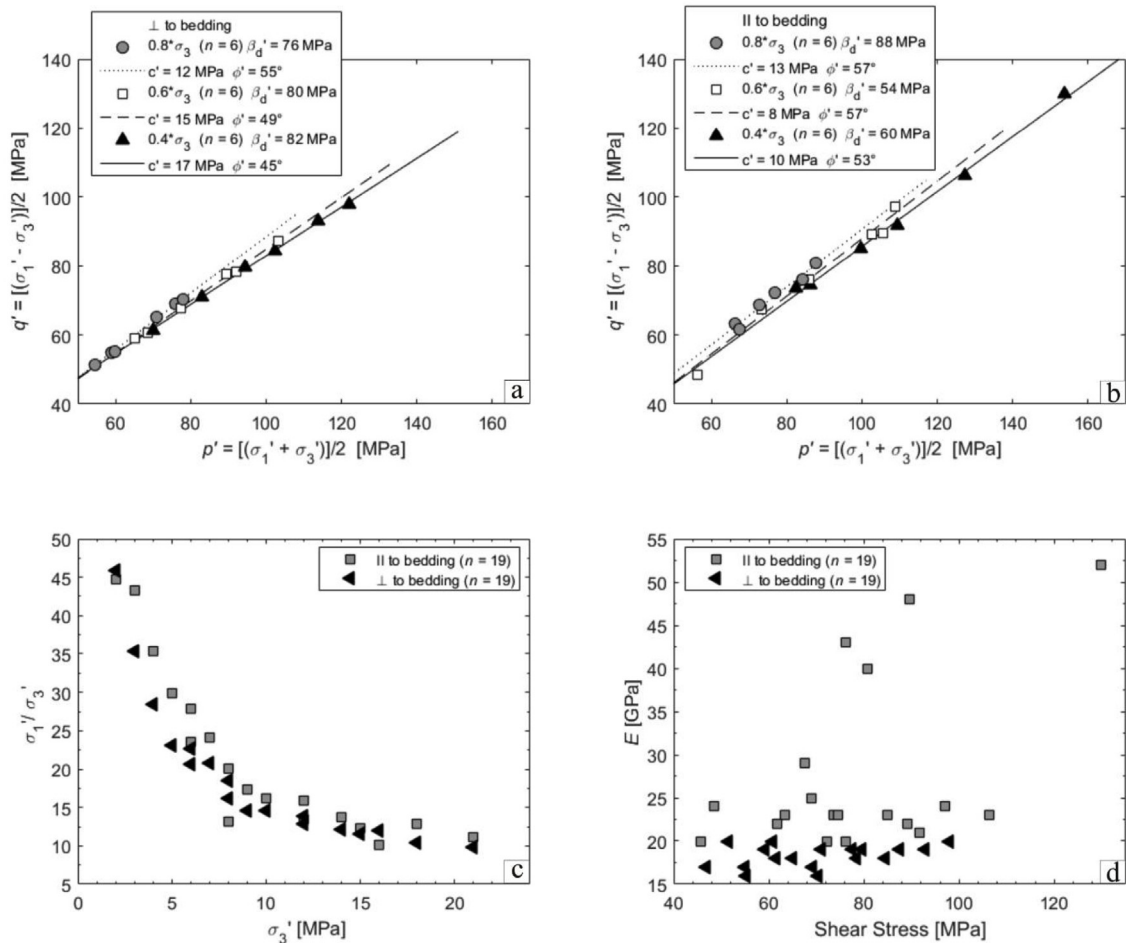


**Fig. 8.** Brittle failure envelopes after Mohr-Coulomb failure criterion represented in terms of effective middle stress (or radius of Mohr's circle,  $p'$ ) and shear stress (or center of Mohr's circle), for bedding transverse (a) and parallel (b) to major stress axis. An envelope is given for each pore pressure level (0.4, 0.6 and 0.8 of  $\sigma_3$ ). The effective uniaxial compressive strength ( $\beta_d$ ) could be calculated by using effective shear parameters, namely cohesion ( $c'$ ) and friction angle ( $\phi'$ ). In (c), brittleness is shown as the development of the effective deviator ratio (on the y-axis) over the effective lithostatic pressure ( $\sigma_3$ ). In (d), a graphical summary of all moduli of deformation determined under triaxial stress as a function of shear stress. In (c) and (d), the structural anisotropy is represented as parallel (gray squares) and transverse (black triangles) to bedding. Total confining pressure varies from 10 to 40 MPa and pore pressure from 6 to 32 MPa.

deformation (from  $\sim 1.2$  to  $\sim 2.8$ ) and in work (from  $\sim 1.1$  to  $\sim 2.9$ ) as a function of confining and pore-pressures (Fig. 7), we could assume that anisotropy effects tend to increase with effective pressure.

An indirect observation about volume change can be made by analysing the stress-strain curves on Fig. 7. The initial bending of these curves is traditionally attributed to the closure of micro-cracks during initial loading (Alejano et al., 2017). Therefore, the different appearances of the stress-axial strain curve may be evidence that structural anisotropy enhances different expressions of volumetric strain, in other words exerting an influence in the development of compression (volume decrease) and dilation (volume increase) domains. Further investigations on the Bunter sandstone are currently being carried out to provide a better understanding in the interaction between anisotropic dilatancy-induced permeability, and the analysis of residual mechanical properties and fabric reaction after reloading.

A substantial advantage of the investigation of anisotropy at core sample scale is the possibility to observe anisotropy effects in terms of fracture patterns. For the Trendelburg beds, we frequently observe pairs of oblique to the shortening direction, in shape of conjugating sets bisected by  $\sigma_1$ , corresponding to the description of shear-enhanced compaction bands as presented by Fossen et al. (2015), that fit the kinematics of a contractant regime. Moreover, the fracture pattern is highly affected by the direction of bedding and by the porosity of the layer (Fig. 9). The spatial clustering of subordinate joints, as seen on the

sample WGS 6–11 (Fig. 9), would suggest a porosity anisotropy due to different porous layers.

Considering another scale of observation, Louis et al. (2003) attributed the nature of anisotropic behaviour to the anisotropy of pore shape. Subsequently, Heap et al. (2017) corroborated this statement and related the presence (or absence) of permeability anisotropy to the shape of pores and grains, as well as to the nature of pore-filling materials. Although we did not carry any microscopic investigation so far, we observed that similar rock blocks with equivalent values of porosity and density (1 and 5, 2 and 12, on Fig. 2a), are nevertheless differently anisotropic on their strength, velocity and permeability. In other words, absolute changes of porosity or density could control the mechanical behaviour of rocks, but not their anisotropy. Thus it appears that structural anisotropy should be induced not only from physical factors but also from microstructural attributes, such as in the literature mentioned above (different arrangements or shapes of grains and pores in sandstone's framework). Louis et al. (2003) mentioned the matrix and the voids as the two principal features that enhance anisotropy in rocks, however a combination between both is also possible. Bearing in mind the wide range of compositions and structures in the Bunter sandstone, we cannot generalize the findings of this work to the whole formation. However, we can consider that the anisotropic behaviour in the Trendelburg beds is especially dominated by the shape and distribution of pore spaces, rather than by the matrix.

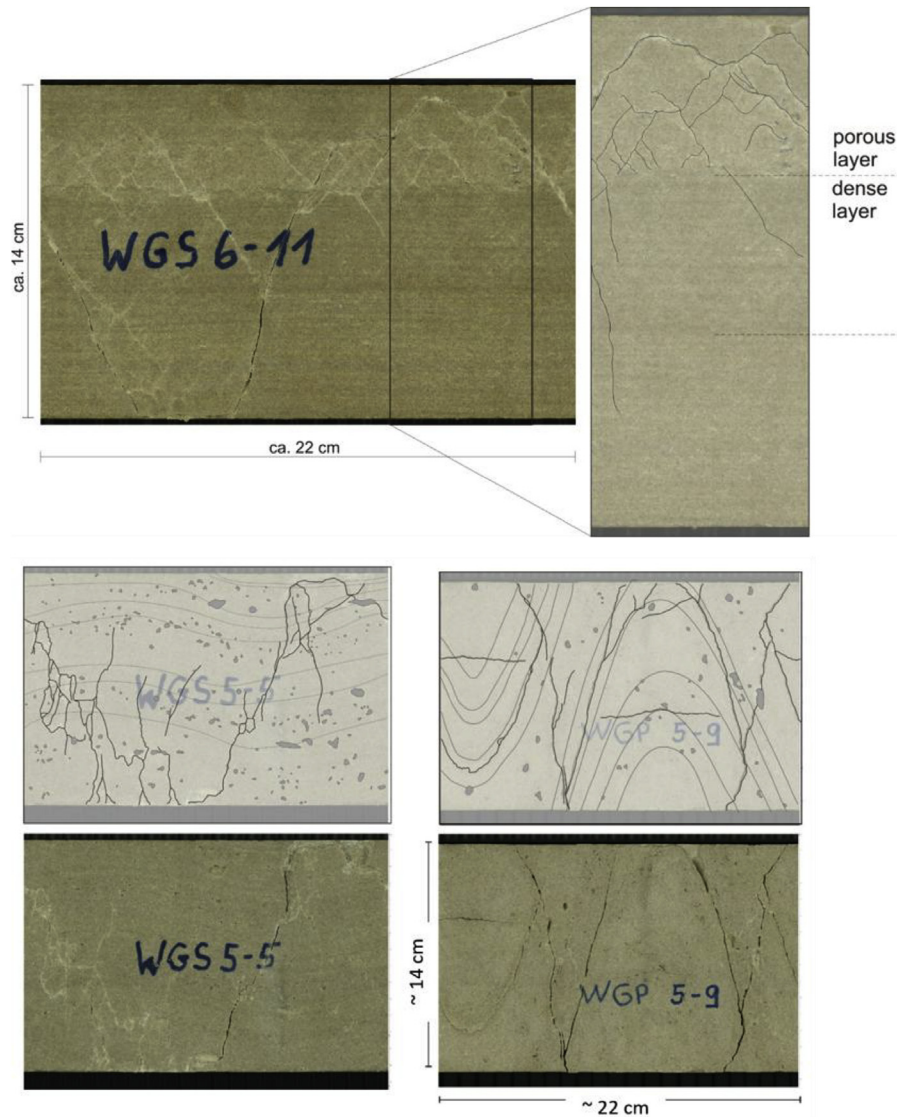


**Fig. 9.** Lateral surface of three cylindrical specimens with regard to their fracture pattern. WGS 6–11 (drilled transverse to bedding) shows a cluster of shear fractures on the more porous upper layer of the sample (test conditions  $\sigma_3 = 40$  MPa,  $p_f = 8$  MPa). WGS 5–5 and WGP 5–9 exhibit the influence of bedding on the development of fracture patterns. Details of the shear fracture, bedding and subordinate joints were emphasized after visual inspection. Pictures taken with a core sample scanner.

## 5. Conclusion

In this paper the effects of anisotropy on the Trendelburg beds are being analysed, a clearly layered subarkose sandstone with anisotropic layers, by taking into consideration two angles of anisotropy (parallel and transverse to bedding). By matching physical and mechanical properties evaluated under atmospheric and lithostatic conditions at core scale, we were able to conduct a comparative study on the anisotropy effects of a siliciclastic cemented Bunter Sandstone and to reach the following conclusions:

- Despite the low to middle anisotropy ratio ( $\sim 1.1$ – $\sim 1.4$ ), the Trendelburg beds show a significant anisotropy in ultrasonic velocity, permeability and uniaxial compression strength. Under atmospheric conditions, samples from different rock blocks may hardly be compared among themselves, as the anisotropy significantly differs.
- Shear parameters and modulus of deformation show that when applying loading parallel to bedding, the harder the sandstone turns correspondingly.
- Structural anisotropy could indirectly be observed as a time

depending property. Parallel to bedding, more force can be built up in a shorter period of time with less deformation and therefore spending less mechanical work up to failure.

- The influence of pore pressure as a weakening effect on the mechanical behaviour of the Bunter Sandstone could be observed for both directions of anisotropy. Moreover, the anisotropy effect increases at high pore pressure levels.
- In direction transverse to bedding, the influence of lithological variation and brittleness may be reduced by increasing effective pressure. However, the influence of lithological heterogeneities (cracks, void spaces, veins) may be maximised if they are arranged parallel to  $\sigma_1$ . As a consequence, the mechanical response in direction transverse to bedding could be better correlated with stress changes, which makes its behaviour more pleasant to foresee.

In conclusion, we found that the Trendelburg bed is markedly anisotropic in its behaviour, either in atmospheric conditions as well as under lithostatic stresses. The effects of anisotropy are influenced by pore pressure and tend to increase as effective pressure increases. However, the influence of lithological factors diverge between both directions of anisotropy as pressure increases. Lastly, anisotropy affects

deformation patterns. Further investigations are being carried out with the Trendelburg beds, in order to gain insights on its anisotropic behaviour considering its volumetric behaviour and permeability properties under triaxial stress conditions.

## References

- Alejano, L.R., Arzúa, J., Bozorgzadeh, N., Harrison, J.P., 2017. Triaxial strength and deformability of intact and increasingly jointed granite samples. *Int. J. Rock Mech. Min. Sci.* 95, 87–103.
- Bauch, E., Lempp, C., 2004. Rock Splitting in the Surrounds of Underground Openings: an Experimental Approach Using Triaxial Extension Tests, vol. 104. pp. 244–254.
- Baud, P., Louis, L., David, C., Rawling, G.C., Wong, T.F., 2005. Effects of bedding and foliation on mechanical anisotropy, damage evolution and failure mode. *Geol. Soc. Lond. Spec. Publ.* 245 (1), 223–249.
- Baud, P., Wong, T.-f., Zhu, W., 2014. Effects of porosity and crack density on the compressive strength of rocks. *Int. J. Rock Mech. Min. Sci.* 67, 202–211.
- Baud, P., Reuschlé, T., Ji, Y., Cheung, C.S., Wong, T.F., 2015. Mechanical compaction and strain localization in Bleurswiller sandstone. *J. Geophys. Res.: Solid Earth* 120 (9), 6501–6522.
- Benson, P.M., Meredith, P.G., Platzman, E.S., White, R.E., 2005. Pore fabric shape anisotropy in porous sandstones and its relation to elastic wave velocity and permeability anisotropy under hydrostatic pressure. *Int. J. Rock Mech. Min.* 42, 890–899.
- Bigdoli, M.N., Jing, L., 2014. Anisotropy of strength and deformability of fractured rocks. *J. Rock Mech. Geotech. Eng.* 6, 156–1654.
- Broch, E., 1983. Estimation of strength anisotropy using the point-load test. *Int. J. Rock Mech. Min. Sci. Geomech. Abstr.* 20 (4), 181–187.
- Bubeck, A., Walker, R.J., Healy, D., Dobbs, M., Holwell, D.A., 2017. Pore geometry as a control on rock strength. *Earth Planet Sci. Lett.* 457, 38–48.
- DGGT (Deutsche Gesellschaft für Erd- und Grundbau e.V.), 1987. Mehrstufentechnik bei dreiaxialen Druckversuchen und direkten Scherversuche, Empfehlung Nr. 12 des Arbeitskreises 19 – Versuchstechnik Fels. In: Technische Prüfvorschriften für Boden und Fels im Straßenbau. (TP BF-StB).
- DIN-18130-1, 1998. Baugrund – Laboratory Tests for Determining the Coefficient of Permeability of Soil – Teil 1: Laborversuche. Beuth Verlag, Berlin.
- DIN EN 1936, 2007-02. Natural Stone Test Method – Determination of Real Density and Apparent Density, and of Total and Open Porosity. German version EN 1936, pp. 2006.
- Erickson, K., Lempp, C., Pöllmann, H., 2015. Geochemical and geomechanical effects of scCO<sub>2</sub> and associated impurities on physical and petrophysical properties of Permian sandstones (Germany): an experimental approach. *Environ. Earth Sci.* 74.
- Farrel, N.J.C., Healy, D., Taylor, C.W., 2014. Anisotropy of permeability in faulted porous sandstones. *J. Struct. Geol.* 63, 50–67.
- Fossen, H., Zuluaga, L.F., Ballas, G., Soliva, R., Rotevatn, A., 2015. Contractual deformation of porous sandstone: insights from the Aztec sandstone, SE Nevada, USA. *J. Struct. Geol.* 74, 172–184.
- Geng, Z., Chen, M., Jin, Y., Yang, S., Yi, Z., Fang, X., Du, X., 2016. Experimental study of brittleness anisotropy of shale in triaxial compression. *J. Nat. Gas Sci. Eng.* 36, 510–518.
- Goodman, R.E., 1989. *Introduction to Rock Mechanics*, second ed. John Wiley & Sons, USA.
- Griffiths, L., Heap, M.J., Xu, T., Chen, C.-f., Baud, P., 2017. The influence of pore geometry and orientation on the strength and stiffness of porous rock. *J. Struct. Geol.* 96, 149–160.
- Heap, M.J., Kushnir, A.R., Gilg, H.A., Wadsworth, F.B., Reuschlé, T., Baud, P., 2017. Microstructural and petrophysical properties of the Permo-Triassic sandstones (Buntsandstein) from the Soultz-sous-Forêts geothermal site (France). *Geoth. Energy* 5 (1), 26.
- Jaeger, J.C., Cook, N.G.W., 1979. *Fundamentals of Rock Mechanics*, third ed. Chapman and Hall, London.
- Louis, L., David, C., Robion, P., 2003. Comparison of the anisotropic behavior of undeformed sandstones under dry and saturated conditions. *Tectonophysics* 370 (1–4), 193–212.
- Marbler, H., Erickson, K.P., Schmidt, M., Lempp, C., Pöllmann, H., 2015. Geomechanical and geochemical effects on sandstones caused by the reaction with supercritical CO<sub>2</sub>: an experimental approach to in situ conditions in deep geological reservoirs. *Environ. Earth Sci.* 69, 1981–1998.
- Means, W.D., 1976. *Stress and Strain*. Springer-Verlag, New York.
- Pöllmann, H., Neumann, A., Menezes, F., Svensson, K., Lempp, C., Göске, J., Winter, S., 2017. Quartz habits and secondary pseudomorphs from secondary filled lenses in Triassic grey Wesersandstein. *Boletim do Museu de Geociências da Amazônia* 3 Ano 4.
- Ramsay, J.G., Huber, M.I., 1983. *The techniques of modern structural geology*. In: *Strain Analysis Vol. 1* Academic Press, London.
- Rawling, G.C., Baud, P., Wong, T.F., 2002. Dilatancy, brittle strength, and anisotropy of foliated rocks: experimental deformation and micromechanical modelling. *J. Geophys. Res. Solid Earth* 107 (B10).
- Reyer, D., Philipp, S.L., 2004. Empirical relations of rock properties of outcrop and core samples from the Northwest German Basin for geothermal drilling. *Geotherm. Energy Sci.* 2 (1), 21.
- Thuro, K., 1997. Drillability prediction: geological influences in hard rock drill and blast tunnelling. *Int. J. Earth Sci.* 86, 426–438.
- Vishnu, C.S., Lahiri, S., Mamtani, M.A., 2018. The relationship between magnetic anisotropy, rock-strength anisotropy and vein emplacement in gold-bearing metabasalts of Gadag (South India). *Tectonophysics* 722, 286–298.
- Weber, J., Ricken, W., 2005. Quartz cementation and related sedimentary architecture of the triassic Solling Formation, Reinhardswald basin, Germany. *Sediment. Geol.* 175, 459–477.
- Wong, T.F., David, C., Zhu, W., 1997. The transition from brittle faulting to cataclastic flow in porous sandstones: mechanical deformation. *J. Geophys. Res. Solid Earth* 102 (B7), 3009–3025.
- Zhu, W., Baud, P., Vinciguerra, S., Wong, T.-f., 2011. Micromechanics of brittle faulting and cataclastic flow in Alban Hills tuff. *J. Geophys. Res.* 116.

Die dritte Publikation wurde mit den ersten geomechanischen Ergebnissen aus dem vom BMWi geförderten CLUSTER-Projekt erstellt. Hierbei soll die physikalisch-mechanische Wechselwirkung anhand anwendungsbezogener Aspekte der gesamten Prozesskette bei der CO<sub>2</sub>-Speicherung in geologischen Formationen veranschaulicht werden. Die physikalischen Gesteinsparameter und die makroskopische Beschreibung des beispielhaft gewählten Sandsteines konnten anhand von Prüfkörpern aus verschiedenen Gesteinsblöcken bestimmt werden. Für diese Untersuchung wurden von mir als Promovendin geomechanische Experimente und mikroskopische Untersuchungen an Sandsteinen durchgeführt. Die Themenstellung sowie die zunächst im Projekt vorgegebenen Fragestellungen basieren auf den von den Professoren Lempp und Pöllmann verfassten Projektantragsunterlagen. Die im Projekt vorgesehenen und in dem Manuskript einbezogenen ersten Untersuchungen und die dazugehörigen Probeherstellungen und mineralogischen Untersuchungen haben die Mitautoren A. Neumann und K. Svensson durchgeführt. Diese Arbeit wurde im September 2018 bei der International Association of Engineering Geology vorgetragen und ist veröffentlicht unter dem folgenden Link zu finden:

[https://link.springer.com/chapter/10.1007/978-3-319-93124-1\\_14](https://link.springer.com/chapter/10.1007/978-3-319-93124-1_14)

[https://link.springer.com/chapter/10.1007/978-3-319-93124-1\\_14](https://link.springer.com/chapter/10.1007/978-3-319-93124-1_14)



[https://link.springer.com/chapter/10.1007/978-3-319-93124-1\\_14](https://link.springer.com/chapter/10.1007/978-3-319-93124-1_14)

[https://link.springer.com/chapter/10.1007/978-3-319-93124-1\\_14](https://link.springer.com/chapter/10.1007/978-3-319-93124-1_14)

[https://link.springer.com/chapter/10.1007/978-3-319-93124-1\\_14](https://link.springer.com/chapter/10.1007/978-3-319-93124-1_14)

[https://link.springer.com/chapter/10.1007/978-3-319-93124-1\\_14](https://link.springer.com/chapter/10.1007/978-3-319-93124-1_14)

[https://link.springer.com/chapter/10.1007/978-3-319-93124-1\\_14](https://link.springer.com/chapter/10.1007/978-3-319-93124-1_14)



[https://link.springer.com/chapter/10.1007/978-3-319-93124-1\\_14](https://link.springer.com/chapter/10.1007/978-3-319-93124-1_14)

[https://link.springer.com/chapter/10.1007/978-3-319-93124-1\\_14](https://link.springer.com/chapter/10.1007/978-3-319-93124-1_14)

### 3. Schlussfolgerung

In diesem letzten Abschnitt werden nochmals alle Feststellungen der drei Veröffentlichungen kurz erläutert, um deren Wechselwirkung deutlich darzulegen. Als Leitfaden dient dabei der Einfluss des Porenraums auf das mechanische Verhalten des Rotliegend und des Buntsandsteines. Die experimentellen Ergebnisse werden mit einem entsprechenden Spannungszustand korreliert; dabei wird der Einfluss der Anisotropie betrachtet. Alle Ergebnisse beziehen sich auf die physikalischen Eigenschaften des Gesteines und sind wie dieses zu verstehen: Sie lassen sich zwar erklären und unter besonderen Randbedingungen korrelieren, sind jedoch tendenziell chaotisch und unvorhersehbar.

Die meisten der sedimentären Gesteine sind von Natur aus anisotrop – aufgrund verschiedener Faktoren, die auf das Gestein einwirken, aus der Zeit der Entstehung bis zur Diagenese, Deformation und zunehmender Überlagerung (bzw. Setzung) (Abbass et al. 2020). Anisotropie-Effekte unterscheiden sich aufgrund der Struktur oder durch lithologische Variabilität. Ersteres bezieht sich auf eine Variation der physikalischen und mechanischen Gesteinseigenschaften, die durch die Orientierung der Schichtung geprägt wird. Für die untersuchten Gesteine haben sich Eigenschaften wie die Ultraschallgeschwindigkeit, Verformbarkeit, maximale Scherspannung, Scherparameter, Volumenänderung, Permeabilität und sogar die Entwicklung der Bruchfigur als richtungsabhängig gezeigt. Dichte und Porosität werden zwar nicht von der Orientierung der Schichtung beeinflusst, sind also nicht richtungsabhängig, dennoch sind sie maßstababhängige Parameter, also von der Größe des betrachteten Bereiches abhängig (3. Publikation, Abb. 2 links).

Die Anisotropie wird nicht nur durch eine planare Struktur verursacht, wie z.B. die Schichtung, sondern auch durch den natürlichen lithologischen Kontrast (z. B. Wechsel in der Korngrößenverteilung, heterogene Porenraumverteilung, Klüfte, Adern, Zementierungsgrad) zwischen abgelagerten Schichten. Solche lithologischen Heterogenitäten können sich ebenfalls als planare Struktur kenntlich machen und daher als anisotropes Element auswirken. Am Beispiel des Buntsandsteines werden solche Strukturen deutlich hervorgehoben, wenn sie parallel zur Hauptspannungsrichtung angeordnet sind. Daraus folgt, dass die Einschätzung der Bedeutung der Verhaltenstendenz eines Sedimentgesteins wegen dieses Anisotropieeinflusses erschwert wird. Anisotropie-Effekte, die durch einen physikalischen Kontrast zwischen den Schichten erzeugt werden, sind besonders abhängig vom jeweiligen Maßstab (2. Publikation, Abb. 9 oben). Daraus ergibt sich die Notwendigkeit, eine reichliche Menge

Untersuchungsmaterial zu sichten, um einen angemessen breiten Überblick über physikalische und mechanische Eigenschaften des Gesteines zu erhalten.

Durch den Vergleich zweier fein- bis mittelkörniger, silikatisch gebundener Sandsteine wurde veranschaulicht, dass der anisotrope Charakter eines Gesteins nicht von absoluten physikalischen Eigenschaften bestimmt, sondern von der gesamten internen Struktur des Gefüges beeinflusst wird. Der Winkel, bei dem solche Parameter den am stärksten ausgeprägten Charakter zeigen, hängt mit der Gestalt des Porenraums und dessen Beschaffenheit zusammen. Anisotropie ist demzufolge eine kontinuierlich veränderliche Eigenschaft innerhalb der Probe (bzw. der Formation) und wird nicht mit einem absoluten Wert, Modul oder Verhältnis ausreichend charakterisiert. Hierfür können wir als Beispiel die Ergebnisse der einaxialen Kompressionsversuche anführen (1. Publikation, Abb. 7a und 7b). Trotz des Porositätskontrasts innerhalb des Buntsandsteins, haben alle untersuchten Blöcke dieser Formation unter einaxialen Spannungsbedingungen den gleichen anisotropen Charakter gezeigt, genauer gesagt, die Zunahme der Festigkeit bei paralleler Anordnung der Schichtung zur mechanischen Beanspruchung (2. Publikation, Fig. 7d). Obwohl beide untersuchten Sandsteine eine „geogenetisch“ angelegte Anisotropie aufweisen, wirkt sich dies durch die interne Struktur des Gefüges unterschiedlich aus.

Im Rahmen dieser Arbeit wurden zwei Fluide zur Sättigung des Porenraumes und als Medium zum Porendruckaufbau angewendet: Einerseits destilliertes Wasser (bei Raumtemperatur) und andererseits flüssiges  $\text{scCO}_2$  (bei  $50^\circ\text{C}$ ). Sollte dieses Fluid mit dem Wirtsgestein in Reaktion kommen, dann ergibt sich ein neuer Einflussfaktor auf dessen mechanisches Verhalten, d. h. die Reaktion zwischen Gestein und Fluid kann das mechanische Verhalten ebenfalls ändern. Dies wurde hier als „induzierte Anisotropie“ bezeichnet und bedeutet lediglich eine verstärkte Auswirkung bereits vorhandener anisotroper Elemente, die durch Reaktionszeit, Temperatur und effektiven Druck beeinflusst werden. Aufgrund der physikalischen Eigenschaften des Gesteins (v.a. Porosität, Durchlässigkeit, Durchströmungsrichtung) kann diese induzierte Anisotropie allerdings begrenzt ausgeprägt sein. Daraus folgt, dass die induzierte Anisotropie sowohl einen strukturellen, als auch einen lithologischen Charakter besitzt, da das Fluid auf verschiedene Schichten unterschiedlich reagiert. Eine induzierte Anisotropie wurde bei den langzeitigen mechanischen Experimenten zwischen Buntsandstein und  $\text{scCO}_2$  beobachtet (3. Publikation).

Die Porosität ist ein sehr wichtiger Einflussfaktor bei der Streuung der lithologischen Parameter, besitzt aber allein keine ausschlaggebende Auswirkung auf das geomechanische Verhalten des Gesteins. Wie beim Buntsandstein gezeigt wurde, weisen die Zunahme der



effektiven Porosität und die Verminderung der Festigkeit nicht unbedingt ein proportionales Verhältnis auf (2. Publikation, Abb. 5e und 5d, 1. Publikation, Abb. 7d). Ein gewisser Anteil der effektiven Porosität bietet einen „Freiraum“, der die Verdichtung des Materials während der Kompression ermöglicht, ohne das Korngerüst dabei erheblich umzustrukturieren. Je höher die Porosität eines Gesteins ist, desto höher ist die Wahrscheinlichkeit einer guten Vernetzung des Porenraums. Ist dieser Anteil an Freiraum zu klein, oder ist die Vernetzung des Porenraums sehr begrenzt, dann findet eine nur reduzierte oder gar keine Verdichtung statt. Dies führt zu einer frühen Strukturänderung des Korngerüsts, gefolgt vonzeitigem Versagen des Materials, wie dies bei dem Beispiel Rotliegend zu sehen ist.

Der Porenraum des Rotliegend hat einen untergeordneten Einfluss auf die gesamte Verformbarkeit des Gesteins, im Vordergrund stehen die Matrix und die „geogenetisch“ angelegte Anisotropie. Besonders ist hier die Anisotropie hervorzuheben (1. Publikation). Aufgrund der niedrigen, effektiven Porosität und der schlechten Konnektivität im Porensystem des Rotliegend ist eine Volumenabnahme (auch als Kontraktanz oder Volumenkompression bezeichnet) unter lithostatischen Bedingungen nicht zwingend erforderlich. In diesem Fall spielt der effektive lithostatische Druck eine besondere Rolle: Ein zunehmender Porendruck führt zu einem höheren Innenwiderstand im Porenraum, welcher die Steifheit der Matrix abschwächt. Dadurch ist die Entwicklung einer Volumenabnahme bei niedrigem effektivem Druck begünstigt (1. Publikation, Abb. 10). Diese Wechselwirkung zwischen physikalischen Eigenschaften und mechanischem Verhalten wird noch deutlicher bei dem Vergleich zwischen Buntsandstein und Rotliegend (1. Publikation, Abb. 8 und 10). Durch die gute Porenkonnektivität des Buntsandsteines ist die klassische Volumenänderung mit Kontraktanz und Dilatanz immer sichtbar – und zwar für beide Haupt-Richtungen der Anisotropie.

Hierbei ergeben sich Übereinstimmungen mit Laborergebnissen früherer Studien. Dilatanz sollte generell als Funktion des Manteldruckes und des Gesteinszustandes betrachtet werden, und ist nicht mit Festigkeitskennwerten zu korrelieren (Kim et al. 1997). Der physikalische Zustand eines Gesteines unter lithostatischem Druck ist prinzipiell kein genau erfassbarer Zustand, sondern eine stetige Anpassung des Gefüges an die Randbedingungen. Demzufolge ist die An- oder Abwesenheit einer Kompression des Porenvolumens (mit Volumenabnahme = Kontraktanz-Phase) relevant als Vorstufe für die Entstehung zukünftiger Trennflächen und für die Durchlässigkeitsentwicklung. Während der Kontraktanz-Phase kollabieren Poren und Mikrorisse entstehen, sodass diese Phase eine plastische Änderung des Gefüges hervorruft.

In dieser Arbeit sind die beobachteten Trennflächen im Bereich der spröden Verformung einzuordnen. Eine spröde Gefügereaktion lässt sich im Wesentlichen in Form von Scherflächen bzw. Scherrissen beschreiben. Häufig werden zur Beschreibung auch die Begriffe „Risse“ und „Scherbänder“ verwendet. Wie ausgeprägt diese Scherstruktur durch die Probe ist, steht in Zusammenhang mit der Konzentration an Verzerrung in einer bevorzugten Orientierung (Cox & Scholz, 1988). Zu dieser ursprünglichen Überlegung „warum bilden sich Scherbänder überhaupt?“ sind Gudehus & Karcher (2007) ebenfalls gekommen und stellten fest, wie die Scherung sich in eingegrenzten, fraktal verteilten Bereichen von Abschiebungen und antithetischen Scherflächen konzentriert.

Wenn man die Strukturmuster von Rotliegend und Buntsandstein Proben aus den Triaxialversuchen miteinander vergleicht, wird klar, dass die lithologischen Eigenschaften und deren Anisotropie eine wesentliche Rolle spielen (2. Publikation, Abb. 9 und 1. Publikation, Abb. 13 und 14). Bezüglich dieser Verteilung von Rissen in porösen Medien sind Cox & Scholz (1988) zu ähnlichen Schlussfolgerungen gekommen, allerdings beschränken sie sich auf den Einfluss der Lithologie. Durch den Vergleich zwischen Kalkstein und Granit stellten sie fest, dass Korngrenzen als potentielle Rissansatzstellen wirken, besonders bei wenig zementierten Gesteinen. Aus mechanischer Sicht ist der Granit härter, nimmt mehr Energie auf und teilt diese in Form komplexer Scherbänder auf. Dagegen ist der Kalkstein spröder, wobei die Risse länger werden und sich weniger miteinander vernetzen. Allerdings sind Entstehung und Wachstum spröder Trennflächen nicht nur materialabhängig, sondern auch spannungsbedingt und anisotrop. Des Weiteren sind sie kaum zufällig. Ein Material darf unterschiedliche mechanische Verhaltensweisen aufweisen, je nach Spannungszustand, in dem es sich befindet – schließlich ergeben sich daraus unterschiedliche Strukturmuster (Risse und Scherbänder).

Die hier präsentierten Ergebnisse bezüglich der Durchlässigkeit unterstützen die Idee, dass unter lithostatischen Spannungsbedingungen eine stetige Neuordnung von Porenraum und Matrix im Sandstein gefördert wird, die irreversibel ist (1. Publikation, Abb. 4, 18, 19). Wie entwickelt sich eine so kontinuierliche Umgestaltung des Gefüges und welche Folgen ergeben sich daraus in späteren, modifizierten Zuständen? Wie bei Mandelbrot (1982) beschrieben, wird selbst eine homogene Spannungsverteilung zu einer fraktalen Form zerstreut. In einem konventionellen Kompressionsversuch wird eine gleichmäßige Verteilung des Manteldrucks (auf der lateralen Oberfläche) und der Axialspannung (auf der oberen und unteren Fläche) stattfinden, aber es bleibt unbestimmt, wie die vorliegende Gesteinsstruktur der Probe mit ihrer vorgegebenen Porenraumstruktur und –verteilung auf die gewählten äußeren Einwirkungen reagiert, die durch die Außenflächen begrenzt sind.

Elemente, die diese fraktale Verteilungsgeometrie in Sandsteinen beeinflussen können, werden nicht nur von den Eigenschaften des Gesteins (z.B. Poren, Körner, Korngrenze, Zement, Risse, Anisotropie) und den Randbedingungen des Spannungszustandes bestimmt, sondern hauptsächlich durch deren Wechselwirkungen, die während der Einwirkung laufend modifiziert werden. Diese Wechselwirkung ist deshalb so umfangreich wie die Randbedingungen selbst und wird im Spannungsfeld kontinuierlich geändert. Das zu definierende strukturelle Muster des aktuellen Zustandes ist implizit als Ursache des nächsten Strukturzustandes zu bezeichnen, wenn die Einwirkung fortgeführt wird. Eine durch elastische Veränderung des Spannungszustandes hervorgerufene Veränderung der Gefügestruktur lässt sich unter lithostatischen Druckbedingungen nicht experimentell nachweisen (1. Publikation, Abb. 4).

Eine ähnliche Meinung über den Charakter der Deformation teilt Kolymbas et al. (2016), bei der das Versagen von Feststoffen eher als Prozess statt als Zustand zu erkennen ist. Dafür benutzt er den Begriff „progressiver Bruch“, welcher für die hier vorliegende Arbeit als eine besonders treffende Definition anzusehen ist. Ord & Hobbs (2010) verstehen diese Wechselwirkung als eine Art Konkurrenz, die zwischen Verzerrungstensor und der dazugehörigen Diffusionsdichte stattfindet – schließlich ergeben sich ebenfalls unterschiedliche Kluftscharen und -muster.

In der vorliegenden Arbeit wurde festgestellt, dass das Verhältnis zwischen Poren- und Manteldruck eine wichtige Rolle bei der Strukturmusterbildung innerhalb der Probe spielt. Diese Wechselwirkung konnte bei dem Rotliegend, aufgrund seiner niedrigen effektiven Porosität und der sehr begrenzten Durchlässigkeit am besten dargestellt werden. In diesem Fall fördern niedrige Porendruckverhältnisse eine breitere Verteilung der Verzerrung innerhalb der Probe und bilden ein Netzwerk aus vielen konjugierten Scherflächen, das von Vardoulakis (1984) als Scherbandbildung bezeichnet wird. Bei hohen Porendruckverhältnissen wird die Verzerrung auf einer mittleren Hauptscherfläche konzentriert. In dem Buntsandstein wurden weniger Varianten von Riss- oder Kluftmusterbildungen erkannt; die Bruchfiguren bestehen häufiger aus einer Hauptscherfläche mit mehreren vernetzten und dazu untergeordneten Scherflächen, teilweise mit verkeilten Enden. Für dieses Material gilt wiederum eine klassische Abhängigkeit von Festigkeit, Volumenänderung und Durchlässigkeit zum Porendruck (2. Publikation). Zunehmender Porendruck führt zu einem früheren Kollaps der Struktur und entsprechend zu niedrigerer Festigkeit (2. Publikation, Abb.6a, 6b und 8a) und weniger Volumenänderung (1. Publikation Abb. 8 und 9). Durchlässigkeitskennwerte (Kf) und Filtergeschwindigkeit (Vf) steigen mit zunehmendem Porendruck (1. Publikation, Abb. 15 und 16), bis die maximale Scherspannung erreicht wird. Nach dem Erreichen der maximalen

Scherspannung nehmen Kohäsions- und Reibungskräfte ab. Dieser „Wendepunkt“ ist in der klassischen Literatur als Übergang zum Diskontinuum beschrieben, wobei man diesen auch als eine weitere Stufe innerhalb des Deformationsprozess ansehen kann. Je fortgeschrittener die Deformation ist, desto schwieriger ist es, herkömmliche Schlussfolgerungen zwischen Spannungszustand und Lithologie anzunehmen. Eine durchgehende Scherfläche oder ein vernetztes, konjugiertes Schermuster (Scherbänder) bringen eine komplett neue anisotrope Struktur mit sich, die nun an erster Stelle der zukünftigen mechanischen Antwort des Gesteins steht. Dieser Zustand ist bereits Ausgangspunkt für weitere Forschungen, die der Fraktalität der Geomaterie eine hohe Bedeutung zumisst (Lempp et al., in Bearbeitung).

Mit dieser Arbeit wurde der Zusammenhang zwischen Lithologie, Spannungsfeld und Anisotropie dargestellt, welcher anhand einer systematischen Porendruckänderung abgebildet werden konnte. Dadurch wird ein vertieftes Verständnis über den skaleninvarianten Charakter der Anisotropie und des Porendruckes auf die Strukturänderung von Gesteinen erlangt. Durch die Zusammenstellung von Festigkeitsparametern (mechanische Arbeit, Verformungsmoduln, Scherparameter, Verformungskurven), Dilatanzkurven und Permeabilitätsentwicklung kann die geomechanische Beurteilung ergänzt und bewertet werden, da ein großes Spektrum an Ergebnissen gezeigt wird. Demzufolge bietet diese Arbeit eine umfassende Darstellung der Auswirkungen zufälliger Faktoren in die Strukturänderung von Gesteinen und ist damit von Bedeutung für diverse Fragestellungen zur Druckänderung in Gesteinsmassen.

#### 4. Literatur- und Quellenangaben

Abbass, H. A., Mohamed, Z., Yasir, S. F. 2018. A review of methods, techniques and approaches on investigation of rock anisotropy. AIP Conference Proceedings 2020, 020012. Doi: 10.1063/1.5062638

Alejano, L. R., Alonso, E. 2005. Considerations of the dilatancy angle in rocks and rock masses. International Journal of Rock Mechanics & Mining Sciences Volume 42, Issue 4, Pages 481-507.

Alejano, L. R., Arzúa, J., Bozorgzadeh, N., Harrison, J. P. 2017. Triaxial strength and deformability of intact and increasingly jointed granite samples. International Journal of Rock Mechanics & Mining Sciences (95), 87-103.

Alkan, H. 2009. Percolation model for dilatancy-induced permeability of the excavation damaged zone in rock salt. International Journal of Rock Mechanics & Mining Sciences 46, 716-724.

Anders, M. H., Laubach, S. E., Scholz, C. H. 2014. Microfractures: A review. Journal of Structural Geology, 1-18.

Arzúa, J., Alejano, L. R. 2013. Dilation in granite during servo-controlled triaxial strength tests. International Journal of Rock Mechanics & Mining Sciences. 61, 43-56.

Bauch, E., Lempp, C. 2004. Rock splitting in the surrounds of underground openings: an experimental approach using triaxial extension tests. -In: Hack, R., Azzam, R. & Charlier, R. (Eds.): Engineering geology for Infrastructure planning in Europe. - LNES 104, Springer: 244-254.

Baud, P., Louis, L., David, C., Rawling, G. C., & Wong, T. F. 2005. Effects of bedding and foliation on mechanical anisotropy, damage evolution and failure mode. Geological Society, London, Special Publications, 245(1), 223-249.



Baud, P., Wong, T-f., Zhu, W. 2014. Effects of porosity and crack density on the compressive strength of rocks. *International Journal of Rock Mechanics & Mining Sciences* 67, 202-211.

Baud, P., Reuschlé, T., Ji, Y., Cheung, C. S., & Wong, T. F. 2015. Mechanical compaction and strain localization in Bleurswiller sandstone. *Journal of Geophysical Research: Solid Earth*, 120(9), 6501-6522.

Bauer, J. F., Meier, S., Philipp, S. L. 2015. Architecture, fracture system, mechanical properties and permeability structure of a fault zone in Lower Triassic sandstone, Upper Rhine Graben. *Tectonophysics* 647-648, 132-145.

Benson, P. M., Meredith, P. G., Platzman, E. S., White, R. E. 2005. Pore fabric shape anisotropy in porous sandstones and its relation to elastic wave velocity and permeability anisotropy under hydrostatic pressure. *International Journal of Rock Mechanics and Mining* (42), 890-899.

Bertrand, F., Collin, F. 2017. Anisotropic modelling of Opalinus Clay behavior: From triaxial tests to gallery excavation application. *Journal of Rock Mechanics and Geotechnical Engineering* 9, 435-448.

Bigdoli, M. N., Jing, L. 2014. Anisotropy of strength and deformability of fractured rocks. *Journal of Rock Mechanics and Geotechnical Engineering* (6), 156-1654.

Broch, E. 1983. Estimation of Strength Anisotropy Using the Point-Load Test. *International Journal of Rocks Mechanics and Mining Sciences & Geomechanics Abstracts*, 20 (4), 181-187.

Bubeck, A., Walker, R. J., Healy, D., Dobbs, M. & Holwell, D. A. 2017. Pore geometry as a control on rock strength. *Earth and Planetary Science Letters*, 457, 38-48.

Cox, S. J. D., Scholz, C. H. 1988. On the formation and growth of faults: an experimental approach. *Journal of Structural Geology*, Vol. 10. Nr. 4, pp. 413 – 430.

Cook, N. G. W. 1965. The failure of rock. *International Journal of Rock Mechanics and Mining science* Volume 2, pp. 389-403.

David, C., Menéndez, B., Zhu, W., Wong, T-f. 2001. Mechanical compaction, microstructures and permeability evolution in sandstones. *Physics and Chemistry of the Earth, Part A: Solid Earth and Geodesy* 26, 45-51.

DGGT (Deutsche Gesellschaft für Erd- und Grundbau e.V.): Mehrstufentechnik bei dreiaxialen Druckversuchen und direkten Scherversuche, Empfehlung Nr. 12 des Arbeitskreises 19 – Versuchstechnik Fels. In: Technische Prüfvorschriften für Boden und Fels im Straßenbau (TP BF-StB) (1987).

DIN-18130-1 (1998): Baugrund – Laboratory tests for determining the coefficient of permeability of soil – Teil 1: Laborversuche. – Beuth Verlag, Berlin.

DIN EN 196-1:2005-05, Methods of testing cement - Part 1: Determination of strength; German version EN 196-1:2005.

DIN 22024:1958-10, Investigations of the raw material in hard-coal-mining; indirect tensile strength determination on solid rocks.

DIN EN 1936:2007-02, Natural stone test method – Determination of real density and apparent density, and of total and open porosity. German version EN 1936:2006.

Erickson, K., Lempp, C., Pöllmann, H. 2015. Geochemical and geomechanical effects of scCO<sub>2</sub> and associated impurities on physical and petrophysical properties of Permian Sandstones (Germany): an experimental approach. *Environmental Earth Sciences* Volume 74, Issue 6, pp 4719-4743. <https://doi.org/10.1007/s12665-015-4437-0>

Farrel, N. J. C., Healy, D., & Taylor, C. W. 2014. Anisotropy of permeability in faulted porous sandstones. *Journal of Structural Geology*, 63 50-67.

Fischer, C. Dunkl, I., von Eynatten, H., Wijbrans, J. R., Gaupp, R. 2012. Products and timing of diagenetic processes in Upper Rotliegend sandstones from Bebertal (North German Basin, Parchim, Formation, Flechtingen High, Germany). *Geol. Mag.* 149(5), 827-840.

Förster, A., Lempp, C. 2014. Determination of states of stress in hard rocks: Results of laboratory conducted finite deformation analysis. *Rock engineering and rock mechanics:*

Structures in and on rock masses – Alejano, Perucho, Olalla & Jiménez (Eds). Taylor & Francis group, London, 978-1-138-00149-7.

Fossen, H., Zuluaga, L. F., Ballas, G., Soliva, R., Rotevatn, A. 2015. Contractional deformation of porous sandstone: Insights from the Aztec Sandstone, SE Nevada, USA. *Journal of Structural Geology*, 74, 172-184.

Fossen, H., Schultz, R. A., Torabi, A. 2011. Conditions and implications for compaction band formation in the Navajo Sandstone, Utah. *Journal of Structural Geology* 33, 1477-1490.

Gehne, S., Benson, P. M. 2017. Permeability and permeability anisotropy in Crab Orchard sandstone: Experimental insights into spatio-temporal effects. *Tectonophysics* 712-713, 589-599.

Geng, Z., Chen, M., Jin, Y., Yang, S., Yi, Z., Fang, X., Du, X. 2016. Experimental study of brittleness anisotropy of shale in triaxial compression. *Journal of Natural Gas Science and Engineering* (36), 510-518.

Goodman, R. E. 1989. *Introduction to rock mechanics*. 2nd edn. John Wiley & Sons, USA

Greve, R. 2003. *Kontinuumsmechanik – ein Grundkurs*. Springer.

Griffiths, L., Heap, M. J., Xu, T., Chen, C-f., Baud, P. 2017. The influence of pore geometry and orientation on the strength and stiffness of porous rock. *Journal of Structural Geology* 96, 149-160.

Gudehus, G., Karcher, C. 2007. Hypoplastic simulation of normal faults without and with clay smears. *Journal of Structural Geology* 29, 530-540.

Gußmann, P. 2018. Ein Beitrag zur Traglastermittlung mit der Kinematischen-Elemente-Methode (KEM) bei Dilatanz. *Geotechnik* 4, 272 – 278.

Healy, D., Rizzo, R. E., Cornwell, D. G., Farrell, N. J. C., Watkins, H., Timms, N. E., Gomes-Rivas, E., Smith, M. 2017. FracPaQ: A MATLAB toolbox for the quantification of fracture patterns. *Journal of Structural Geology* 95, 1-16.

Heap, M. J., Kushnir, A. R., Gilg, H. A., Wadsworth, F. B., Reuschlé, T., & Baud, P. 2017. Microstructural and petrophysical properties of the Permo-Triassic sandstones (Buntsandstein) from the Soultz-sous-Forêts geothermal site (France). *Geothermal Energy*, 5:26. <https://doi.org/10.1186/s40517-017-0085-9>

Hecht, C. A., Bönsch, C., Bauch, E. 2005. Relations of rock structure and composition to petrophysical and geomechanical rock properties: examples from Permocarboniferous Red-Beds. *Rock Mechanics Rock Engineering* 38, 197-216.

Henningsen, D. Katzung, G. 2006. Einführung in die Geologie Deutschlands. 6. Auflage, Spektrum Verlag.

Hobbs, B. E. 1993. The significance of Structural geology in rock mechanics. In: *Comprehensive rock engineering – practices, principles & projects*. Volume 1. Pergamon Press.

Iglauer, S., Sarmadivaleh, M., Al-Yaheri, A., Lebedev, M. 2014. Permeability evolution in sandstone due to injection of CO<sub>2</sub>-saturated brine or supercritical CO<sub>2</sub> at reservoir conditions. *Energy Procedia* 63, 3051-3059.

IPCC 2005: IPCC Special Report on Carbon Dioxide Capture and Storage. Prepared by Working Group III of the Intergovernmental Panel on climate change [Metz, B. O. Davidson, H. C. de Coninck, M. Loos, and L. A. Meyer (eds.)]. Cambridge University Press, Cambridge, UK and New York, NY, USA, 442 pps

Jaeger, J. C., Cook, N. G. W.. 1979. Fundamentals of rock mechanics. 3<sup>rd</sup> edn. Chapman and Hall, London.

Jeannin, L., Bignonnet, F., Agostini, F., Wang, Yi. 2018. Stress effects on the relative permeabilities of tight sandstones. *Comptes Rendus Geoscience* 350 (3), 110-118.

Josh, M., Esteban, L., Delle Piane, C., Sarout, J., Dewhurst, D. N., Clennell, M. B. 2012. Laboratory characterisation of shale properties. *Journal of Petroleum Science and Engineering* 88-98, 107-127.

Kim, B-H., Walton, G., Larson, M. K, Berry, S. 1997. Experimental study on the confinement-dependent characteristics of a Utah coal considering the anisotropy by cleats. *International Journal of Rock Mechanics and Mining Sciences* 105,182-191.

Kluge, C., Milsch, H., Blöcher, G. 2017. Permeability of displaced fractures. *Energy Procedia* 125, 88-97.

Kolymbas, D., Fellin, W., Schneider-Muntau, B., Medicus, G., Schranz, F. 2016. Zur Rolle der Materialmodelle beim Standsicherheitsnachweis. *Geotechnik*. Doi: 10.1002/gete.201500017

Kolymbas, D., Herle, I. 2017. Stoffgesetze für Böden. *Grundbau-Taschenbuch, Teil 1: Geotechnische Grundlagen*, 8. Auflage, Ernst & Sohn, p. 457-509.

Lempp, C., Menezes, F. F., Schöner, A. in Bearbeitung. Evolution of shear bands and cracks in multi-stage triaxial tests with water-saturated sandstone: a micro-tectonic analogon (a never ending paper).

Li, J. Z., Laubach, S.E., Gale, J. F.W., Marrett, R. A. 2018. Quantifying opening-mode fracture spatial organization in horizontal wellbore image logs, core and outcrop: Application to Upper Cretaceous Frontier Formation tight gas sandstones, USA. *Journal of Structural Geology* 108, 137-156.

Li, J., Wang, M., Xia, K., Zhang, N., Huang, H. 2017. Time-dependent dilatancy for brittle rocks. *Journal of Rock Mechanics and Geotechnical Engineering* 9, 1054-1070.

Louis, L., David, C., & Robion, P. 2003. Comparison of the anisotropic behavior of underformed sandstones under dry and saturated conditions, *Tectonophysics*, 370 (1-4), 193-212.



Luo, W., Qin, Y-p., Zhang, M-m., Wang, C-x., Wang, Y-r. 2011. Test study on permeability properties of the sandstone specimen under triaxial stress conditions. First international symposium on mine safety science and engineering. *Procedia Engineering* 26, 173-178.

Marbler, H., Erickson, K. P., Schmidt, M., Lempp, C., Pöllmann, H. 2015. Geomechanical and geochemical effects on sandstones caused by the reaction with supercritical CO<sub>2</sub>: an experimental approach to in situ conditions in deep geological reservoirs. *Environmental Earth Sciences* 69:1981-1998.

Mandelbrot, B. 1982. *The fractal geometry of nature*. W.H. Freeman and Company, USA.

Means, W. D. 1976. *Stress and Strain*. Springer-Verlag, New York.

Menéndez, B., Zhu, W., Wong, T-F. 1995. Micromechanics of brittle faulting and cataclastic flow in Berea sandstone. *Journal of Structural Geology* 18, 1-16.

Menezes, F. F., Lempp, C. 2018. On the structural anisotropy of physical and mechanical properties of a Bunter sandstone. *Journal of Structural Geology* 114, 196-205.

Mitchell, T. M., Faulkner, D. R. 2008. Experimental measurements of permeability evolution during triaxial compression of initially intact crystalline rocks and implications for fluid flow in fault zones. *Journal of Geophysical Research* 113.

Naumann, M., Hunsche, U., Schulze, O. 2007. Experimental investigation on anisotropy in dilatancy, failure and creep of Opalinus Clay. *Physics and Chemistry of the Earth* 32, 889-895.

Neumann, A., Svensson, K., Menezes, F., Lempp, C., Pöllmann, H. 2018. Mineralogical analyses of the impact of CO<sub>2</sub> and associated compounds on sandstone in the presence of formation waters at non-ambient conditions. Conference: 40th international conference on cement microscopy, At Deerfield, FA, USA.

Oda, M., Takemura, T., Aoki, T. 2002. Damage growth and permeability change in triaxial compression tests of Inada granite. *Mechanics of Materials* 34, 313-331.

Ord, A. 1990. Mechanical Controls on dilatant shear zones. Geological Society London Special Publications 54 (1):183-192.

Ord, A. 1991. Deformation of rock: A pressure-sensitive, dilatant material. Pure and applied Geophysics. Volume 137, N° 4, pp 337-366.

Ord, A., Hobbs, B. E. 2010. Fracture pattern formation in frictional, cohesive, granular material. Phil. Trans. R. Soc. A (2010) 368, 95-118. Doi: 10.1098/rsta.2009.0199

Pérez-Flores, P., Wang, G., Mitchell, T. M., Meredith, P. G., Nara, Y., Sarkar, V., Cembrano, J. 2017. The effect of offset on fracture permeability of rocks from the Southern Andes Volcanic Zone, Chile. Journal of Structural Geology 104, 142-158.

Pimentel, E. 2017. Stoffgesetze und Bemessungsansätze für Festgestein. Grundbau-Taschenbuch, Teil 1: Geotechnische Grundlagen, Ernst & Sohn, p. 397-450.

Pludo, D., Albrecht, D., Ganzer, L., Gaupp, R., Kohlhepp, B., Meyer, R., Reitenbach, V., Wienand, J. 2011. Petrophysical, Facies and mineralogical-geochemical investigations of Rotliegend sandstones from the Altmark natural gas field in central Germany. Energy Procedia 4, 4648-4655.

Pöllmann, H, Neumann, A., Menezes, F., Svensson, K., Lempp, C., Göske, J., Winter, S. 2017. Quartz habits and secondary pseudomorphs from secondary filled lenses in Triassic grey Wesersandstein. Boletim do Museu de Geociências da Amazônia (3), Ano 4.

Ramsay, J. G., Huber, M. I. 1983. The techniques of modern Structural geology. Vol.1, Strain analysis. Academic Press, London.

Rawling, G. C., Baud, P., & Wong, T. F. 2002. Dilatancy, brittle strength, and anisotropy of foliated rocks: Experimental deformation and micromechanical modelling. Journal of Geophysical Research: Solid Earth, 107 (B10).

Reyer, D., & Philipp, S. L. 2004. Empirical relations of rock properties of outcrop and core samples from the Northwest German Basin for geothermal drilling. *Geothermal Energy Science*, 2(1), 21.

Scholz, C. H. Dawers, N. H., Yu, J.-Z., Anders M. H. 1993. Fault growth and fault scaling laws: Preliminary results. *Journal of Geophysical Research*, Vol. 98. N° 12, 21.951-21.961.

Scholz, C. H. 1968. Microfracturing and the inelastic deformation of rock in compression. *Journal of Geophysical Research* 73 (4), pp. 1417-1432.

Scholz, C. H. 1967. Microfracturing of rock in compression. PhD Thesis.

Sheldon, H. A., Ord, A. 2005. Evolution of porosity, permeability and fluid pressure in dilatant fault post-failure: implications for fluid flow and mineralization. *Geofluids* 5, 272-288.

Sheldon, H. A., Barnicoat, A. C., Ord, A. 2006. Numerical modelling of faulting and fluid flow in porous rocks: An approach based on critical state soil mechanics. *Journal of Structural Geology* 28, 1468-1482.

Tan, T. K., Shi, Z. Q. Yu, Z. H., Yang, W. X. 1989. Dilatancy, creep and relaxation of brittle rocks measured with the 8000 kN multipurpose triaxial apparatus. *Physics of the Earth and Planetary Interiors*, 55, 335-352.

Thuro, K. Drillability prediction. 1997. Geological influences in hard rock drill and blast tunnelling. *International Journal of Earth Sciences*. 86, 426-438.

Tavallali, A., Vervoort, A. 2010. Effect of layer orientation on the failure of layered sandstone under Brazilian test conditions. *International Journal of Rock Mechanics and Mining Sciences*, Volume 47, Issue 2, 313:322.

Turcotte, D. L. 1990. Implications of chaos, scale-invariance, and fractal statistics in geology. *Palaeography, Palaeoclimatology, Palaeoecology (Global and Planetary Change Section)*, 89 (1990) 301-308. Elsevier Science Publishers B. V., Amsterdam.

Uehara, S-i., Takahashi, M. 2013. How rock mechanical properties affect the fault permeability in Neogene mudstones? *Energy Procedia* 37, 5588-5595.

Vardoulakis, I. 1984. Rock bursting as a surface instability phenomenon. *International Journal of Rock Mechanics, Mining Sciences and Geomechanics Abstracts*. Vol. 21, N° 3, pp. 137-144.

Vardoulakis, I., Mühlhaus, H. B. 1986. Technical note: Local rock surface instabilities. *International Journal of Rock Mechanics and Mining Sciences* 23, No. 5 379-383.

Verdon, J. P., Stork, A. L. 2016. Carbon capture and storage, geomechanics and induced seismic activity. *Journal of Rock Mechanics and Geotechnical Engineering* 8 (2016), 928-935.

Vilarrasa, V., Ramírez, J. C., Olivella, S., Rutqvist, J., Laloui. 2019. Induced seismicity in geologic carbon storage. *Solid Earth*, 10, 871-892.

Vishnu, C. S., Lahiri, S., Mamtani, M. A. 2018. The relationship between magnetic anisotropy, rock-strength anisotropy and vein emplacement in gold-bearing metabasalts of Gadag (South India). *Tectonophysics* (722), 286-298.

von Soos, P., Engel, J. 2017. Eigenschaften von Boden und Fels – ihre Ermittlung im Labor. *Grundbau-Taschenbuch, Teil 1: Geotechnische Grundlagen*, 8. Auflage, Ernst & Sohn, p. 139-242.

Watkins, H., Healy, D., Bond, C. E., Butler, R. W. H. 2018. Implications of heterogeneous fracture distribution on reservoir quality; an analogue from the Torridon Group sandstone, Moine Thrust Belt, NW Scotland. *Journal of Structural Geology*, 108, pp. 180-197.

Weber, J., Ricken, W. 2005. Quartz cementation and related sedimentary architecture of the Triassic Solling Formation, Reinhardswald Basin, Germany. *Sedimentary Geology* (175), 459-477.

Wittke, W. 2014. *Rock mechanics based on an anisotropic jointed rock model (AJRM)*. Wiley – Ernst & Sohn, p.875

Wong, T. F., David, C., & Zhu, W. 1997. The transition from brittle faulting to cataclastic flow in porous sandstones: Mechanical deformation. *Journal of Geophysical Research: Solid Earth*, 102 (B2), 3009-3025.

Wu, J. Feng, M., Yu, B., Zhang, W., Ni, X., Han, G. 2018. Experimental investigation on dilatancy behavior of water saturated sandstone. *International Journal of Mining Science and Technology* 28, 323-329.

Xu, P. Yang, S-Q. 2016. Permeability evolution of sandstone under short-term and long-term triaxial compression. *International Journal of Rocks Mechanics & Mining Sciences*. Volume 85, pp. 152-164.

Zhao, X. C., Cai, M. 2010. A mobilized dilation angle model for rocks. *International Journal of Rock Mechanics & Mining Sciences* 47, 368-384.

Zhu, W., Baud, P., Vinciguerra, S., Wong, T-f. 2011. Micromechanics of brittle faulting and cataclastic flow in Alban Hills tuff. *Journal of Geophysical Research*, Vol. 116, Issue B6. <https://doi.org/10.1029/2010jb008046>



### **Eidesstattliche Erklärung / *Declaration under Oath***

Ich erkläre an Eides statt, dass ich die Arbeit selbstständig und ohne fremde Hilfe verfasst, keine anderen als die von mir angegebenen Quellen und Hilfsmittel benutzt und die den benutzten Werken wörtlich oder inhaltlich entnommenen Stellen als solche kenntlich gemacht habe.

*I declare under penalty of perjury that this thesis is my own work entirely and has been written without any help from other people. I used only the sources mentioned and included all the citations correctly both in word or content.*

---

Datum / Date Unterschrift des Antragstellers / *Signature of the applicant*

# Flora Feitosa Menezes

---

floramenezes@gmx.de

## Persönliche Daten

- Geburtsdatum: 31. Dezember, 1989
- Nationalität: brasilianisch

## Universitätsausbildung

### 02/2016 - 02/2019 | PHD-STUDENTIN AN DER MARTIN-LUTHER-UNIVERSITÄT (MLU), HALLE, DEUTSCHLAND

Vertiefungen: Felsmechanik und Ingenieurgeologie

Titel der PhD-Thesis: Experimentelle Studie über die fortschreitende Strukturänderung von anisotropen Sandsteinen.  
Betreuer: Prof. Dr. Christof Lempp.

### 08/2013 - 10/2015 | M.SC. ANGEWANDTE GEOWISSENSCHAFTEN AN DER MARTIN-LUTHER-UNIVERSITÄT (MLU), HALLE, DEUTSCHLAND

Vertiefungen: Ingenieurgeologie, Geodynamik und Bodenmechanik

Titel der Masterarbeit: Der Rotliegend Sandstein: geomechanisches Verhalten von Kontinuum ins Diskontinuum.  
Betreuer: Prof. Dr. Christof Lempp und Dr. Annika Förster.

### 03/2008 - 03/2013 | DIPLOM IN GEOLOGIE AN DER BUNDESUNIVERSITÄT VON PARÁ (UFPA), BELÉM, BRASILIEN

Vertiefungen: Strukturgeologie, Kartierung und Sedimentologie

Titel der Abschlussarbeit: Caracterizacao da porosidade secundária em zonas de falha do Granito Tracuateua, nordeste paraense. Betreuer: Prof. Dr. Roberto Vizeu Lima Pinheiro und Prof. Dr. Fábio Henrique Domingos.

Stipendiatin des UniBral-Programmes (DAAD und CAPES) von April 2011 bis März 2012 als Austauschstudentin an der Universität Halle.

## Schlüsselqualifikationen

### SPRACHEN

Portugiesisch: Muttersprache

Deutsch: fließend

Englisch: fließend

Spanisch: fließend

Französisch: gute Kenntnisse

### SOFTWARE

• ADINA • ANSYS • ArcGis • CAD • CorelDraw • GGU • FLAC 2D • MatLab • R

## Veröffentlichungen

### POSTER UND ABSTRACTS

SVENSSON, K., MENEZES, F. F., NEUMANN, A., LEMPP, C., PÖLLMANN, H. Impact of scCO<sub>2</sub> injection and chloride rich brine on a CEM III cement at lithostatic conditions. In: „AEG 61<sup>st</sup> Annual Meeting / IAEG XIII Congress“, in San Francisco, Vereinigte Staaten von Amerika (2018). Poster und Abstract.

**MENEZES, F. F.**, LEMPP, C. Anisotropy of Volume Change and Permeability in Hard Sandstones under Triaxial Stress Conditions. In: „AEG 61<sup>st</sup> Annual Meeting / IAEG XIII Congress”, in San Francisco, Vereinigte Staaten von Amerika (2018). Poster und Abstract.

**MENEZES, F. F.**, LEMPP, C., SVENSSON, K. NEUMANN, A. PÖLLMANN, H. Geomechanical behaviour changes of a Bunter Sandstone and of a borehole cement due to scCO<sub>2</sub> injection effects. In: „AEG 61<sup>st</sup> Annual Meeting / IAEG XIII Congress”, in San Francisco, Vereinigte Staaten von Amerika (2018). Poster, Abstract und Vortrag.

**MENEZES, F. F.**, LEMPP, C. Anisotropy of Volume Change and Permeability in Hard Sandstones under Triaxial Stress Conditions. In: „Young Researchers in Structural Geology and Tectonics (YORSGET)”, in Montgenèvre, Frankreich (2018). Poster und Abstract. Auf der Internetseite <https://conferences.leeds.ac.uk/yorsget/programme/> verfügbar.

**MENEZES, F. F.**, SCHLÜTER, S., KÖHNE, J. M., SVENSSON, LEMPP, C., K. NEUMANN, A. PÖLLMANN, H. Geomechanical effects in a Bunter Sandstone due to impure scCO<sub>2</sub> injection. In: „Young Researchers in Structural Geology and Tectonics (YORSGET)”, in Montgenèvre, Frankreich (2018). Poster und Abstract. Auf der Internetseite <https://conferences.leeds.ac.uk/yorsget/programme/> verfügbar.

**MENEZES, F. F.**, SCHLÜTER, S., KÖHNE, J. M., SVENSSON, LEMPP, C., K. NEUMANN, A. PÖLLMANN, H. Geomechanical effects in a Bunter Sandstone due to impure scCO<sub>2</sub> injection. In: „Geoscience challenges in the 21<sup>st</sup> century: What difference does your research make? “2<sup>st</sup> Geologists’ Association Student Symposium, GASS (2018), in London, England. Poster und Abstract.

**MENEZES, F. F.**, LEMPP, C., SVENSSON, K. NEUMANN, A. PÖLLMANN, H. Geomechanical behaviour changes of a Bunter Sandstone and of a borehole cement due to scCO<sub>2</sub> injection effects. In: GeoBremen 2017, in Bremen, Deutschland. Poster und Abstract.

SVENSSON K., NEUMANN, A. PÖLLMANN, H., **MENEZES, F. F.**, LEMPP, C. Carbonation of Wollastonite. In: GeoBremen 2017, in Bremen, Deutschland. Poster und Abstract.

SVENSSON K., NEUMANN A., PÖLLMANN H., **MENEZES F.**, LEMPP C. (2017). Curing by Carbonation of Wollastonite. GDCh, at Bauhaus-University Weimar, Deutschland. Poster und Abstract.

NEUMANN, A., SVENSSON K., PÖLLMANN, H., **MENEZES, F. F.**, LEMPP, C. Mineralogy and microstructure of small secondary modified lenses in the grey Weser sandstone. In: GeoBremen 2017, in Bremen, Deutschland. Poster und Abstract.

PÖLLMANN, H., NEUMANN, A., SVENSSON K., **MENEZES, F. F.**, LEMPP, C. Microstructure and Mineralogy of the Trendelburg Sandstone Beds. In: GeoBremen 2017, in Bremen, Deutschland. Poster und Abstract.

**MENEZES, F. F.**, LEMPP, C., NEUMANN, A. SVENSSON, K. PÖLLMANN, H. Geomechanical behaviour changes of a Bunter Sandstone due to scCO<sub>2</sub> injection effects. In: „Geology and societal change: What difference does your research make? “1<sup>st</sup> Geologists’ Association Student Symposium, GASS (2017), in London, England. Poster und Abstract.

**MENEZES, F. F.**, LEMPP, C. The Rotliegend fracture patterns: a transition between continuous and discontinuous geomechanical behaviour. In: 21<sup>st</sup> International Conference on „Deformation mechanisms, Rheology and Tectonics“, DRT 2017 in Inverness, Scotland. Poster und Abstract.

**MENEZES, F. F.**, LEMPP, C., NEUMANN, A. SVENSSON, K. PÖLLMANN, H. Geomechanical behaviour changes of a Bunter Sandstone due to scCO<sub>2</sub> injection effects. In: 21<sup>st</sup> International Conference on „Deformation mechanisms, Rheology and Tectonics“, DRT 2017 in Inverness, Scotland. Poster und Abstract.

**MENEZES, F. F.**, PINHEIRO, R. V. L., FERREIRA, E. L. Caracterizacao mecânica da porosidade secundária em zonas de falha do Granito Tracuateua, nordeste paraense. In: Simpósio de Geologia da Amazônia, 2013, Belém (PA), Brasilien. Poster und Abstract.

#### CONFERENCE PAPER

NEUMANN A., SVENSSON K., PÖLLMANN H., **MENEZES F.**, LEMPP C. (2018). Mineralogical analyses of the impact of CO<sub>2</sub> and associated compounds on sandstone in the presence of formation waters at non ambient conditions. Conference: 40<sup>th</sup> International conference on cement microscopy. Deerfield, USA.

SVENSSON K., NEUMANN A., PÖLLMANN H., **MENEZES F.**, LEMPP C. (2017). Curing by Carbonation of Wollastonite. GDCh Conference Bauchemie 2017, 52, 80–83, ISBN: 978-3-947197-02-6.

**MENEZES, F. F.**, LEMPP, C., SCHÖNER, A. Der Rotliegend Sandstein: geomechanisches Verhalten vom Kontinuum ins Diskontinuum. In: Fachsektionstage Geotechnik, Forum für junge Ingenieurgeologen 2017 in Würzburg, Deutschland. Vortrag und extended Abstract.

**MENEZES, F. F.**, PINHEIRO, R. V. L., FERREIRA, E. L. Caracterizacao da porosidade secundária em zonas de falha do Granito Tracuateua, nordeste paraense. In: Reuniao Anual de Avaliacao dos prhs ANP Norte-Nordeste, 2012, Natal (RN), Brasilien. Auf der Internetseite [http://www.nupeg.ufrn.br/raanne2012/prh06/resumos\\_prh06.pdf](http://www.nupeg.ufrn.br/raanne2012/prh06/resumos_prh06.pdf) verfügbar. Poster und extended Abstract.

#### PEER-REVIEWED PUBLICATIONS

SVENSSON, K.; NEUMANN, A.; **MENEZES, F.**; LEMPP, C.; PÖLLMANN, H. 2019. Carbonation of natural pure and impure Wollastonite.

**MENEZES, F. F.**: Anisotropy of volume change and permeability evolution of hard sandstones under triaxial stress conditions.

**MENEZES, F. F.**, LEMPP, C., SVENSSON, K., NEUMANN, A., PÖLLMANN, H. 2019. Geomechanical behaviour changes of a Bunter Sandstone and a of a borehole cement due to CO<sub>2</sub> injection effects. In: IAEG/AEG Annual Meeting Proceedings, San Francisco, CA, 2018 - Volume 1: Slope Stability: Case Histories, Mapping, Emerging Technologies. DOI: 10.1007/978-3-319-93124-1\_14.

**MENEZES, F. F.**, LEMPP, C. 2018. On the structural anisotropy of physical and mechanical properties of a Bunter Sandstone. 2018. In: Journal of Structural Geology 114 (2018) 196-205. DOI: 10.1016/j.jsg.2018.06.010.

SVENSSON, K.; NEUMANN, A.; **MENEZES, F.**; LEMPP, C.; PÖLLMANN, H. 2018. The conversion of Wollastonite to CaCO<sub>3</sub> considering its use for CCS application as cementitious Material. Applied Sciences 2018, 8, 304. Open Access. <http://www.mdpi.com/2076-3417/8/2/304>

LEMPP, C., **MENEZES, F. F.**, SACHWITZ, S. 2016. Tonstein als Wirtsgestein: Ein geomechanischer Beitrag über Opalinuston (2016). In: Geotechnik. DOI: 10.1002/gete.2015400025.

#### **AUSZEICHNUNGEN**

2. Platz an den Plakatwettbewerb der „AEG 61<sup>st</sup> Annual Meeting / IAEG XIII Congress“, in San Francisco, Vereinigte Staaten von Amerika (2018). Titel: „Anisotropy of Volume Change and Permeability in Hard Sandstones under Triaxial Stress Conditions“.

#### **MITGLIEDSCHAFT**

Deutsche Gesellschaft für Geotechnik (DGGT), Deutschland